Utilization of bistatic TanDEM-X data to derive land cover information

Dissertation
(kumulativ)

zur Erlangung des akademischen Grades doctor rerum naturalium (Dr. rer. nat.)

vorgelegt dem Rat der Chemisch-Geowissenschaftlichen Fakultät der Friedrich-

Schiller-Universität Jena

von Michael Schlund (Master of Science)

geboren am 24.06.1985 in Sonneberg

Gutachter:

Prof. Dr. Christiane Schmullius (Friedrich-Schiller-Universität Jena)

Prof. Dr. Steffen Kuntz (Albert-Ludwigs-Universität Freiburg)

Tag der Verteidigung: 16.12.2015

List of manuscripts and publications

Chapter 4: Schlund, M., F. von Poncet, S. Kuntz, D.H. Hoekman & C. Schmullius (2014). Importance of bistatic SAR features from TanDEM-X for forest mapping and monitoring. *Remote Sensing of Environment* 151, 16-26.

Chapter 5: Schlund, M., F. von Poncet, S. Kuntz, C. Schmullius & D.H. Hoekman (2015). TanDEM-X data for aboveground biomass retrieval in a tropical peat swamp forest. *Remote Sensing of Environment* 158, 255-266.

Chapter 6: Schlund, M., F. von Poncet, S. Kuntz, H.D.-V. Boehm, D.H. Hoekman & C. Schmullius (2015). WorldDEM™ data for canopy height and aboveground biomass retrieval in a tropical peat swamp forest. *ISPRS International Journal of Photogrammetry & Remote Sensing*. (Submitted on March 31, 2015)

Editorial note

All publications and manuscripts were edited to obtain a common style and format in this dissertation. Editorial modifications were made regarding: 1) fonts, and layout of text and tables; 2) numbering of chapters, figures, and tables. 3) A common citation style was used for the whole thesis, which may differ to the journal's citation style.

References of Chapter 1, 2, 3, 7 and 8 are at the end of the dissertation. References of the individual publications and manuscripts are at the end of the respective chapter.

Kurzzusammenfassung

Wälder haben eine wichtige Bedeutung als natürliche Kohlenstoffsenke für den Klimawandel und den globalen Kohlenstoffkreislauf. Insbesondere tropische Wälder und vor allem tropische Torfsumpfwälder spielen trotz ihrer relativ geringen Ausdehnung eine große Rolle im globalen Kohlenstoffkreislauf. Entwaldung und Walddegradierung sind die zweitgrößten Ursachen anthropogen verursachter Kohlenstoffemission und deren Raten sind in tropischen Ländern am höchsten. Daher soll Entwaldung und Walddegradierung beispielsweise durch das UN (*United Nations*) Programm REDD+ (*Reducing Emissions from Deforestation and Degradation*) verhindert bzw. minimiert werden. Um dieses Ziel zu erreichen, ist es von großer Bedeutung Landnutzungsänderungen zu erfassen und den Status der Wälder als Kohlenstoffsenke zu schätzen. Dies kann für nachhaltiges

Waldmanagement, Landnutzungsplanung, Kohlenstoffmodellierung und zur Umsetzung von internationalen Initiativen wie REDD+ nützlich sein, indem tropische Länder für den Schutz ihrer Wälder finanziell belohnt werden. Tropische Wälder sind in der Regel schwer zu erreichen und Feldmessungen sind daher nur mit großem Aufwand möglich. Eine Kombination von Feldmessungen und Fernerkundung wird daher als am nützlichsten betrachtet, um tropische Wälder zu überwachen.

Radarsensoren haben großes Potential für die Überwachung tropischer Wälder, da sie von Wetter und Tageszeit unabhängig sind. Zusätzlich sind bereits oftmals die Nützlichkeit von SAR-Rückstreuung (SAR=*synthetic aperture radar*) und deren interferometrische Fähigkeiten in der Waldüberwachung und Biomasseschätzung unter Beweis gestellt worden. SAR-Sensoren mit kurzen Wellenlängen erzielen eine geringe Eindringtiefe in die Waldbedeckung. Daher wird häufig angenommen, dass kurzwellige SAR-Sensoren ein geringes Potential für die Abschätzung der Waldbiomasse mithilfe der Radarrückstreuung haben. Dies beruht auf der unzureichenden Interaktion der kurzen Wellenlänge mit tieferen bodennäheren Baumteilen, wie Asten und Stämmen, aufgrund der geringen Eindringung. Interferometrische Fähigkeiten von SAR-Sensoren könnten diese Limitierungen überwinden, wobei eine geringe Eindringtiefe sich als Vorteil erweisen kann. Die interferometrische Höhe kann bei geringer Eindringung als Waldbedeckungshöhe angenommen werden, die wiederum mit der Waldbiomasse korreliert ist. Daher sollen in dieser Arbeit die Möglichkeiten eines interferometrischen SAR-Systems mit kurzen Wellenlängen zur Waldüberwachung und zur Abschätzung der Biomasse untersucht werden. Die Zielsetzung dieser Arbeit ist somit die Erfassung des Potentials von interferometrischen TanDEM-X Daten für die Landnutzungskartierung und Biomasseschätzung.

Die TanDEM-X Mission ist ein X-Band SAR, das in geringen Eindringtiefen in den Wald resultiert. TanDEM-X ist eine bistatische SAR-Mission bestehend aus zwei Satelliten, die in enger Formation fliegen. Zusammen bilden die beiden Satelliten ein *single-pass* (einfacher Überflug mit simultanen Aufnahmen) interferometrisches System. Die Landmassen der Erde wurden dabei mehrere Male zwischen 2010 und 2014 in hoher Auflösung aufgenommen, um ein globales, digitales Höhenmodell zu erstellen. Daher bieten Radardaten der TanDEM-X Mission die potentielle Möglichkeit die Gesamtheit der Tropenwälder der Erde innerhalb dieses Zeitraums multi-temporal und in hoher Auflösung zu untersuchen. Gleichzeitig eröffnen sie die Möglichkeit als hochgenaue Grundlage für ein globales Waldmonitoring zu dienen. Die Sensoren von TanDEM-X können gleichzeitig aufnehmen, wobei ein Sensor als Sender und Empfänger (aktiv/monostatisch) und der andere lediglich als Empfänger (passiv/bistatisch) dient. Die Rückstreuinformationen beider Sensoren

können genutzt werden. Weiterhin können interferometrische Daten, wie interferometrische Kohärenz und Höhe, abgeleitet werden. Diese Informationen können für Landnutzungsüberwachungen sowie für biophysikalische Parameterabschätzung wie Waldbiomasse genutzt werden.

Für die Untersuchung des Informationsgehalts einer interferometrischen X-Band SAR-Aufnahme für das Tropenwaldmonitoring wurden TanDEM-X Daten genutzt. Rückstreukoeffizienten sowie Texturinformationen und interferometrische Kohärenz wurden in einer Klassifikation von tropischen Torfsumpfwald in Zentralkalimantan (Indonesien) angewendet, um zwischen grundlegenden Landbedeckungsklassen (Wald, Wasser, Buschland, Grasland) und unterschiedlichen Waldtypen zu trennen. Die Signifikanz der abgeleiteten SAR-Merkmale wurde mit einem Merkmalsauswahlprozess analysiert, um den zusätzlichen Nutzen einer bistatischen SAR-Aufnahme im Vergleich zu einer üblichen monostatischen Aufnahme zu bestimmen. Der resultierende optimale Merkmalsdatensatz bestehend aus monostatischen und bistatischen SAR-Merkmalen wurde anschließend in einer Klassifikation angewendet, um die Verbesserung der Trennbarkeit und Klassifikationsgenauigkeit von bistatischen TanDEM-X Merkmalen im Vergleich zu monostatischen zu evaluieren.

Die Ergebnisse der Merkmalsauswahl und Klassifikation indizierten, dass die interferometrische Kohärenz die Trennbarkeit von thematischen Klassen signifikant im Vergleich zu monostatischen Aufnahmen erhöhte. Die interferometrische Kohärenz verbesserte Ergebnisse im Vergleich zu Landnutzungsklassifikationen ohne Kohärenz um 10 % (75 % vs. 85 %). Speziell die Unterscheidung zwischen Waldklassen und Wald/Nicht-Wald profitierte von der Kohärenz aufgrund der Volumendekorrelation in Wäldern. Im Gegensatz dazu lieferten Rückstreukoeffizienten keine signifikanten Informationen zur Trennung von Waldklassen. Diese Analysen wurden in dem Artikel "Importance of bistatic SAR features from TanDEM-X for forest mapping and monitoring", erschienen in *Remote Sensing of Environment*, beschrieben.

Feldmessungen wurden als Referenz für Waldbiomasse in den Jahren 2013 und 2014 im Untersuchungsgebiet von Zentralkalimantan durchgeführt. Diese Feldmessungen wurden mit Waldbedeckungshöhen von LiDAR (*Light Detection and Ranging*) korreliert. Diese Korrelation diente zur Herleitung eines Regressionsmodells, um über die gemessenen LiDAR-Baumhöhen die Biomasse innerhalb der beflogenen Gebiete abzuschätzen. Die *in situ* erhobenen Biomassemittelwerte entsprachen den mittels des Regressionsmodells geschätzten Biomassewerten aus den LiDAR-Daten. Die LiDAR basierende Biomasseschätzung konnte somit als eine verlässliche Datenquelle angesehen werden, um Korrelationen der Biomasse mit Rückstreuung und interferometrischer Kohärenz

von TanDEM-X zu untersuchen. Zusätzlich wurde das Potential des global verfügbaren digitalen Höhenmodells der TanDEM-X Mission WorldDEM™ in Bezug auf Biomasseschätzungen in dem tropischen Torfsumpfwald in Zentralkalimantan untersucht. Auch hier wurden die Feldmessungen mit verschiedenen Waldhöhenmodellen korreliert. Diese Waldhöhenmodelle wurden auf Basis des TanDEM-X *intermediate digital elevation model* (iDEM; als Präkursor für WorldDEM™) und LiDAR-Messungen berechnet. Diese Korrelationen resultierten wiederum in Regressionsmodellen, die zur Skalierung der Biomasse der kleinräumigen Feldmessungen auf großräumige Fernerkundungsdaten genutzt wurden.

Die interferometrische Kohärenz war hilfreich bei Klassifikationen (wie oben beschrieben) sowie bei der Schätzung der Waldbiomasse. Volumendekorrelation der X-Band SAR-Daten in Wäldern nahm mit der Biomasse zu. Die Kohärenz korrelierte daher mit der Biomasse mit einer Modellgenauigkeit von 0,5, beschrieben durch das Bestimmtheitsmaß (R^2). Diese Korrelation resultierte in einem Fehler von 14 %, der mithilfe der Wurzel aus dem mittleren quadratischen Fehler (*root mean square error*=RMSE) in Bezug auf unabhängigen Validierungsdaten berechnet wurde. Der beobachtete Biomassewertebereich lag zwischen 183 t/ha und 495 t/ha. Degradierte Waldgebiete ließen sich aufgrund von Auflockerung der Bestände und damit verbundener geringerer Biomasse im Vergleich zu intaktem Wald identifizieren.

Im Vergleich zu den LiDAR-Referenzmessungen lagen die mittleren Abweichungen der aus den TanDEM-X Daten abgeleiteten Höhenmodelle unter 5 m. Die interferometrische Höhe kombiniert mit einem genauem Geländemodell erreichte höhere Korrelationen mit der Biomasse (R^2 = 0,68) im Vergleich zur Kohärenz und resultierte in einem kreuz-validiertem RMSE von 7,5 %. TanDEM-X Höhen korrelierten jedoch geringer mit der Biomasse ohne externes Geländemodell (R^2 = 0,2) resultierend in höherem RMSE (16 %).

Sehr genaue Geländemodelle stehen jedoch nicht auf globalem Maßstab zur Verfügung. Dennoch zeigen die Ergebnisse, dass ein Ansatz basierend auf WorldDEM™ alleine in Gebieten ohne genauem Geländemodell genutzt werden kann. Dies resultiert zwar in geringeren Genauigkeiten, kann aber global angewendet werden. Diese Analysen sind in den Artikeln "TanDEM-X data for aboveground biomass retrieval in a tropical peat swamp forest", erschienen in *Remote Sensing of Environment*, und "WorldDEM™ data for canopy height and aboveground biomass retrieval in a tropical peat swamp forest", eingereicht bei *ISPRS Journal of Photogrammetry & Remote Sensing*, beschrieben.

Die Ergebnisse zeigen, dass TanDEM-X als nützliche und konsistente Datenquelle für Waldüberwachung angewendet werden kann. Speziell die interferometrische

Information ist nützlich in der Landbedeckungskartierung und Biomasseschätzung. TanDEM-X Daten können daher beispielsweise für Stratifizierung im Kontext von REDD+ oder Walddegradierungsdetektion genutzt werden, um die räumliche Verteilung von Waldtypen und Biomasse abzubilden. Der global verfügbare TanDEM-X Datensatz könnte daher auch als Referenz für zukünftige, weltweite Entwaldungs- und Degradationsüberwachung dienen. Hierbei könnte der Status Quo von Wäldern für die Jahre 2010 bis 2014 mit TanDEM-X präzise analysiert werden. Änderungen des Status könnten anschließend mit bereits existierenden¨ oder zukünftigen SAR oder optischen Fernerkundungsmissionen erfasst werden.

Abstract

Forests are of significance as natural carbon sink in climate change mitigation and the global carbon cycle. Tropical forests and tropical peat swamp forests in particular play an important role in the global carbon cycle despite their relatively small extent. Deforestation and forest degradation are the second largest source of anthropogenic caused carbon emissions and and the highest rates are found in tropical regions. Therefore, deforestation and forest degradation should be prevented or minimized. In order to achieve this goal, it is of high importance to track land use changes as well as to estimate their status as carbon sink. This is useful for sustainable forest management, land use planning, carbon modeling, and supports to implement international initiatives like REDD+ (Reducing Emissions from Deforestation and Degradation), through which tropical countries are incentivized to protect their forests. However, tropical forests are difficult to reach and field measurements are only feasible with high effort. Therefore, the combination of field measurements and remote sensing seems most suitable for tropical forest monitoring purposes.

Radar sensors are considered having high potential for tropical forest monitoring due to their weather and daytime independence. In addition, SAR (synthetic aperture radar) backscatter and interferometric capabilities have been proved in many cases to be useful in forest monitoring and aboveground biomass estimation. However, short wavelengths like X-band SAR systems have a low penetration depth into the forest canopy. Therefore, it is assumed that such systems have limited potential for forest biomass estimation via backscatter information due to insufficient interaction with lower forest constituents. However, the interferometric capabilities of X-band SAR can overcome such limitations, whereas the low penetration depth can be considered an advantage. The interferometric height is assumed as canopy height as the signal mainly stems from the upper canopy due to the low penetration depth. The resulting canopy height over forest stands is

assumed to have a high correlation with aboveground biomass (AGB). Thus, the capabilities of a short wavelength interferometric SAR system for tropical forest monitoring and biomass estimation is analyzed in this study. The main objective is to assess the potential of single-pass bistatic interferometric information from TanDEM-X mission for land use mapping and biomass estimation.

TanDEM-X is a SAR mission consisting of two X-band SAR satellites flying in close formation and realizing a single-pass interferometric SAR mission in space. TanDEM-X delivers backscatter information from active/monostatic (transmitting and receiving) and passive/bistatic (transmitting only) sensor as well as interferometric data, such as interferometric coherence and surface height. The interferometric coherence is mainly governed by volume decorrelation, whereas temporal decorrelation is minimized due to simultaneous acquisition of single-pass interferometric data. The interferometric coherence and height can be used for land use monitoring as well as for estimation of biophysical parameters, like aboveground biomass of forests. Earth's land mass has been acquired between 2010 and 2014 multiple times in high resolution in order to create a global digital elevation model. Therefore, radar data from the TanDEM-X mission provide a unique opportunity to monitor large areas of tropical forests with the multi-temporal global coverage and in high resolution.

TanDEM-X data was used in this study to assess the information content delivered by a bistatic SAR acquisition for land cover information derivation and biomass estimation in a tropical peat swamp forest in Central Kalimantan, Indonesia. Backscatter coefficients of active and passive sensors including texture measures as well as interferometric coherence served for the classification of tropical peatland in order to distinguish basic land use categories suggested from IPCC (Intergovernmental Panel on Climate Change) and different forest types. Feature importance was assessed with a feature selection process in order to assess the added value of a bistatic SAR acquisition from TanDEM-X mission data compared to the monostatic case, available from all other spaceborne SAR missions in the past and at present. The resulting optimal feature sets, representing a monostatic and a bistatic SAR dataset, were used in a subsequent classification to assess the improvement of classification accuracies using the bistatic TanDEM-X features in order to separate land cover and forest type classes.

The feature selection and classification results obtained demonstrated that the interferometric coherence significantly increased the separability of thematic classes compared to a dataset of monostatic acquisitions. The interferometric coherence improved results in comparison to land use classifications without coherence about 10 % (75 % vs. 85 %). Especially the differentiation between forest classes and forest/non-forest profited from coherence due to the volume

decorrelation in forests and subsequent information about forest structure. In contrast, backscatter coefficients did not provide significant information content to separate forest classes. This analysis was described in the article "Importance of bistatic SAR features from TanDEM-X for forest mapping and monitoring", published in *Remote Sensing of Environment*.

In order to quantify the quality of aboveground biomass estimates from TanDEMX mission data, field analysis was conducted in the years 2013 and 2014 as a reference for forest biomass in the study area in Central Kalimantan. LiDAR (Light Detection and Ranging) data was available for the study area in addition to field measurements. LiDAR data was used as a reference for aboveground biomass estimation from TanDEM-X for larger areas compared to field measurements alone. The field measurements were correlated with canopy height models of LiDAR. This correlation calibrated a regression model used to up-scale the limited number of *in situ* measurements in this difficult accessible area in order to increase the number of observations. This regression model resulted in similar mean values of biomass for the area of interest. Thus, the LiDAR biomass estimation represented a reliable data source to correlate biomass and TanDEM-X features like backscatter and interferometric coherence. In addition, the potential of the globally available digital elevation model from the TanDEM-X mission, namely WorldDEM™, was investigated for aboveground biomass estimation in this tropical peat swamp forest in Central Kalimantan, Indonesia. Again, existing field measurements were correlated with different canopy height models. These canopy height models were derived from an intermediate TanDEM-X DEM (iDEM; as a precursor for WorldDEM™) and LiDAR measurements. These correlations resulted in regression models, which were used to transfer pointwise biomass estimations from field measurements to aerial estimations via remote sensing data.

The interferometric coherence was helpful in classifications, as mentioned above, as well as for the estimation of aboveground biomass. Volume decorrelation in forests increased with aboveground biomass. Therefore, it was shown that the interferometric coherence correlated with the aboveground biomass with a coefficient of determination (R^2) of about 0.5. This resulted in an error of 14 % (calculated as root mean square error (RMSE) with an independent validation dataset) within highly variable forest stands showing variations of biomass in the range of 183 t/ha to 495 t/ha. Degraded forest areas were clearly identified due to openings in the forest canopy and lower biomass compared to relatively undisturbed forest.

The canopy height models derived from TanDEM-X achieved accuracies of about 5 m compared to the LiDAR reference. Correlation of canopy height models, derived by subtracting interferometric height models from TanDEM-X with high accurate

terrain heights from LiDAR, and biomass achieved a R^2 of 0.68. This was an even higher correlation with biomass compared to coherence and resulted in cross-validated RMSE of 7.5 %. TanDEM-X heights correlated lower to the biomass without an external terrain height (R^2 = 0.2) resulting in higher RMSE (16 %).

High accurate terrain models are not available on global scale. Nevertheless, the results of this study suggest that the estimation of aboveground biomass exclusively based on WorldDEM™ can be used in areas where no accurate terrain model is available. Even though this will result in moderately lower accuracies, it can be applied globally in a consistent way. The analysis of biomass estimation with interferometric coherence and height from TanDEM-X is explained in "TanDEM-X data for aboveground biomass retrieval in a tropical peat swamp forest", published in *Remote Sensing of Environment*, and "WorldDEM™ data for canopy height and aboveground biomass retrieval in a tropical peat swamp forest", submitted to *ISPRS Journal of Photogrammetry & Remote Sensing*.

These results indicate that TanDEM-X can be considered as a valuable and consistent data source for forest monitoring in particular - but not only for tropical forests. Especially interferometric information seems suitable for land cover mapping and biomass estimation. TanDEM-X data is thus usable at least for stratification purposes in the context of REDD+ or forest degradation identification in order to assess the spatial distribution of forest types and aboveground biomass. Therefore, the global TanDEM-X database can serve as a reference for future deforestation and forest degradation assessment worldwide. The status quo of forests for the years 2010 to 2014 can be analyzed accurately with TanDEM-X and changes of this status can be assessed with existing or future SAR or optical remote sensing missions.

Danksagung

Table of contents

Table of contents

List of Figures

List of Tables

Abbreviations & symbols

AGB	Aboveground biomass
CoSSC	Co-registered Single-Look Slant Range Complex
DEM	Digital Elevation Model
DSM	Digital Surface Model
DTM	Digital Terrain Model
EEC	Enhanced Ellipsoid Corrected
ERS	European Remote Sensing Satellite
GEC	Geocoded Ellipsoid Corrected
GPS	Global Positioning System
HS	High Resolution SpotLight
ICESat	Ice, Cloud, and land Elevation Satellite
iDEM	intermediate DEM
InSAR	Interferometric synthetic aperture radar
IPCC	Intergovernmental Panel on Climate Change
GLAS	Geoscience Laser Altimetry System
LULUCF	Land Use, Land-Use Change and Forestry
LiDAR	Light Detection and Ranging
Modis	MODerate Resolution Imaging Spectroradiometer
MGD	Multi Look Ground Range Detected
MRP	Mega Rice Project
MRV	Measurement Reporting and Verification
PPP	Public-Private-Partnership
Radar	RAdio Detection And Ranging
REDD+	Reducing Emissions from Deforestation and Degradation
RCS	radar cross section
RVoG	Random Volume over Ground
SAR	Synthetic Aperture Radar
SC	ScanSAR
SL	SpotLight
SM	StripMap
SRTM	Shuttle Radar Topography Mission

SSC   Single Look Slant Range Complex

ST   Staring SpotLight

TanDEM-X   TerraSAR-X-Add-on for Digital Elevation Measurements

List of Tables

UN   United Nations

$B_\perp$ perpendicular baseline

B_k parallel baseline

B_h horizontal baseline B_v

vertical baseline *bef* biomass expansion

factor

bv   bole volume *c*speed of

light

dbh   diameter at breast height

h   tree height

p   *p*=1 if bistatic acquisition used *p*   *p*=2   if

monostatic acquisition used

R   range

vob   volume   over   bark   *wd*

        wood density

α   baseline orientation angle *β*

bistatic angle *λ*   wavelength *θ* look

angle

1 Introduction

TanDEM-X is a single-pass interferometer in space acquiring the whole Earth multiple times (Krieger et al. 2007). This makes TanDEM-X an unique dataset, resulting in plenty of application possibilities. The most obvious is the creation of a digital elevation model (DEM), which is also the main mission objective of TanDEM-X (Krieger et al. 2010, Krieger et al. 2007). The interferometric dataset, which is used to create the elevation model, as well as the elevation model itself are again of use for many applications. These applications can be found in topographic mapping, orthorecrification, radiometric correction, glaciology, hydrology and also ecology and vegetation analysis (Rosen et al. 2000, Bamler & Hartl 1998, Krieger et al. 2010). Such dataset could be also of high interest for the mapping and monitoring of tropical forests. These are usually not easy to access and high temperature, high moisture level together with high tree density hinder field measurements in tropical forests. Thus, *in situ* measurements can only be conducted with high effort resulting in small spatial coverage with regard to the huge extent and variability of tropical forests (Rosenqvist et al. 2003, Asner 2009).

Tropical forests are relevant due to their function as carbon sink and can also act as carbon emission source via deforestation and forest degradation (Werf et al. 2009, Page et al. 2002). Therefore, programs like REDD+ (Reducing Emissions from Deforestation and Degradation) are developed in order to incentivize tropical countries to protect their forests. However, the implementation of such a program needs effective monitoring systems. The combination of high accurate field measurements and remote sensing seems most promising for such a purpose (De Sy et al. 2012).

A global dataset like TanDEM-X has high potential for forest monitoring since the dataset is globally consistent. In addition, interferometric SAR (synthetic aperture radar) was already used in vegetation analysis (e.g. Solberg et al. 2010, Wegmuller & Werner 1995, Santoro et al. 2007, Kugler et al. 2014). The objective of this thesis is the analysis of TanDEM-X in the context of tropical forest mapping, monitoring and aboveground biomass estimation. It is expected that the methodology can be used for measurement, verification and reporting (MRV) systems in REDD+. Special emphasis is on a study area in Central Kalimantan. This study area consists of tropical peat swamp forest, which on the one hand functions as huge carbon store and on the other hand is highly endangered through deforestation, degradation and drainage (Page et al. 2002, Hooijer et al. 2010, Werf et al. 2009, Aldhous 2004). Therefore, the estimation and monitoring of biomass in such an area is of high *1 Introduction*

interest (Lawson et al. 2014).

The thesis on hand is structured as follows: TanDEM-X is a bistatic SAR formation consisting of two similar SAR satellites. Therefore, basics of radar remote sensing are explained in Chapter 2.1. Subsequently, bistatic SAR systems, their properties and utilization are illustrated (Chapter 2.2). A description of the main data source TanDEM-X follows (Chapter 2.3.2). Some fundamentals of REDD+ and the implementation via measurement, verification and reporting concepts with remote sensing are explained further (Chapter 2.4). The need for research is presented in Chapter 3: The significance of tropical peat swamp forests and thus the study area is discussed (Chapter 3.1). Subsequently, the necessity for research of using TanDEM-X in the context of tropical forest mapping, monitoring and biophysical parameter estimation is outlined guiding to the research questions of this thesis (Chapter 3.2).

The research questions are examined in the following chapters. These chapters comprise research published in three publications in scientific journals. Chapter 4 represents a publication in the journal *Remote Sensing of Environment* about the usage of TanDEM-X for land cover classifications. The usage of interferometric coherence of TanDEM-X for biomass estimation is analyzed in Chapter 5, which is also based on a publication in *Remote Sensing of Environment*. The derivation of a canopy height model and subsequently the estimation of aboveground biomass with interferometric height from TanDEM-X DEM with regard to the final global product WorldDEM™ is described in Chapter 6, which is based on a submitted publication in *ISPRS Journal of Photogrammetry & Remote Sensing*.

Finally, the findings of the papers are reflected and discussed in Chapter 7 and an outlook to further potential research is presented. Chapter 8 concludes the thesis.

2 Technical background & state of the art

2.1 Radar remote sensing

Radar sensors acquire data in the microwave domain of the electromagnetic spectrum with wavelengths between 1 mm and 1 m (Henderson & Lewis 1998). Figure 2.1 represents the electromagnetic spectrum, the corresponding remote sensing sensors and the atmospheric transmissibility. Penetration into media like vegetation or soil is possible with radar due to the long wavelength. Microwaves are barely influenced by atmospheric conditions and are able to penetrate through clouds depending on the wavelength. In addition, radars are active systems, which transmit and receive the electromagnetic wave making them independent of external sources of energy (Ulaby et al. 1981). Systems receiving only microwaves

are called passive microwave radiometers (Lillesand et al. 2008). The independence of illumination of the sun and the (almost) all-weather capability are advantages compared to optical sensors (Leckie 1998). Furthermore, the penetration into media is another advantage leading to possible information extraction from beneath the surface of media. This is appropriate especially for vegetation and soil analysis (Ulaby et al. 1981). Radars are also able to record the phase of the electromagnetic wave, which yields additional applications and advantages compared to optical systems. The phase information of coherent radar acquisitions are comparable, which is called interferometry. Topographic heights and surface motion can be estimated with this technique (Massonnet & Souyris 2008, Chapter 2.2).

Remote sensing radars where transmitter and receiver of the electromagnetic wave are spatially at the same position are called monostatic. Systems where transmitter and receiver are spatially separated are referred to as bistatic (Richards 2009, Chapter 2.2). Three major types of radar systems are differentiated in remote sensing, which are imaging radar, altimeter and scatterometer (Ulaby et al. 1981). Major part of the thesis is about TanDEM-X, which is an imaging radar. Therefore, in the following only the imaging radar is described.

The radar cross section (RCS) per unit area is of high importance for remote sensing with such systems. The radar cross section describes the backscattered signal of a target. The unit area is defined by the resolution cell. Different properties of the
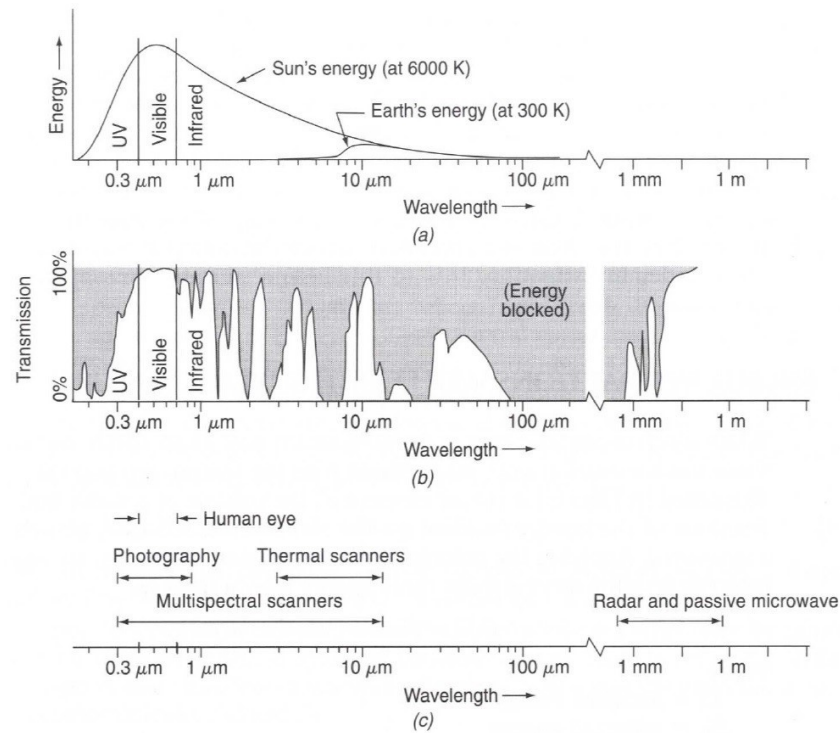
Fig. 2.1: Properties of energy sources (a), atmospheric transmissibility (b) & sensors
(c) (from Lillesand et al. 2008:11)

illuminated elements, like electric and geometric properties, as well as sensor
properties, like wavelength (frequency), polarization and incidence angle, have
influence on the backscatter and thus on radar cross section (Klausing & Holpp
2000). These properties are described in the next chapter.

2.1.1 Influences on radar backscatter & backscatter processes

The backscatter is influenced by many factors. These can be differentiated into
object and system properties (Lewis & Henderson 1998). Two major factors
influencing the properties of illuminated objects are the geometry and
electromagnetic properties of those objects. Geometric properties are determined
by the orientation to the sensor and the roughness. Generally, backscatter increases
if the objects tend towards the sensor (Raney 1998). The orientation of objects with
respect to the sensor is described by the local incidence angle, which is the angle
between the line of sight and a normal at the illuminated object (Fig. 2.2). Therefore,
the slope of the object and the position of the sensor with the resulting look angle
influence the local incidence angle. The look angle is defined by the line of sight and
a vertical to a reference height (Lewis & Henderson 1998, Fig. 2.2). The look angle
or the depression angle, which is complementary to the look angle, and the local
incidence angle are of high significance for the description of the acquisition
geometry.

Another geometric property is the roughness of the illuminated surface of the objects. The roughness is a description of height variability with respect to the
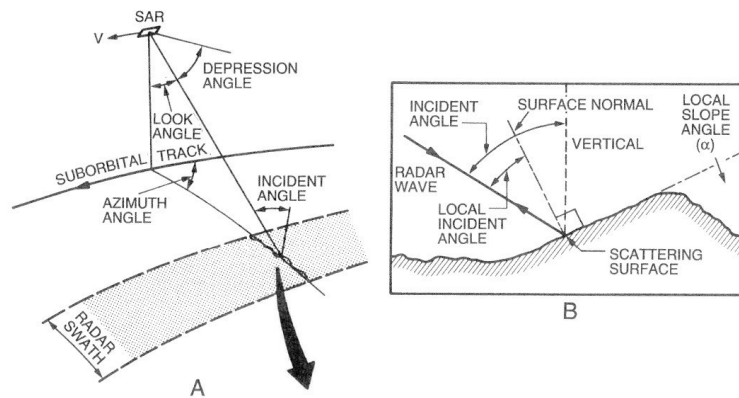
Fig. 2.2: Important angles of a SAR system (A) & illustrations of local incidence angle (B) (from Lewis & Henderson 1998:133)

wavelength (Raney 1998). The backscatter at rough objects can be separated into two components, on the one hand are scattering and on the other hand specular portion (Ulaby et al. 1981, Raney 1998). Increased roughness results in decreased specular portion. The signal is scattered away from the transmitter with the same exit angle as the incidence angle at specular surfaces. Side looking monostatic imaging radar does not receive any signal in this case. Therefore, the term backscatter is commonly used in radar remote sensing, because the radar measures the scattering back to the sensor and hence the scattering object is referred as scatterer (Raney 1998, Knott 1990).

The moisture content is similarly influencing the radar backscatter. The moisture content determines the complex dielectric constant, which is an electromagnetic property of objects. Increased moisture of an object results in higher dielectric constant and thus causes higher backscatter (Ulaby & Dobson 1989). Other electromagnetic properties are the permeability and electrical conductivity. However, the dielectric constant has the highest consequence on radar backscatter (Richards 2009).

The moisture and thus the dielectric constant have influence on the penetration depth. Increased moisture of an object results in decreased penetration (Lewis & Henderson 1998). However, the wavelength has also a major impact on the penetration. Long wavelengths penetrate deeper compared to short wavelengths. The penetration into a medium with many scatterers results in multiple reflections. This is called volume scattering and occurs mainly in vegetation and in sea ice (Raney 1998, Richards 2009). This kind of scattering is based on the dielectric heterogeneity of the medium (Ulaby et al. 1982). The spatial distribution of the dielectric differences is normally random. Therefore, the volume scattering is not

directed and thus the signal is scattered into every direction (Raney 1998, Ulaby et al. 1982). The intensity of backscatter at volume scattering depends on one hand on dielectric differences, their density and size with respect to the wavelength and on the other hand on the surface roughness and the average dielectric constant of the medium (Ulaby et al. 1982).

Besides direct backscattering mainly at rough objects (Fig. 2.3 left) or objects tending to the sensor (Fig. 2.3 right) and the volume scattering (Fig. 2.3 center) dihedral, trihedral or polyhedral scattering is possible. Dihedral scattering is also called double bounce and depends on the orientation to the sensor (Fig. 2.3 right). Double bounce is possible at artificial or natural objects. For instance, a specular surface and stem of a tree can create a double bounce. Trihedral and polyhedral scattering occurs mainly at artificial objects like ships or vehicles and in cities (Raney 1998).
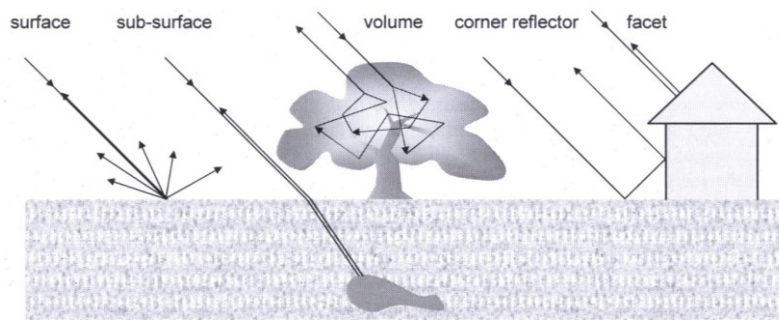
Fig. 2.3: Exemplary illustration of backscatter mechanisms (from Richards 2009:136)

Sensor properties have influence on backscatter as well. The look angle is one influencing sensor property as described above. Additional important sensor properties are the frequency and polarization. The radar frequency (f_c) defines the wavelength (λ) of the system ($\lambda = {}^{c}\!/\!{}_{f_c}$, where c is the velocity of light) (Massonnet & Souyris 2008). A specific wavelength is acquired in contrast to optical systems with bands of wavelengths (Henderson & Lewis 1998). The used frequencies are abbreviated with letters stemming from World War II (Table 2.1). Each frequency has individual properties and advantages for different applications (Skolnik 1990). Two additional important elements are sampling and pulse repetition frequency, which influence the resolution of the system (Massonnet & Souyris 2008, Chapter 2.1.2).

In addition, the polarization of the transmitting wave can be determined by the system. The receiver can also define the receiving polarization. The polarization is a description of the orientation of the electrical field vector, which influences the interaction between the electromagnetic wave and the object (Raney 1998).

Scattering processes alter the polarization of the electromagnetic wave (Raney 1998). A horizontal plane is used as reference for defining the polarization. Linear polarizations, which are mainly used in remote sensing, are separated into horizontal (H) and vertical (V) polarization. The transmitted polarization is in first place and received polarization in the second place when describing the system. Since transmitter and receiver are able to define their used polarization individually, four possibilities can result (HH, HV, VH, VV). Nevertheless, cross-polarizations HV and Tab. 2.1: Examples of used frequencies, wavelengths and abbreviations (after Lillesand et al. 2008)

Abbreviation	Wavelength λ (in cm)	Frequency f_c (in MHz)
Ku	1.67-2.4	18000-12500
X	2.4-3.75	12500-8000
C	3.75-7.5	8000-4000
S	7.5-15	4000-2000
L	15-30	2000-1000
P	30-100	1000-300

VH are identical after the reciprocal theorem (Klausing & Holpp 2000).

2.1.2 Imaging radar & resolution

The image representation of an object is based on the amplitude or intensity of its backscatter. The intensity is the square of amplitude (Lillesand et al. 2008). Resolution cells must be used in order to create an image representation. Spatial resolutions in direction of the movement of the sensor (along-track or azimuth) and orthogonal to that (across-track or range) are differentiated (Richards 2009).

Measurement of wave run time is possible using radar sensors due to their active nature. Objects can be separated via this measurement, if they have not the same distance to the sensor. Therefore, radars are side looking in order to avoid ambiguities (Massonnet & Souyris 2008). Imaging radar is a 3-dimensional representation due to the side looking effect. The representation along a linear plane towards the sensor is called slant range (Raney 1998). Radars transmit the electromagnetic wave in continuous pulses. Close neighboring objects superimpose each other and cannot be separated by the radar (Richards 2009). The resolution in range (r_R) is thus defined by the pulse length (τ_P):

$$r_R = \frac{c\tau_P}{2} = \frac{c}{B_C 2} \tag{2.1}$$

where 2 means the path of the wave to target and back, c the velocity of light and B_C the chirp bandwidth (Ulaby et al. 1982). The representation relative to a horizontal plane (ground range) is dependent on the look angle (Raney 1998):

$$r_R = \frac{c\tau_P}{2\sin\theta} = \frac{c}{B_C 2\sin\theta} \tag{2.2}$$

where θ describes the look angle (Ulaby et al. 1982). Some conclusions can be drawn from these equations. Firstly, a look angle of 0 ($\theta = 0$) results in no resolution. Therefore, imaging radar must acquire side looking. Secondly, no term for range is included in these equations resulting in independence of range for the resolution in across-track. However, the resolution is dependent on the look angle, whereas an increase of the look angle results in an increase of spatial resolution (Richards 2009). Furthermore, higher resolutions are only achievable by decreasing the pulse length. A substantial increase of the look angle is usually not possible. A decrease of the pulse length results in less signal energy and thus decreased probability to detect objects. Another possibility is the application of long pulses with linear oscillating and modulated frequency, which is called chirp (B_C; Klausing & Holpp 2000).
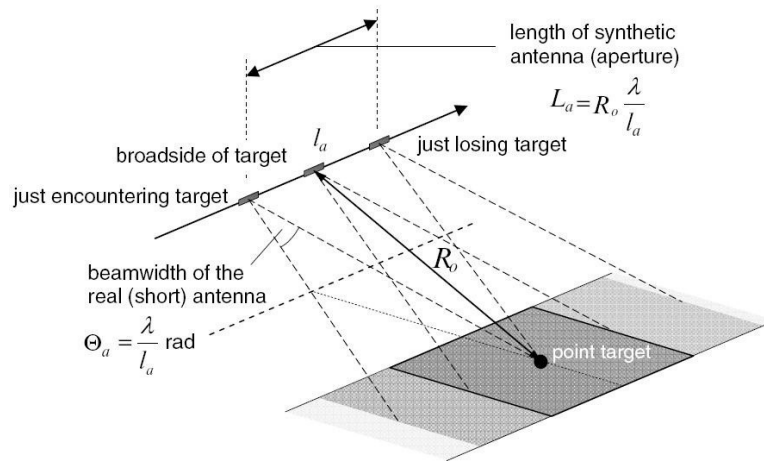
Fig. 2.4: Principle of SAR system (from Richards 2009:62)

The resolution in along-track is calculated from bandwidth in azimuth B_A and range to the target (R). The bandwidth in azimuth is defined by the ratio of wavelength (λ) and length of aperture (l_A) (Ulaby et al. 1981):

$$r_A = B_A R = \frac{\lambda R}{l_A} \tag{2.3}$$

The range distance can be calculated by the velocity of light and the time from transmitter to target or target to receiver ($R = c \cdot t$), which is similar in the monostatic case (Ulaby et al. 1982). Formula 2.3 emphasizes that the resolution depends on wavelength, aperture length and range. Therefore, such a system is not feasible for high flying altitudes of the sensor due to the large range. An increase in resolution is only possible by increasing the aperture size (Klausing & Holpp 2000). The development of SAR systems can overcome those limitations of a system with real aperture (RAR=real aperture radar or SLAR=side looking aperture radar). A long aperture is synthesized at SAR systems via forward movement of the sensor (Lewis & Henderson 1998). Signals are transmitted and backscatter is coherently stored during the movement. The resulting multiple single images are coherently processed and phase differences are corrected via knowledge about the relative position of points to the target (Cutrona 1990, Klausing & Holpp 2000). The final image is thus a combination out of multiple images, while synthesizing a long aperture (Raney 1998; Fig. 2.4). The length of the synthetic aperture depends on the illumination time of the target. The illumination time and thus the potential length of the aperture is directly proportional to the range to the target, whereby the resolution in azimuth at SAR is independent from the range (Ulaby et al. 1982, Klausing & Holpp 2000). The theoretical resolution of a SAR in azimuth is calculated by (Ulaby et al. 1981):

$$r_A = \frac{l_A}{2} \tag{2.4}$$

where l_A is the length of the real aperture. Formula 2.4 shows that an increased resolution is achievable by using smaller antennas. The pulse repetition frequency and velocity of the sensor platform determine the actual azimuth resolution (r_A). The Doppler frequency of space borne sensors is high and thus potentially results in ambiguities (Ulaby et al. 1982). Therefore, Massonnet & Souyris (2008) suggest transmitting a pulse every half length of the antenna. Furthermore, the width should not be too large in order to minimize ambiguities (Ulaby et al. 1982). The usage of a synthetic aperture requires system specification like coherent processing, a stable platform and movement compensation since a constant antenna along the flight direction is assumed in the processing (Cutrona 1990).

Pixel size and resolution is usually similar within passive optical systems. This is different for imaging radar. The pixel size depends on sampling of the signal and synthesis of the aperture. In contrast, the resolution depends only on the synthesis of aperture. An oversampling of 15 to 20 % is common resulting in a lower geometrical resolution compared to pixel size (Massonnet & Souyris 2008).

The final image is created via determining the coordinate of the resolution cell in azimuth using the Doppler frequency gradient. The coordinate in range is recorded via run time measurement of the signal (Raney 1998). It is obvious that this could result in image distortions. This is, for instance, the case if an object is higher compared to surroundings and hence closer to the sensor compared to its surroundings. Consequently, the run time is shorter and the object is represented closer to the sensor as the real position (Ulaby et al. 1982). The pixel may result out of multiple superimposed objects, which have a similar distance to the sensor. This phenomenon is known as layover, which occurs if the look angle is smaller than the slope of the object (Fig. 2.5, Raney 1998). A similar geometric distortion is foreshortening, where the distance of two points is represented smaller than it is in reality (Fig. 2.5). This is also caused by the run time measurement. In contrast, radar shadow occurs if an object is not visible for the radar and thus is not illuminated by the electromagnetic wave (Fig. 2.5, Ulaby et al. 1982). These distortions increase with steeper look angles (Fig. 2.5) as well as with strong relief (Lillesand et al. 2008).
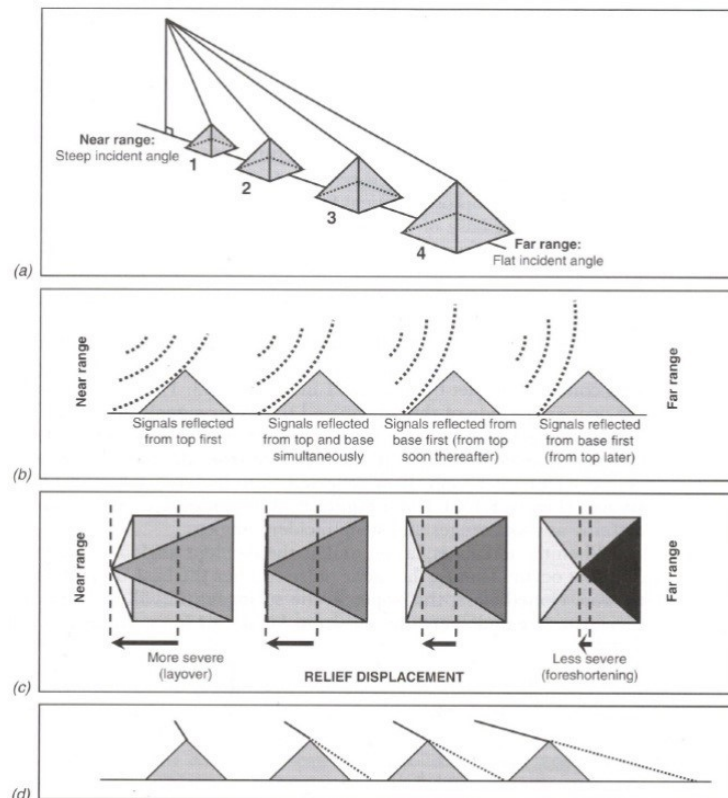
Fig. 2.5: Influences of topographic relief & geometric distortions in radar image
(from Lillesand et al. 2008:644)

2.1.3 Speckle

A resolution cell consists of multiple individual distributed scatterers. The received signal is the vector sum of all signals of the individual scatterers within a resolution

cell (Raney 1998, Klausing & Holpp 2000, Chitroub et al. 2002). Therefore, the radar signal is a complex sum, which can be described by phase and amplitude (Fig. 2.6). The phase is randomly and uniformly distributed between 0 and 2π (Raney 1998). The addition of scattering from individual scatterers results in phase displacement, which results in constructive or destructive noise depending on the type of displacement (Raney 1998, Klausing & Holpp 2000, Chitroub et al. 2002, Fig. 2.6). This noise, which is called speckle, leads to a radiometrically weaker or stronger signal (Massonnet & Souyris 2008). Surfaces with similar properties can have different backscatter due to the speckle resulting in a granular texture in the image (Durand et al. 1987). It is usually assumed that the speckle is a multiplicative and random noise. Therefore, the speckle is stronger in higher backscatter areas (Klausing & Holpp 2000). However, this assumption is simplified and in reality not appropriate (Raney 1998).

After Raney (1998) fully developed speckle occurs at targets fulfilling the following criteria: The resolution cell consists of a large amount of scatterers, no dominant scatterer exists in the resolution cell, the scatterers are statistically independent and the phase is uniformly distributed. An average of multiple pixels should be used in
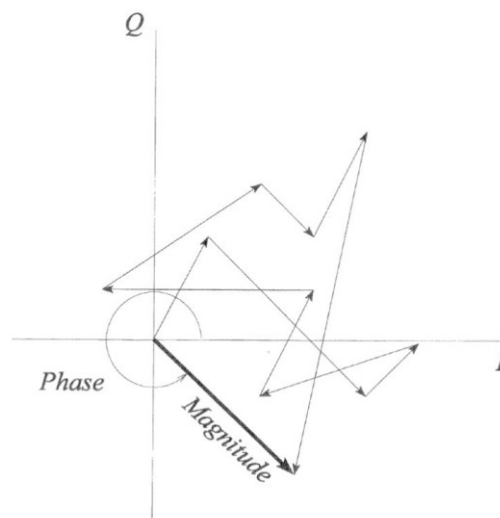
Fig. 2.6: Illustration of complex sum within a resolution cell (from Raney 1998:69)

order to estimate the radar cross section of a surface (Ulaby et al. 1982). The radar cross section is explained in more detail in Section 2.2.1.

Interpretations, classifications and segmentations are difficult because of the speckle, since similar land cover surfaces have fluctuations in their backscatter intensity and edges are difficult to detect (Huang & Liu 2007). Therefore, reduction of speckle is usually necessary (Ulaby et al. 1982). Different methods exist to reduce speckle. They can be separated into multi-looking and filtering approaches. The

incoherent addition of single sub-images reduces the speckle (= multi-looking), whereas the resolution decreases. The number of looks determines the number of additions (Massonnet & Souyris 2008, Raney 1998). In contrast, filters are applied locally on the pixel. Grey values are changed on the basis of neighboring pixels (Lillesand et al. 2008). Filters have a high noise suppression resulting in potential improvement of the subjective perception of the image. However, simple filters suppress also high grey values and anomalies, whereas loosing details and edges. Therefore, adaptive filters were developed, which suppress noise and preserve edges. Frost, Gamma-MAP and Lee filters are examples of adaptive speckle filters (Massonnet & Souyris 2008, Huang & Liu 2007). The choice of filter and/or number of looks should fit to the application and requires a good understanding of the object properties (Gupta & Gupta 2007).

2.2 Bistatic radar systems, properties & utilization

Bistatic radar systems are defined by a spatial separation of the transmitter and the receiver of the electromagnetic wave (Willis 1991). Definitions of bistatic systems are not commonly used in literature. For instance, quasi-monostatic, pseudo-monostatic and others are used for bistatic systems (Willis 1990). If transmitter and receiver are spatially separated, but are at the same place or within short distance compared to the distance to the target, it is called a monostatic system (Klausing & Holpp 2000, Willis 1991). Therefore, the distance of transmitter and receiver is important for some definitions (Willis 1991). The term bistatic will be used in the following if spatially separation is fulfilled without considering the distance. Figure 2.7 shows the principle of a bistatic system, whereas Figure 2.7 (a) represents a bistatic system with spatially separated transmitter and receiver and Figure 2.7 (b) a monostatic system.
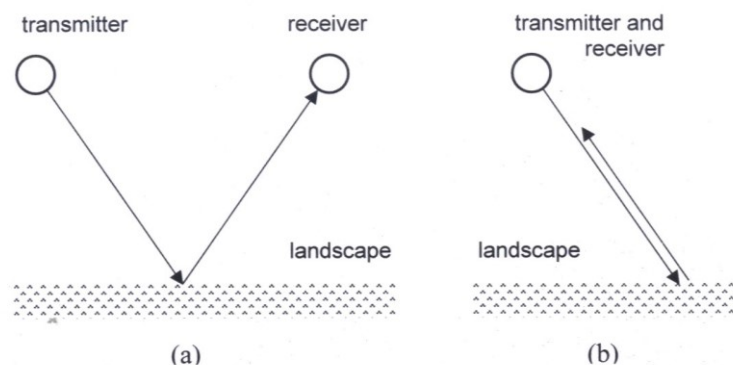
Fig. 2.7: Bistatic (a) & monostatic (b) system (from Richards 2009:54)

A transmitter can normally act as receiver as well and thus a combination of monostatic and bistatic system exists. Willis (1991) refers to that as hybrid radar. Hybrid radars have huge potential for applications. The transmitting and receiving

antenna is usually referred to as active or monostatic and the antenna which only receives is referred to as passive or bistatic (Krieger et al. 2007, Richards 2009). The radar formation of TanDEM-X is such a hybrid system (see Section 2.3, Krieger et al. 2007).

The spatial separation of the sensors is called baseline (L in Fig. 2.8). The angle between the target and both sensors is referred to as bistatic angle (β, Fig. 2.8). It is a monostatic system if baseline and β equal 0 (Willis 1990). Therefore, the bistatic angle (β) is unique for bistatic systems (Willis 1991). Furthermore, two different look angles exist, one for active and one for passive sensors (Fig. 2.8). The backscatter of a bistatic system differs compared to the monostatic case due to the spatial separation of transmitter and receiver (Kell 1965).
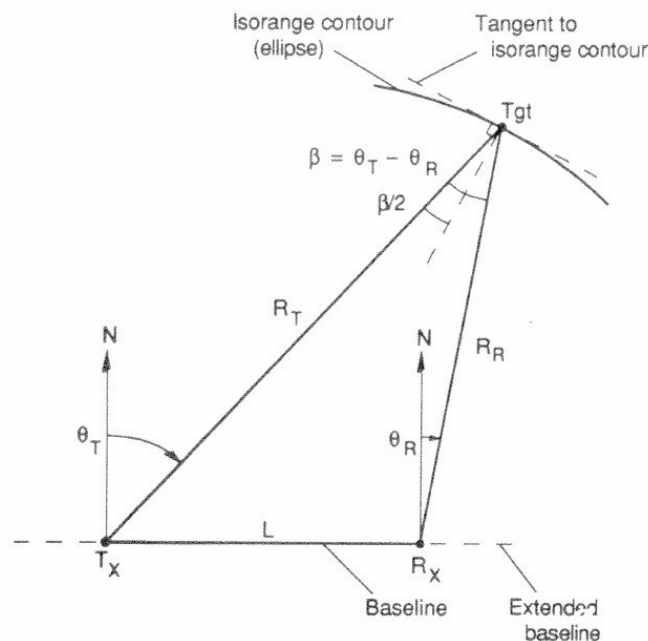
Fig. 2.8: Bistatic coordinate system (from Willis 1991:60)

2.2.1 Monostatic & bistatic radar cross section

The concept of radar cross section (RCS) was developed to define interactions of radar, target and the received signal. The target is described by size, shape and orientation. The radar cross section was introduced in order to characterize those properties (Knott 1990). The interactions can be divided in three steps. First, the signal is transmitted directional by the radar. Second, the radar signal hits and interacts with the target. Third, the receiver receives the signal (Massonnet & Souyris 2008). Formula 2.5 describes the receiving signal at sensor (P_r, Ulaby et al. 1982):

$$P_t G_t A_r \sigma$$

$$P_\mathrm{r} = (4\underline{\qquad\qquad}\pi)2R_\mathrm{t}R_\mathrm{r} \qquad\qquad (2.5)$$

The indexes *t* and *r* mean transmit and receive. *R* is the range from transmitter to target or target to receiver. P_t means the density of electromagnetic energy, which was transmitted with gain G_t. σ means cross section in square meter (Skolnik 1990). This cross section is the area of a metal sphere, which would result in the same backscatter as the actual target (Knott 1990). The loss of energy via spreading is defined as $(4\pi)^2 R_\mathrm{t} R_\mathrm{r}$ (Ulaby et al. 1982). The scattered energy to the sensor in square meter is calculated by P_t, G_t and σ. The actual received energy is described by the effective aperture A_r (Skolnik 1990). R_t and R_r, A_t and A_t as well as G_t and G_r are equal in the monostatic case. Therefore, formula 2.5 is valid for the bistatic case. The effective aperture is defined by the wavelength (λ) and gain (G), thus formula 2.5 can be formulated for the monostatic case:

$$\qquad\qquad (2.6)$$

This formula is valid for point scatterers, whereas mainly areas are observed in remote sensing (Ulaby et al. 1982). Thus, most important in radar remote sensing is the RCS per unit area. This is calculated by the differential coefficient (▮▮▮▮), which is simplified by substituting the unit area *A* with the resolution cell (Klausing & Holpp 2000). The formula for area targets is:

$$\qquad\qquad (2.7)$$

Two conditions must be fulfilled in order to use this model. The unit area must consist of multiple scatterers and a large amount of scatterers must exist in the whole observed area (Ulaby et al. 1982). These conditions are usually fulfilled in natural areas. In contrast, in urban areas or in acquisitions with high resolution the first condition may fail since often one scatterer dominates resulting in a single scatterer in the unit area (Bamler & Hartl 1998).

The bistatic RCS is more complex compared to monostatic RCS, because multiple look angles (σ_t and σ_r) as well as the bistatic angle (β) influence the backscatter (Richards 2009, Villard & Borderies 2015). Normally, the bistatic cross section is different and often smaller compared to the monostatic one (Willis 1991). Kell (1965) suggest three major sources of differences between bistatic and monostatic RCS:

- Difference in relative phase of the individual scatterer

- Difference in backscatter of scatterers

- Difference in existence of scatterers (appearance or disappearance)

The first source is similar to fluctuations in a monostatic system when the look angle changes. However, the difference in bistatic systems is caused by the bistatic angle. The second source is based on reduced backscattered energy due to separation of transmitter and receiver (Willis 1990). The third source is caused by additional shadow or appearances of new targets due to the different look angles (Willis 1990, Richards 2009). However, a comprehensive analysis of bistatic radar cross sections does not exist (Krieger & Moreira 2006).

2.2.2 Utilization of a bistatic SAR system

Nowadays, most of the radar sensors are monostatic. Bistatic systems must have substantial advantages in order to justify the increased costs, reduced extent and higher complexity than monostatic systems (Willis 1991). However, the first developments in radar were mainly based on bistatic radars. Most of the first radar experiments were bistatic and focused on target recognition. The developments stopped after the World War II, but were continued again in the 1950s for military purposes (Willis 1990). Willis (1990) and Willis (1991) provide more historic information on bistatic radar.

As mentioned above, bistatic systems have some drawbacks. Usually, the common imaged extent of monostatic and bistatic sensor is used. Therefore, the extent is at best the same as in monostatic case, but it is mostly smaller (Willis 1991). However, bistatic systems have multiple advantages. Some advantages are of special interest for military purposes. For instance, the safety of the systems can be improved by placing the transmitter out of reach for enemies and the detection of the position of a receiver is challenging (Walterscheid et al. 2004). In addition, the difference of look angles can be used to increase the RCS for some targets in order to detect better those that are undetectable. E.g. specular reflecting targets are not visible for a monostatic system but may be detected by bistatic systems due to the different look angle (Willis 1991). Generally, a combination of monostatic and bistatic systems delivers more information since they observe objects out of different angles (Krieger & Moreira 2006). However, this cannot be used only for military purposes. Bistatic systems may serve for an improved feature selection and classification. On one hand, objects may be detected that are not visible for monostatic only. On the other hand, dihedral and trihedral backscatter is reduced, which is especially the case in urban areas (Villard & Borderies 2015, Walterscheid et al. 2006). Therefore, the grey value range of bistatic SAR amplitude can be smaller compared to monostatic acquisition (Richards 2009), resulting in a more homogeneous image

(Walterscheid et al. 2006). Dubois-Fernandez et al. (2006) reported such advantages in airborne experiments in urban areas as well as in agricultural areas even with a very small bistatic angle of 0.1°. The biggest advantage of hybrid systems (combination of monostatic and bistatic) is the single-pass interferometry (Krieger & Moreira 2006).

2.2.3 SAR interferometry

The usage of phase information from SAR is, according to Hanssen (2001), the main idea of interferometry and for Massonnet & Souyris (2008) it is an unique feature compared to other sensors. Interferometry can deliver information about topography and surface movement making interferometry a key application for radar remote sensing (Bamler & Hartl 1998). SAR interferometry (InSAR) expands the two dimensional imaging of SAR to a third dimension (Rosen et al. 2000). Operational application of interferometry started in early 1990s and plays an important role in remote sensing (Krieger et al. 2010). Interferometry means the comparison of phase information from two or more SAR acquisitions in order to retrieve information (Bamler & Hartl 1998). Radar cannot separate targets having the same distance to the sensor (Chapter 2.1.2). However, two sensors with (slightly) different positions and comparable phases can result in the separation of those targets.

The main principle of interferometry is the comparison of the phases of two complex SAR images (Bamler & Hartl 1998). A resolution cell consists of multiple scatterers with different distance to the sensor. Therefore, the phase can be assumed as random. The phase information is only useful if compared to another (Massonnet & Souyris 2008). The images must be acquired either from another position and/or another time. The distance between the acquisitions is defined as baseline. The spatial separation (spatial baseline) defines the geometry of the acquisitions, whereas the separation in time is called temporal baseline (Hanssen 2001). The comparison of the phases shows differences in run time of the signal between the acquisitions, which is named interferogram. These differences can be measured in the order of a fraction of the wavelength (Madsen & Zebker 1998).

Two different kinds of interferometry exist, which are differentiated in acrosstrack and along-track interferometry. An acquisition at different positions with a spatial separation across the flight direction is across-track interferometry (Klausing & Holpp 2000). Both sensors should acquire the same area from different position resulting in different look angles. In this case, two sensors with spatial separation but simultaneous acquisition are used (Bamler & Hartl 1998). This configuration is called single-pass interferometry (Klausing & Holpp 2000). Hybrid

radar (see Chapter 2.2) enables such a configuration. Nevertheless, the same or a similar sensor can be used which overflies the area of interest at another time. This means at least two overflights are necessary, which is called repeat-pass interferometry (Bamler & Hartl 1998). The phase differences reflect differences in run time of the signal, which can be attributed to topography resulting from a function of look angle and spatial baseline (Rosen et al. 2000, Fig. 2.9).
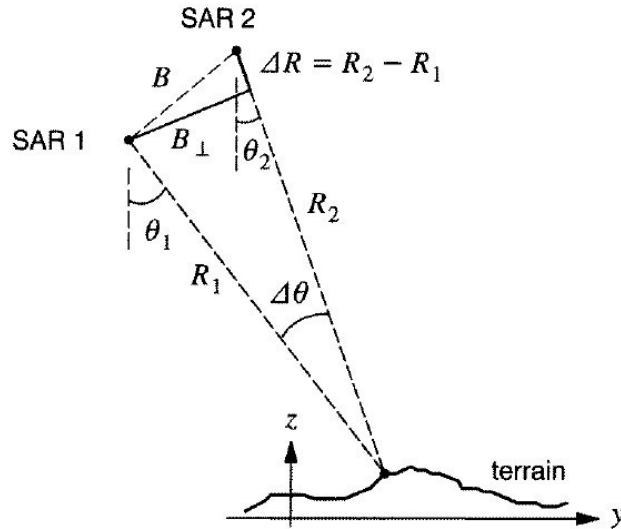
Fig. 2.9: Across-track interferometry for topographic derivation (from Bamler & Hartl 1998:R12)

The interferogram is created by precise co-registration of the complex images and their multiplication of one image with the complex conjugate of the second image (Madsen & Zebker 1998, Bamler & Hartl 1998):

$$\blacksquare \qquad (2.8)$$

where u_1 means complex image 1 and $\blacksquare$ means complex conjugate of complex image 2. This results in the interferomteric phase (φ), representing the phase difference of image 1 (φ_1) and image 2 (φ_2):

$$\varphi = \varphi_1 - \varphi_2 \qquad (2.9)$$

The equality of both phases is eliminated and phase differences are preserved (Rosen et al. 2000). A phase cycle in interferogram of 0 to 2π is a fringe (Hanssen 2001). The phase difference $\Delta\varphi$ depends on differences in distance ΔR:

$$\blacksquare \qquad (2.10)$$

p equals 1 if one transmitter and two receivers are used or p equals 2 if two transmitters and two receivers are used (Madsen & Zebker 1998, Fig. 2.10).
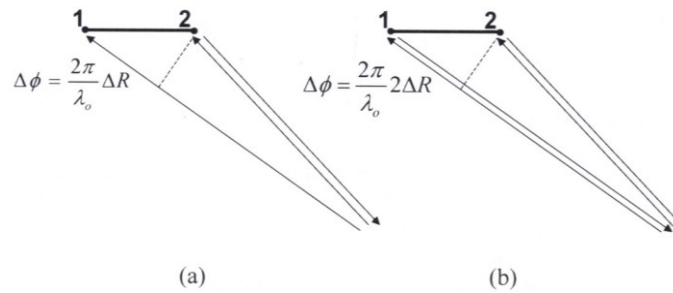
Fig. 2.10: Distances of the signal for a shared (a) & separated (b) transmitting antenna (from Richards 2009:191)

The term ΔR is a function of the acquisition geometry. Horizontal, vertical, parallel, effective and perpendicular baselines describe the geometry (Hanssen 2001, Fig. 2.11). Another important parameter is the baseline orientation angle α (Rosen et al. 2000). The sensors create a right angle triangle, whereas the baseline is the hypotenuse and the vertical and horizontal baseline are the cathetus. The line of sight and a right angle define the parallel and perpendicular baseline (Hanssen 2001). In case of one transmitter and two receivers the perpendicular baseline is double of effective baseline, which is the effective distance between both sensors (Hanssen 2001). In other cases, the perpendicular baseline equals the effective baseline (Hanssen 2001).

The interferometric phase is the modulus of the absolute phase since the phase of complex numbers are calculated by the arc tangent (Klausing & Holpp 2000). This means that every distance difference (ΔR) in the order of half wavelength results in repetition of phase difference (Cloude 2009). Nevertheless, the phase differences can be multiple of the wavelength and thus greater than 2π (Rosen et al. 2000). A phase unwrapping is necessary in order to transform the relative wrapped phase consisting of the multiple phase cycle to absolute phase.
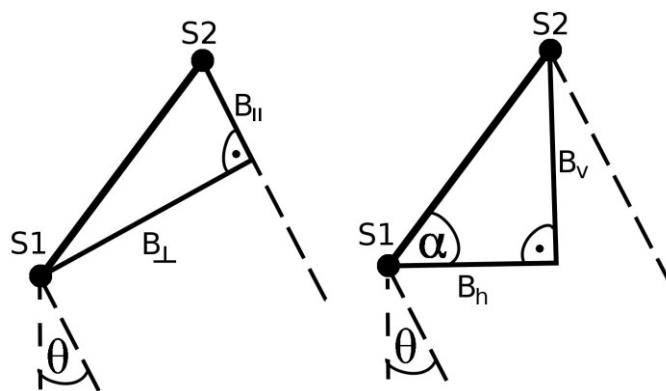
Fig. 2.11: Baselines & baseline orientation angle of SAR interferometry (after Hanssen 2001:115)

The phase difference finally consists of an unwrapped phase and a reference phase. The reference phase is visible in high frequency of phase changes (fringes) in range direction in the interferogram. Therefore, the reference phase has to be subtracted (Cloude 2009). These fringes are caused by the side looking acquisition geometry resulting in distance differences in range direction (Klausing & Holpp 2000). Distance differences to a reference height and both sensors must be converted in phase differences in order to eliminate the reference phase. Finally, the reference is subtracted from the measured interferometric phase (Hanssen 2001). The height of the reference phase compared to a reference height is assumed to be 0 and thus the reference phase is named flat earth phase (Cloude 2009) and the process of subtraction is named flattening (Rosen et al. 2000). The flat earth phase (φ_{fe}) is calculated as follows:

$$\blacksquare \tag{2.11}$$

whereby the measured interferometric phase is defined:

$$\blacksquare, \tag{2.12}$$

where λ means the wavelength, B the baseline, α the baseline orientation angle, D_p the surface movement, H_p the topographic component, θ the look angle of transmitter and R the range from transmitter to scatterer (Hanssen 2001). The removal of the flat earth phase is mostly the first step in interferometric processing and is achieved by the multiplication of complex images (Cloude 2009):

$$\blacksquare \tag{2.13}$$

where again u_1 means complex image 1 and $\blacksquare$ means complex conjugate of complex image 2.

Formula 2.12 shows that the interferometric phase is based on the look angle (θ), the baseline (B) and the baseline orientation angle (α). Some calculations, e.g. after Madsen et al. (1993) and Madsen & Zebker (1998), are necessary in order to retrieve the topographic height (h) above the reference height (H) and exact position in range (y):

$$\blacksquare \tag{2.14}$$

$$h = H - R\cos\theta \tag{2.15}$$

$$y = R\sin\theta \tag{2.16}$$

If the acquisitions differ in time but are taken from the same position, the sensors are separated spatially in flight direction. This is called along-track interferometry (Klausing & Holpp 2000). This formation is applicable for change detection and surface movement since the phase difference is mainly based on changes between the acquisition dates. The sensors should have similar orbits in order to minimize the topographic effect in the phase difference, which is mostly not possible (Richards 2009). Formula 2.12 shows that phase differences are mainly based on surface movement if the topographic component is minimized. The topographic component can be eliminated by using differential interferometry, where a digital elevation model is used to eliminate the topographic effect (Rosen et al. 2000).

The interferometric phase of along-track interferometry consists of the same components as across-track interferometry. Therefore, topographic height retrieval is also possible with along-track InSAR. However, the along-track interferometry has major drawbacks in topographic height retrieval depending on the size of the spatial and temporal baseline (Madsen & Zebker 1998).

2.2.4 Conditions for interferometry & description of performance

It has been explained in chapter 2.1 that radar is (almost) independent from atmospheric influences due to the long wavelengths. This is not completely true for radar interferometry. The phase is sensitive to changes (e.g. changes in acquisition conditions), which result in phase differences causing errors in retrieval of topographic height or surface movement (Massonnet & Souyris 2008). Interferometry is only possible with coherent images and thus the coherence is a descriptor of the quality of the interferogram (Bamler & Hartl 1998). The coherence enables the separation between useful and useless image parts. It is the modulus of the complex interferogram and defined between 0 and 1 (Massonnet & Souyris 2008, Bamler & Hartl 1998):

$$\blacksquare \tag{2.17}$$

E means expectation value, u_i denotes complex image i and vertical lines are for magnitude of complex data. The expectation value is difficult to estimate. Therefore, it is replaced by mean value of neighboring pixels. This is valid due to the assumption of ergodicity for coherence (Hanssen 2001). It is assumed that neighboring pixels have similar mean value for their phase and thus the phase is not random resulting in high coherence (Massonnet & Souyris 2008). The complex cross-correlation is then calculated as follows:

(2.18)

where u_i denotes complex image i, the brackets mean ensemble average and vertical lines are for magnitude of complex data (Rosen et al. 2000). Low coherence values mean that the signal is decorrelated and no extraction of interferometric information is possible. At $|\gamma| = 0$ there does not exist any interferometric phase information (Bamler & Hartl 1998). Decorrelation is caused by different factors, which are related to the system or the scatterers. However, definitions of decorrelation are not distinct. Geometric decorrelation, Doppler centroid decorrelation, thermal noise, processing, temporal decorrelation and volume decorrelation as well as atmospheric decorrelation are such factors (Hanssen 2001). Atmospheric decorrelation is not a decorrelation term for Hanssen (2001), but should be mentioned here. Generally, every factor which changes the signal results in decorrelation (Richards 2009). In addition, it should be mentioned that single-pass interferometers like TanDEM-X have the significant advantage of simultaneous acquisition and thus there does not exist any decorrelation by the atmosphere since it is similar for both images (Bamler & Hartl 1998, Krieger et al. 2007). The decorrelation is the product of all decorrelation factors:

$$\gamma_{Total} = \gamma_{Geom} \cdot \gamma_{Doppler} \cdot \gamma_{SNR} \cdot \gamma_{Proc} \cdot \gamma_{Temp} \cdot \gamma_{Vol} \cdot \gamma_{Atmospheric} \qquad (2.19)$$

The difference of the look angles results in geometric decorrelation (γ_{Geom}) causing a spectral shift (Hanssen 2001). This decorrelation can be described by the critical baseline, which calculates the maximal spectral shift for interferometric exploitation (Bamler & Hartl 1998):

(2.20)

where λ represents the wavelength, B the system bandwidth, R the range, θ the look angle of transmitter and α the slope of the area. No interferometry is possible if the spectral shift is too high and thus the images are completely decorrelated. Therefore, the effective baseline should not exceed the critical baseline otherwise a phase difference of more than 2π exists and thus the signal is completely decorrelated (Richards 2009, Bamler & Hartl 1998). The geometric decorrelation is reducable by applying bandpass filters (Rosen et al. 2000). The filter is applied before the interferogram calculation and reduces the spectral shift. Similar to geometric decorrelation is the Doppler centroid decorrelation ($\gamma_{Doppler}$). This decorrelation is in azimuth and stems from different Doppler centroid frequencies (Hanssen 2001).

Noise concerns the individual SAR images and thus causes also decorrelation in the interferogram (γ_{SNR}), depending on the sensor and the observed area (Rosen et al. 2000). Decorrelation via processing (γ_{Proc}) means, on the one hand, imprecise co-registration and, on the other hand, errors via interpolation (Hanssen 2001). Coregistration means the fitting of position of the images, whereas corresponding pixels are overlaying. This should be conducted in sub-pixel accuracy. In addition, pixels must be resampled in order to create pixels of the same size for the images, which means an interpolation of pixels (Hanssen 2001).

The γ_{Geom}, γ_{Doppler}, γ_{SNR}, and γ_{Proc} are decorrelation terms concerning the system and its processing. Two other important terms are the temporal and volume decorrelation. Temporal decorrelation occurs if the scattering properties of the objects change between the acquisitions and in this way changes also the phase. Temporal decorrelation is caused by movement of objects or/and change of dielectric properties (Wegmuller & Werner 1995). This decorrelation is observable for some surfaces like water bodies already after a fraction of seconds. Temporal decorrelation can also occur after a short amount of time in vegetation, whereas movement of leaves, twigs and branches through wind can cause changes of scattering properties resulting in temporal decorrelation (Bamler & Hartl 1998).

Another decorrelation factor occurring mostly in vegetation is the volume decorrelation. This decorrelation occurs in all volume scattering processes, where the backscatter is random (Ulaby et al. 1982). The resolution cell consists of multiple vertical layered scatterers due to the penetration into the volume, which contribute to the backscatter and are projected into the resolution cell (Krieger et al. 2010, Rosen et al. 2000). The projection of the vertical layered scatterers may be different for two images due to the randomness of the volume backscatter causing the volume decorrelation (Rosen et al. 2000). However, this can also include information about the vertical structure (Krieger et al. 2010, Rosen et al. 2000). Figure 2.12 shows the principle of volume decorrelation. The resolution cell in range ($\Delta\rho$) is projected and the size of the projected area (in grey) is larger in vegetation compared to bare soil.

Therefore, the coherence contains information about the objects due to their temporal and volume decorrelation, whereby Massonnet & Souyris (2008) refer to information about lifetime through temporal decorrelation and volume properties
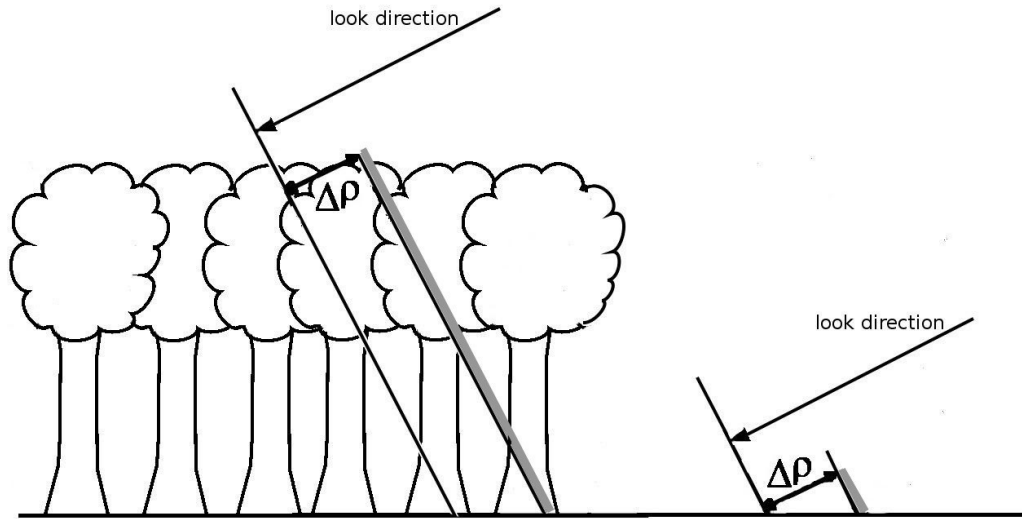
Fig. 2.12: Projection of resolution cell in range at volume scattering (left) & bare soil (right) (after Rosen et al. 2000:351)

through volume decorrelation. Thus, the coherence can be used in classifications or biophysical parameter retrieval adding additional or more information to the backscatter amplitude (e.g. Wegmuller & Werner 1995).

Temporal decorrelation emphasizes that the usage of repeat-pass interferometry may be inappropriate. TanDEM-X is a single-pass interferometer minimizing the temporal and atmospheric decorrelation due to simultaneous acquisition (Krieger et al. 2007). The coherence of a single-pass interferometer is generally higher compared to repeat-pass constellations. This suggests that single-pass interferometers are better suited for topographic height retrieval resulting in better phase information and finally less height errors (Bamler & Hartl 1998).

Different concepts exist in order to describe the height sensitivity of an interferometer. The effective baseline is the most important factor, whereas the sensitivity increases with increasing baseline (Rosen et al. 2000). Two formulas express the height sensitivity:

$$\rule{3cm}{1cm}$$

(2.21)

Bamler & Hartl (1998) suggest using the height of ambiguity (H_{oa}). This expresses the height, which results in a phase difference of 2π:

$$\rule{3cm}{1cm}$$

(2.22)

where λ means the wavelength, $B_\perp$ the perpendicular baseline, θ the look angle of transmitter, R the range from transmitter to scatterer and p is 1 if bistatic and 2 if monostatic acquisition is used.

2.3 TanDEM-X mission

The main objective of TanDEM-X mission is the creation of a global digital elevation model with a vertical relative accuracy of 2 m and a vertical absolute accuracy of 4 m (Krieger et al. 2007, Airbus Defence and Space 2014). Single-pass InSAR is used to accomplish this mission. An almost perfect twin of the TerraSAR-X satellite named TanDEM-X was built and both are flying in close formation. Therefore, the formation TanDEM-X is the first single-pass interferometer in space with two satellites (Krieger et al. 2010).

A comparable mission was SRTM (shuttle radar topography mission), where a space shuttle with a mast was used to create an interferometer. Main objective of this mission was to create a digital elevation model with C-band interferometry between 60° northern latitudes and 56° southern latitudes (Rosen et al. 2000). Here, the additional X-band antenna was used also to create elevation models and achieved higher accuracies than C-band. However, the X-band elevation models had a limited coverage (Rosen et al. 2000). Another important interferometric space mission was Tandem mission of ERS (European Remote Sensing Satellite). ERS-1 and ERS-2 flew with a temporal baseline of one day. Temporal decorrelation was reduced compared to other missions with larger temporal baselines resulting in higher coherences (Zhou et al. 2009). Nevertheless, areas with high vegetation cover still showed high temporal decorrelation after one day. Thus, it was recommended to use single-pass interferometers for digital elevation model creation (Rosen et al. 2000).

2.3.1 TerraSAR-X

The satellite TerraSAR-X was launched on June 06, 2007 from Baikonur. Since then it acquires data with a carrier frequency of 9.65 GHz resulting in a wavelength of about 3 cm (Pitz & Miller 2010). TerraSAR-X is the continuation of German X-band radar technology. TerraSAR-X and TanDEM-X are part of a public private partnership (PPP) between Airbus DS GmbH (former EADS Astrium GmbH) and the German Aerospace Center (DLR) (Werninghaus & Buckreuss 2010).

TerraSAR-X is able to transmit and receive in horizontal and vertical polarization. Single polarization and dual polarization modes are operational. In total, twelve different polarizations are combinable, whereas nine of them include no additional information and thus three combinations for dual-polarization are offered as product (HH/VV, HH/HV and VV/VH) (Fritz & Eineder 2013). For Pitz & Miller (2010) the most significant feature of TerraSAR-X is the phased array aperture enabling different acquisition modes. The antenna has a size of 4.8 m x 0.7 m

(Krieger et al. 2007). The spatial resolution and extent varies within the different modes. The use of single- or dual-polarization affects also the resolution and extent. The acquisition modes and use of polarization are as follows:

Tab. 2.2: Properties of different single-polarization acquisition modes of TerraSARX (after Fritz & Eineder 2013:15ff.)

Mode	Width (km)	Length (km)	Nominal L1B Resolution in azimuth (in product) (m)	Resolution in range (m)	Incidence angle at full performance
SM	30	50	3.3	1.7 – 3.49	20° – 45°
HS	10	5	1.1	1.48 – 3.49	20° – 55°
ST	7.5	2.5	0.24	0.85 – 1.77	20° – 45°
SL	10	10	1.7	1.48 – 3.49	20° – 55°
SC	100	150	18.5	1.7 – 3.49	20° – 45°

- StripMap (SM) (single- or dual-polarization)

- High Resolution SpotLight (HS) (single- or dual-polarization)

- Staring SpotLight (ST) (single-polarization)

- SpotLight (SL) (single- or dual-polarization)

- ScanSAR (SC) (single-polarization) (Fritz & Eineder 2013)

The modes are defined by the configuration of the phased array antenna. The antenna is fixed orthogonal to the flight direction at StripMap mode (Klausing & Holpp 2000). Higher resolutions in azimuth are achieved by longer illumination time (Massonnet & Souyris 2008, see Section 2.1.2). The antenna is squinted forward and backward in SpotLight modes in order to increase the illumination time increasing the synthetic aperture. This results in higher resolution in azimuth (Table 2.2, Raney 1998, Klausing & Holpp 2000). The phased array antenna enables such squinting (Klausing & Holpp 2000). The antenna is panned orthogonal to the flight direction in ScanSAR mode (Klausing & Holpp 2000). Sub-strips are acquired, which are combined to a single big strip resulting in large overall swath width (Table 2.2, Raney 1998). However, each sub-strip is acquired with limited proportion of Doppler bandwidth resulting in lower resolution in azimuth (Massonnet & Souyris

2008). The extent in azimuth direction is extendable to 1,500 km for StripMap and ScanSAR mode (Pitz & Miller 2010). The properties, acquisition modes, etc. of TerraSAR-X are also applicable for TanDEM-X.

StripMap mode is used in this study in order to trade-off resolution and extent. In addition, this mode is also used for the creation of the global digital elevation model and thus worldwide available (see Section 2.3.2). Therefore, results of this study can be transferred globally or to any place on earth. The delivery of the data is in the following product types:

- Single Look Slant Range Complex (SSC)

- Multi Look Ground Range Detected (MGD)

- Geocoded Ellipsoid Corrected (GEC)

- Enhanced Ellipsoid Corrected (EEC) (Fritz & Eineder 2013)

The phase information is the major prerequisite for interferometry. Only SSC data can be used for interferometry since this is the only mode containing complex data and thus phase information (Fritz & Eineder 2013). TanDEM-X mission data is subject to additional processing steps. Both sensors, TerraSAR-X and TanDEM-X, received data simultaneously resulting in an image (SSC) for each sensor. These pairs are co-registered and resampled. Furthermore, common band filtering and Doppler centroid filtering is applied resulting in co-registered single-look slant range complex data (CoSSC, Fritz 2012).

2.3.2 TanDEM-X

The TanDEM-X satellite is a reproduction of TerraSAR-X with minor differences (Krieger et al. 2007). It was launched on June 21, 2010 and completes the TanDEM-X formation. The differences concern mainly the TanDEM-X mission. Therefore, TanDEM-X has an additional cold gas impulsion in order to allow frequent adjustments for the formation flight. An S-band receiver was added for intersatellite communication. However, TerraSAR-X was already built for the mission and thus has horn antennas for synchronization, dual-frequency GPS (global positioning system) for exact orbit positioning and high phase stability (Krieger et al. 2010).

Different interferometric modes are enabled by the TanDEM-X formation, which are bistatic, alternating bistatic and pursuit monostatic (Fig. 2.13). The global digital elevation model is created in the bistatic mode. TanDEM-X or TerraSAR-X is transmitter and both receive synchronously in this mode (center of Fig. 2.13, Krieger et al. 2007). Therefore, TanDEM-X is a fully active system, because both sensors are

able to transmit and receive. Such a system is more flexible compared to semi-active systems, where only one transmitter and multiple receivers are used (Krieger & Moreira 2006). The interferometric modes are combined with the acquisition modes (see Chapter 2.3.1) and thus the global DEM is acquired in bistatic StripMap. Temporal decorrelation and atmospheric effects are minimized due to the simultaneous reception, which results in highest accuracy for topographic height estimation (Krieger et al. 2007).

Different prerequisites must be fulfilled in order to use that mode for interferometry. The Doppler spectra must overlap sufficiently in order to compare the phases.
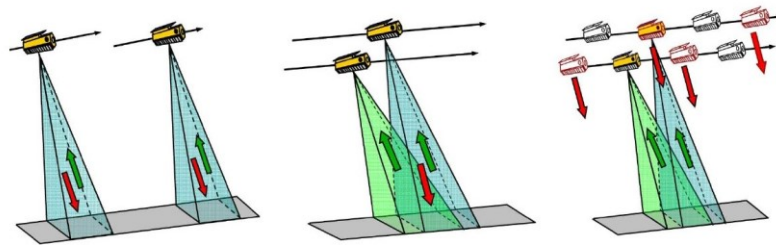
Fig. 2.13: Interferometric modes of TanDEM-X (from Krieger et al. 2007:3318)

The decorrelation by changes in Doppler centroid frequency ($\gamma_{Doppler}$) is described in Chapter 2.2.4. The Doppler spectra is linearly related to the baseline in flight direction (along-track) and consequently the along-track baseline is limited to a maximum of one kilometer for TanDEM-X (Krieger et al. 2010). Another prerequisite is the phase stability. The horn antennas are used to reference the phases and maintain phase stability (Krieger et al. 2007, Krieger et al. 2010).

Another mode is the pursuit monostatic mode (left in Fig. 2.13), where the satellites are flying separated in along-track with a very short distance. The sensors are independent and no synchronization is necessary (Krieger et al. 2007). This mode enables along-track interferometry with very short temporal baselines (in the order of seconds). However, vegetation and water can already affect the coherence. Nevertheless, this mode can be used for object detection, sea current and sea ice movement estimation and monitoring. In addition, super-resolution can be performed where the single images are coherently combined in order to increase spatial resolution (Krieger et al. 2010).

The transmitter is switched from pulse to pulse in alternating bistatic mode (right in Fig. 2.13), whereas both receive every signal. This mode results in one monostatic and two bistatic images in one overflight (Krieger et al. 2007). Two interferograms are calculable, which have doubled height of ambiguity and effective baseline (Krieger et al. 2010). However, the swath width is reduced due to overlap of monostatic images in range and azimuth (Krieger et al. 2007).

The orbit and security play an important role in a formation like TanDEM-X (Krieger & Moreira 2006). The TanDEM-X mission is flying in a helix formation (Fig. 2.14), which maximizes the security of the satellites (Krieger et al. 2010). This helix formation results in a vertical and horizontal baseline component. The satellites never cross their orbits in this formation, which makes that formation very safe (Krieger & Moreira 2006). In addition, flexible along-track baseline is possible. The along-track baseline should be minimal for single-pass interferometry in order to have highest overlap of Doppler spectra. An along-track baseline is necessary for along-track interferometry or other applications like super-resolution (Krieger et al. 2007). Therefore, many applications are possible besides the topographic height estimation (Krieger et al. 2010). Furthermore, the height of ambiguity is almost constant and in this way comparable height accuracies are achievable over the whole Earth. The helix formation is a significant advantage compared to SRTM, because here only one fixed baseline was used due to the mast (Krieger & Moreira 2006, Krieger et al. 2010).
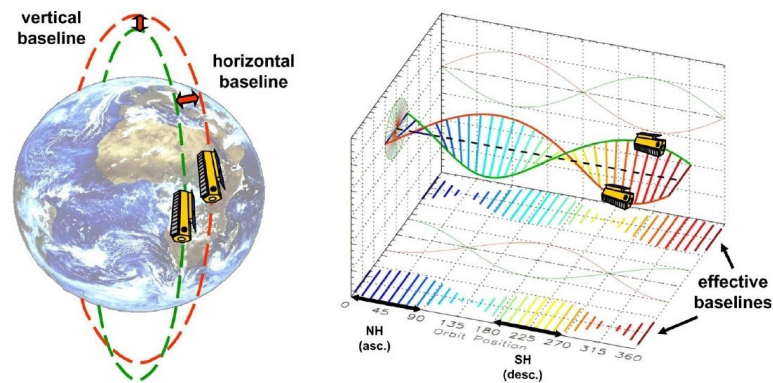
Fig. 2.14: Helix-formation of TanDEM-X mission (from Krieger et al. 2007:3324)

It is worth noting that a TanDEM-X acquisition depends on more parameters than a usual monostatic acquisition from TerraSAR-X mission. The interferometric mode and baseline are important parameters in a TanDEM-X acquisition. The largest across-track baseline is up to four kilometer, whereas the along-track baseline is limited to one kilometer (Krieger et al. 2007). This is based on the critical baseline, the geometric decorrelation and the Doppler centroid decorrelation (Krieger et al. 2010, see Section 2.2.4). An exception to this is the pursuit monostatic mode, where two independent monostatic acquisitions are combined (Fritz 2012).

2.4 REDD+ & remote sensing

Forests have significance in mitigation of greenhouse gas emissions and climate change. They act as carbon sink in the global carbon cycle and at the same time as emitters of carbon via deforestation and degradation. The latter is caused by

burning the forest through fire clearing, harvesting, pests as well as decomposition of organic material and soil organic matter. Therefore, deforestation and degradation are the second largest sources of anthropogenic caused carbon emissions after fossil fuels (Werf et al. 2009). Especially tropical forests are of high importance due to their large extent and high carbon storage related to their high biomasses (Olander et al. 2008, Lucas et al. 2004). The UN (United Nations) program Reducing Emissions from Deforestation and Degradation (REDD+) is aimed to incentivize tropical countries with financial compensation to reduce their deforestation and degradation rates in order to reduce carbon emissions (Olander et al. 2008). Concepts to realize that system are developed, where a carbon emission baseline should be established based on historic data. The emissions should be reduced compared to this baseline. The saved carbon is valuable at the carbon market. Therefore, tropical countries have access to the carbon market and are enabled to reduce their contribution to or mitigate climate change (Gibbs et al. 2007, Olander et al. 2008).

The countries are obliged to verify the reduction of their carbon emissions by using measurement, reporting and verification (MRV) concepts based on proven methods by IPCC Good Practice Guidelines (De Sy et al. 2012). Precise carbon emission estimations are necessary to implement a MRV. Firstly, the area of change between land categories must be assessed (activity data; De Sy et al. 2012). Basic land categories are suggested from IPCC in their Good Practice Guidelines for Land Use, Land-Use Change, and Forestry (LULUCF) and are namely forest land, grassland, cropland, wetland, settlements and other land (IPCC 2003). Secondly, the emitted or lost carbon of the activity data unit has to be estimated (emission factor; De Fries et al. 2007, De Sy et al. 2012). Therefore, the carbon emission is calculated as follows:

$$Emissions = Activity\ data * Emission\ factor \qquad (2.23)$$

The application of methods based on remote sensing is of high importance in order to implement such a MRV system. Field measurements are reliable estimations, but are not applicable to large areas due to high costs based on their labor intensive and time consuming nature. In contrast, remote sensing can be applied at large extent and with low costs compared to field measurements (Rosenqvist et al. 2003, Asner 2009). Hence, De Sy et al. (2012) suggest the combination of field measurements and remote sensing in order to implement cost efficient MRV concepts.

The detection of forest area and deforestation with optical remote sensing is already operational. This is based on the fact that forest, open areas, bare soil and

settlements have different spectral properties and thus they are easily differentiable resulting in high accuracies (Souza et al. 2005, Asner et al. 2009a, Cabral et al. 2010). Therefore, large area deforestation is clearly detectable. Nevertheless, the detection of forest degradation is limited, which is a large part of carbon emission and often indicates subsequent deforestation (De Fries et al. 2007, Carreiras et al. 2006, GOFC-GOLD 2012). Optical sensors with medium and low resolution, like Landsat and Modis (MODerate Resolution Imaging Spectroradiometer), are applied in operational systems like PRODES (Amazon Deforestation Monitoring Project) or DETER (Near Real Time Deforestation Detection System) for forest monitoring with unsupervised classifications (Hansen et al. 2008, Shimabukuro et al. 1998). Nevertheless, supervised classification schemes are also often used (Souza et al. 2005, Cabral et al. 2010). Sub-pixel analysis, like spectral mixture models, are commonly applied using optical data (Franke et al. 2012, Souza et al. 2005, Shimabukuro et al. 1998). Hansen et al. (2013) even provide a global forest cover map and gain/loss information on a global, annual basis. However, a global optical based map has limited consistency due to frequent cloud cover in tropical areas. For example, 39 acquisitions per scene were necessary to produce 5-year composites with a coverage of 99 % of the Democratic Republic of Congo, whereas areas of frequent cloud cover had still gaps of 18 % (Potapov et al. 2012). Similarly, multiple acquisitions are necessary in Southeast Asia to avoid data gaps caused by clouds (Wijedasa et al. 2012).

Optical sensors acquire electromagnetic waves in the visible and infrared spectrum (see Chapter 2.1). These waves are not able to penetrate into a medium due to their short wavelength, and mainly interact with the surface. Differentiation between intact high biomass and lower degraded biomass is very difficult and only applicable to large biomass differences with limited quality (Carreiras et al. 2006, Koch 2010, Thenkabail et al. 2004). Therefore, not any generally accepted method exists to detect forest degradation with remote sensing (De Fries et al. 2007).

Frequent cloud cover hinders consistent spatial and temporal coverage with optical systems. Thus, radar sensors can be a possibility for consistent and large area tropical forest monitoring due to their weather and day/night independence (Castro et al. 2003, Kuntz 2010). The electromagnetic waves interact with forest constituents based on their longer wavelengths and ability to penetrate the forests. This can be used for the retrieval of information about biomass, density or tree height (Leckie 1998). In comparison to optical satellites, SAR sensors achieve similarly high accuracies in detection of forest area and deforestation, but are not used operationally. L- and P-band SAR systems use decimeter wavelengths resulting in deep penetration into the forest. Hence, such wavelengths are considered to be more appropriate for tropical forest information retrieval compared to short wavelengths, like X- and C-band (Castro et al. 2003, Saatchi et al. 1997). JERS-1 L-band mosaics are used for the classification of tropical forests with high accuracies

(Sgrenzaroli et al. 2004, Simard et al. 2000, Simard et al. 2002), which can be improved by using dual-polarized ALOS PALSAR data (Hoekman et al. 2010, Walker et al. 2010). For instance, Dong et al. (2014) used ALOS PALSAR data to create a forest cover map of Southeast Asia. Nevertheless, the detection and classification of degraded forest is still a demanding task resulting in lower accuracies (Morel et al. 2011, Castro et al. 2003, Almeida-Filho et al. 2007). ALOS PALSAR data has limitations when mapping subtle changes and thus is limited when mapping forest degradation due to low spatial resolution (Reiche et al. 2013, Reiche et al. 2015). Hame et al. (2013a) reported also that ALOS PALSAR is not suitable for finer classifications than forest/non-forest.

Nevertheless, high resolution C- and X-band SAR systems are already applied successfully to tropical forest mapping. Especially high resolutions and retrieved texture measurements (Sanden & Hoekman 1999, De Grandi et al. 2015) as well as multiple polarisations (Otukei et al. 2011, Santos et al. 2010, Ullmann et al. 2012) achieved promising results. For instance, De Grandi et al. (2015) separated intact forest from degraded forest with spatial wavelet statistics in C-band, whereas Lband data did not achieve any differentiation. Furthermore, backscatter of X-band was applied to classify tropical forests and estimate aboveground biomass in certain biomass ranges in Central Kalimantan (Englhart et al. 2011, Ullmann et al. 2012). However, limitations exist in X-band data for differentiation of intact and degraded forest (Santos et al. 2010). The use of single-polarization did not achieve sufficient accuracy (Del Frate et al. 2008, Santos et al. 2010, Sanden & Hoekman 1999), which is demanded by REDD+ MRV concepts.

The biomass of a forest is the most important parameter in REDD+ since it is closely related to the stored carbon (Martin & Thomas 2011). The assessment of biomass can be used for the emission factors in MRV systems (De Fries et al. 2007, De Sy et al. 2012). Koch (2010) suggests two basic principles to assess biomass via remote sensing. On the one hand, biomass is directly related to the remote sensing measurement. On the other hand, remote sensing is used to estimate parameters like forest height or density, which are subsequently related to biomass (Lu 2006, Koch 2010). Biophysical parameters like density, height or biomass are hardly assessable via optical remote sensing (Koch 2010, Thenkabail et al. 2004). Indices of optical and hyperspectral data are frequently used in order to retrieve leaf area index and/or biomass (Myneni et al. 2001, Schlerf et al. 2005, Rahman et al. 2008), but usually result in low accuracies (Schlerf et al. 2005, Koch 2010, Beer et al. 2006). This is based on the fact that the spectral response of optical data does not have any physical relationship with biomass and thus spectral properties have a low correlation with biomass (Schlerf et al. 2005, Koch 2010, Le Toan et al. 2011).

Consequently, direct estimations of biomass with optical remote sensing is demanding, because of low saturation values and low differentiation (Lu 2006, Gibbs et al. 2007). However, tropical forests have usually high biomass values with complex structure. Solely qualitative classifications like forest type, health status, and so on are possible, where biomass values could be related. Nevertheless, these methods have low accuracies for biomass estimation (Koch 2010). An additional disadvantage for optical remote sensing is its dependence on sun illumination. Additionally, they are not able to penetrate through clouds, and are influenced by atmosphere. All these disadvantages can result in inconsistent datasets and/or low repetition frequency as explained before (Nezry et al. 1993, Koch 2010).

In contrast to passive optical systems, the potential of active systems (laser scanning or SAR) for biomass estimation is recognized. Combined methods with different active sensor types and field measurements were applied successfully (Asner et al. 2010, Dandois & Ellis 2013, Lefsky et al. 2005, Mitchard et al. 2011, Santoro et al. 2007, Solberg et al. 2013). LiDAR (Light Detection and Ranging) are used for biomass estimation with high accuracies in tropical forests in combination with field measurements (Lefsky et al. 2005, Drake et al. 2002, Asner et al. 2009b, Gonzalez et al. 2010, Dandois & Ellis 2013, Boehm et al. 2013, St-Onge et al. 2008). A big advantage of active systems is their independence from sunlight. However, today's LiDARs are mostly airborne and thus a consistent coverage is time-consuming and expensive (Koch 2010, Koehl et al. 2011). Therefore, the usefulness of LiDAR for large areas is limited (Koehl et al. 2011). ICESat/GLAS (Ice, Cloud, and land Elevation Satellite / Geoscience Laser Altimetry System) is a space borne LiDAR sensor, but it is a pointwise measurement. This can be used for pointwise estimation and up-scaling of MODIS based estimations (Lefsky et al. 2005, Baccini et al. 2008, Simard et al. 2011). Two pan-tropical biomass maps were created with upscaling from field measurements to ICESat/GLAS and further with optical MODIS imagery (Baccini et al. 2008, Saatchi et al. 2011a). Saatchi et al. (2011a) utilized SRTM and quick scatterometer (QSCAT) data in addition to MODIS. Nevertheless, MODIS has a low spatial resolution and is also a passive optical system, resulting in spatial and temporal inconsistencies due to frequent cloud cover. In addition, the pan-tropical biomass maps differed significantly despite similar input data, showing that large uncertainties still exist for such pan-tropical maps (Mitchard et al. 2013).

The potential of SAR data for biomass estimation is already successfully analyzed (e.g. Mitchard et al. 2011, Santoro et al. 2007, Naidoo et al. 2015, Luckman et al. 2000, Solberg et al. 2010). A correlation between radar backscatter and biomass is frequently used and achieved similarly to classifications more accurate results with longer wavelengths like L- and P-band compared to short wavelengths, like C- and

X-band (Saatchi et al. 1997, Luckman et al. 2000, Naidoo et al. 2015, Englhart et al. 2011, Gama et al. 2010, Neeff et al. 2005, Mitchard et al. 2011). This is based on the penetration capacity into the canopy, the subsequent interaction with forest constituents and related volume scattering (Dobson et al. 1995, Leckie 1998, Le Toan et al. 1992, Saatchi et al. 2011b). Especially X-band has been rated as inappropriate for biomass estimation in tropical forests (Gama et al. 2010, Naidoo et al. 2015, Castro et al. 2003). The X-band backscatter can only be used for small biomass values (Englhart et al. 2011), since the wave has a low penetration depth interacting mainly with upper canopy constituents. This results in low correlation with biomass (Gama et al. 2010). However, the synergetic use of different wavelengths achieved improved results compared to single wavelength (Naidoo et al. 2015, Luckman et al. 2000). But simply adding shorter wavelengths to L-band data did not enhance the results significantly (Saatchi et al. 1997, Naidoo et al. 2015, Luckman et al. 2000).

In contrast, phase based approaches can overcome the limitations of short wavelengths (Balzter 2001, Santoro et al. 2007, Solberg et al. 2010, Solberg et al. 2013, Soja et al. 2015). Here, interferometric coherence (Santoro et al. 2002, Santoro et al. 2007, Cartus et al. 2011) as well as InSAR height are usable (Solberg et al. 2010, Gama et al. 2010, Neeff et al. 2005, Solberg et al. 2013). The interferometric coherence seems to be correlated to biophysical parameters like volume and subsequently biomass (Askne et al. 1997). C-band data is frequently used in the interferometric water cloud model to estimate growing stock volume of boreal forests (Askne et al. 2003, Santoro et al. 2002, Santoro et al. 2007, Cartus et al. 2011). Volume decorrelation information is also used in a two-level model in order to assess aboveground biomass of boreal forests (Soja et al. 2015). InSAR height of C- or X-band is frequently used in order to estimate forest canopy height, which is further correlated with biomass (Solberg et al. 2010, Solberg et al. 2013, Neeff et al. 2005). In addition, interferometric coherence can be used in the Random Volume over Ground (RVoG) model in order to estimate canopy height as well (Cloude & Papathanassiou 1998, Papathanassiou & Cloude 2001, Neumann et al. 2010, Hajnsek et al. 2009).

However, generally it is assumed that full-polarimetric and long wavelengths, like L-band data, should be used in order to achieve highest accuracies (Neumann et al. 2010, Hajnsek et al. 2009). If those assumptions are not fulfilled, the model has limitations and assumptions have to be made (Askne et al. 2013, Kugler et al. 2014, Caicoya et al. 2012).

TanDEM-X offers new possibilities for deploying bistatic interferometric information applicable to tropical forest monitoring and biomass estimation. The

use of interferometry and derived products could achieve higher accuracies compared to results without interferometry on high spatial resolution for classification as well as estimation of biophysical parameters. The estimation of biomass with TanDEM-X is possible utilizing the two approaches suggested by Koch (2010). The interferometric coherence can be used for direct estimation of biomass and can overcome limitations of backscatter in higher frequency data, like C- and X-band (Santoro et al. 2007, Santoro et al. 2002, Cartus et al. 2011). The potential of InSAR data for estimation of canopy height models and subsequently biomass was analyzed by e.g. Neeff et al. (2005), Sexton et al. (2009), Solberg et al. (2010), Weydahl et al. (2007) and Gama et al. (2010). However, the use of high resolution space borne X-band interferometric information for such purposes still lacks scientific analysis and results.

3 Need for research

It has been explained that some systems/sensors have high potential for REDD+ MRV concepts and are already operational in use. Nevertheless, all of them have deficiencies (e.g. coarse resolution, inconsistent coverage due to cloud cover, inaccuracies; Koch 2010, Mitchard et al. 2013). It is assumed that radar remote sensing has high potential due to its weather and day/night independence as well as its interaction with forest constituent beneath the canopy (Leckie 1998). But there is still a need for research in the field of (tropical) forest monitoring (Saatchi et al.
2007).

3.1 Significance of the study area in context of climate change and REDD+

The study area is covered by tropical peat swamp forest. Peat areas exist in low drainage areas resulting in acidification of substrates and lack of nutrients as well as gathering of organic material (Phillips 1998, Page et al. 1999, Hooijer et al. 2010). Peat areas can be divided into ombrogene and topogene ones, whereas most are ombrogene (Sorensen 1993). The study area in Central Kalimantan, Indonesia is an ombrogene peat swamp area. Ombrogene peat areas are convex shaped where precipitation is the only water source for plants at the top of the convex shape (Phillips 1998). After Page et al. (2011) 440,000 km^2 are covered by peat swamps, whereas the majority (57 % of total area) exist in Southeast Asia.

Tropical peat swamps are mostly covered with forest. Usually, tropical peat swamp forests are dividable in different zones, which are related to the convex shape. At the center of the convex shape is the top with the deepest peat layer and the lowest nutrient content (Sorensen 1993, Phillips 1998, Page et al. 1999). The convex shape is also often called peat dome. Here, the nutrients are washed away by precipitation (Phillips 1998). Therefore, nutrient content increases to the edge of the peat dome and is highest at the thinnest peat layer. This nutrient distribution causes differences in species composition and forest structure. The tallest trees with highest biomass are at the edge of the peat dome, while the tree height and biomass decreases but with increasing the stem density towards the center of the dome (Sorensen 1993, Page et al. 1999).

Peat formations store a huge amount of carbon in addition to the biomass of the forests (Sorensen 1993, Page et al. 1999). Therefore, peat swamp forests despite

their relatively small extent are of high significance as carbon storage. After Werf et al. (2009) the emissions from peat swamp forests equal 1/4 of the emissions from all deforestation and degradation activities. Deforestation and drainage result in higher vulnerability to fires. For instance, droughts and fires in El Niñ̃o year 1997 resulted in carbon emission equal to 13 - 40 % of emissions from fossil fuels (Page et al. 2002). Werf et al. (2009) address the consideration of peat swamp forests in REDD+. Peat swamp forests have important ecological functions like regulation of local climate and hydrology as well as habitat in addition to carbon sink (Phillips 1998). Indonesia has the highest extent of peat swamp forests (Page et al. 2011) and thus Indonesia is one of largest emission sources via deforestation, degradation and decomposition of peat (Hooijer et al. 2010, Werf et al. 2009). Peat swamps in Indonesia are mostly located at coastal zones and lowlands of Sumatra and Kalimantan (Sorensen 1993, Phillips 1998).

The study area of this study is a peat swamp forest in Central Kalimantan, Indonesia and is located at about 60 km from provincial capital Palangkaraya. Large parts of Central Kalimantan were part of the mega rice project (MRP). The transition of 1 million hectare for agricultural purposes was the main objective of this project, whereas peat swamps were most affected. The project was initiated in 1995 and stopped in 1999 (Muhamad & Rieley 2002, Woesten et al. 2008). Nevertheless, large parts of pristine forest were drained by canals and subsequently deforested (Boehm & Siegert 2001, Aldhous 2004). The forests of Kalimantan are still under pressure despite the abundance of the project. The drainage and fire clearing are still utilized for agricultural purposes, like oil palm cultivation. The huge demand for oil palm products are major drivers (Germer & Sauerborn 2008). Nevertheless, the study area is less affected from drainage and fire clearing due to the declaration as protected conservation area (Aldhous 2004). Today, the study area contains one of the largest populations of wild Orang-Utans (about 3,500 individuals, Wich et al. 2008).

Despite the significance of peat swamp forests, still a huge need for research exists (Lawson et al. 2014). This applies especially to the extent of peat swamp forests, their classification and their estimation of biomass (Hooijer et al. 2010, Lawson et al. 2014). Remote sensing can play an important role to serve those needs. After Hooijer et al. (2010) the need for land cover information as well as for deforestation and degradation rates exist. Further, estimation of biomass in peat swamp forests with remote sensing demands efforts for research (Lawson et al. 2014). Although, this is generally the case for every forest in the world, but a high need for research is recognized in tropical peat swamp forests (Lawson et al. 2014, Kronseder et al. 2012, Englhart et al. 2013). For Phillips (1998), the lack of research results in

tropical peat swamp forests is caused by their difficult accessibility. Peat swamp forests have a high water table at least during half the year, and the high density of trees and underwood hinder the access for field measurements (Phillips 1998). However, the suggestion of Werf et al. (2009) to consider peat swamps in REDD+ also, indicates that the importance of tropical peat swamp forests is recognized at an international level and might increase further. Therefore, need for research of tropical forest monitoring exists and is probably even more important for tropical peat swamp forests.

3.2 Need for research & research questions

It has been mentioned that some applications are already operational with optical data. Nevertheless, these applications have still limitations and drawbacks mainly related to cloud cover and thus inconsistent coverage. Medium to coarse spatial resolution with high revisit are used to achieve large coverage (Hansen et al. 2008, Hansen et al. 2013). But with such data subtle changes in forest, like small scale deforestation or degradation, are not detectable. In addition, biophysical parameter estimation with optical sensors is a demanding task often resulting in low accuracies (Koch 2010). TanDEM-X offers the possibility to use a global, multi-temporal, high-resolution (~3 m) InSAR dataset. This SAR system is almost independent of weather and day/night. Additionally, the acquisitions for the creation of a digital elevation model were finished within 3 years resulting in a consistent global coverage in the time between 2010 and 2013/2014 (Krieger et al. 2010). The high resolution and consistent coverage enables mapping of large (up to global) areas and on every place on earth within a similar time frame. This can be used for baseline mapping supporting deforestation and degradation monitoring (Poncet et al. 2014, Schlund et al. 2014a, Schlund et al. 2014b). Nevertheless, TanDEM-X is the first operational single-pass interferometer in space. The analysis and utilization of this data for land cover classifications is not assessed yet. TerraSAR-X or other X-band systems were used (Breidenbach et al. 2010, Otukei et al. 2011, Santos et al. 2010, Sanden & Hoekman 1999, Ullmann et al. 2012), but had limitations which could be resolved by single-pass interferometry of TanDEM-X. More land cover types distinguishing features could be derived with one acquisition compared to a monostatic TerraSAR-X acquisition. This is especially the case for the coherence and bistatic amplitude. The interferometric coherence was used frequently in classification, but this was limited on repeat-pass coherence (e.g. Bruzzone et al. 2004, Engdahl & Hyyppa 2003, Strozzi et al. 2000). Additionally, a TanDEM-X acquisition results in active and passive amplitudes. The active amplitude is similar to a monostatic acquisition

whereas the passive amplitude can include other information than active amplitude due to the little different look angle (see Section 2.2.1). Dubois-Fernandez et al. (2006) suggested additional information by using the passive amplitude even at very small bistatic angles, but emphasized additional need for research. Therefore, the possibility to use TanDEM-X for highly accurate land cover classifications needs to be analyzed in order to evaluate the additional information which comes with a hybrid radar system like TanDEM-X.

As mentioned before, biomass is one of the most important parameters for REDD+ and generally important for estimation of carbon sinks. Some potential approaches exist for biomass estimations (Koch 2010). Best results are achieved with LiDAR, which is mostly airborne and thus expensive and/or only applicable to small areas (Koehl et al. 2011, Koch 2010). Similarly to classifications, TanDEM-X can be used as basis for global consistent coverages. The backscatter of X-band is considered to be of low potential for biomass estimations due to the short wavelength (Castro et al. 2003, Luckman et al. 2000, Gama et al. 2010). However, the interferometric information could be used for biomass estimations and could overcome the limitations of X-band backscatter. The interferometric coherence was used frequently for volume estimation with C-band or longer wavelengths (Askne et al. 1997, Santoro et al. 2007, Santoro et al. 2002) as well as for tree height estimation with full-polarimetric L-band data (e.g. Hajnsek et al. 2009, Neumann et al. 2010). First analyses indicate the potential of TanDEM-X for tree height estimation (Kugler et al. 2014, Askne et al. 2013, see Section 2.4). The biggest advantage is the minimization of temporal decorrelation (Krieger et al. 2007). The interferometric coherence is thus mainly governed by volume decorrelation, signal-to-noise-ratio and system parameters. This information could be used to estimate biophysical parameters of tropical forests. For instance, canopy cover or tree height could be derived by the interferometric coherence, which are subsequently correlated with the biomass. Consequently, coherence can be also directly correlated with the biomass.

Further information given by TanDEM-X is the global surface height. This is the primary mission objective and is defined with a global accuracy of 2 m relative and 4 m absolute vertical error (Airbus Defence and Space 2014). The TanDEMX height could be assumed as real surface due to the short wavelength and low penetration depth. This represents the height including the vegetation height. The subtraction of the digital surface model (DSM) with a digital terrain model (DTM) results in a canopy height model (CHM). This canopy height model could be used for biomass estimation. Existing studies show the potential of canopy height models and biomass estimations with different data sources like SRTM, LiDAR and airborne SAR

(Sexton et al. 2009, Solberg et al. 2010, Weydahl et al. 2007). The creation of an accurate DTM is of high importance for calculating the CHM, whereas different approaches exist. For instance, LiDAR is used (Sexton et al. 2009, Kellndorfer et al. 2004, Weydahl et al. 2007) and other studies showed also the potential of long wavelength InSAR for creating the DTM (Neeff et al. 2005, Rombach & Moreira 2003, Gama et al. 2010). Most of the aforementioned approaches are airborne, but the global digital surface model (WorldDEM™) could be edited to a terrain model (WorldDEM DTM). The difference of both models would also represent the vegetation height to be used for biomass estimations. This is also globally applicable.

Lawson et al. (2014) emphasize the need for research of mapping and biomass estimations with (radar) remote sensing in tropical peat swamp forests. Optical sensors are also used in peat swamp forests successfully, but Lawson et al. (2014) suggest also high potential of active remote sensing (radar and LiDAR) for fine differentiation and estimation of biophysical parameters in tropical peat swamp forests. Therefore, the following research question can be concluded:

- Do bistatic TanDEM-X data and features have a significant benefit of information for land cover classification compared to usual monostatic acquisitions and for which classes is this relevant?

- Can interferometric information from TanDEM-X be used for estimation of biomass?

  - To what extent is the interferometric coherence correlated with biophysical parameters, like canopy cover and biomass, and is this usable for spatial estimation of biomass?

  - Is the interferometric height of global TanDEM-X data accurate and related to vegetation height in order to create a canopy height model and estimate biomass?

  - Is it necessary to use a high accurate terrain model (e.g. from LiDAR) or is the editing of the global surface model to terrain model sufficient for canopy height and biomass estimation?

The next three chapters analyze these questions by presenting published articles in scientific journals. The first question is analyzed in the paper called *"Importance of bistatic SAR features from TanDEM-X for forest mapping and monitoring"* published in *Remote Sensing of Environment* presented in the next chapter. The second and third question are evaluated in a journal paper entitled *"TanDEM-X data for aboveground biomass retrieval in a tropical peat swamp forest"* published in *Remote*

Sensing of Environment as well. Journal paper *"WorldDEM™ data for canopy height and aboveground biomass retrieval in a tropical peat swamp forest"* submitted to *ISPRS Journal of Photogrammetry & Remote Sensing* analyses the fourth and the fifth question.

4 Importance of bistatic SAR features from TanDEM-X for forest mapping and monitoring

M. Schlund[a,b], F. von Poncet[a], D. H. Hoekman[c], S. Kuntz[a] & C. Schmullius[b]

[a] *Astrium GEO-Information Services, Claude-Dornier-Str., 88090 Immenstaad, Germany* [b] *Department of Earth Observation, Friedrich-Schiller University, 07743 Jena, Germany* [c] *Dept. of Environmental Sciences, Wageningen University, Droevendaalsesteeg 4, 6708 PB Wageningen, The Netherlands*

Abstract

Deforestation and forest degradation are one of the important sources for human induced carbon dioxide emissions and their rates are highest in tropical forests. For man-kind, it is of great importance to track land-use conversions like deforestation, e.g. for sustainable forest management and land use planning, for carbon balancing and to support the implementation of international initiatives like REDD+ (Reducing Emissions from Deforestation and Degradation). SAR (synthetic aperture radar) sensors are suitable to reliably and frequently monitor tropical forests due to their weather independence. The TanDEM-X mission (which is mainly aimed to create a unique global high resolution digital elevation model) currently operates two X-band SAR satellites, acquiring interferometric SAR data for the Earth's entire land surface multiple times. The operational mission provides interferometric data as well as mono- and bistatic scattering coefficients. These datasets are homogeneous, globally consistent and are acquired in high spatial resolution. Hence, they may offer a unique basic dataset which could be useful in land cover monitoring.

Based on first datasets available from the TanDEM-X mission, the main goal of this research is to investigate the information content of TanDEM-X data for mapping forests and other land cover classes in a tropical peatland area. More specifically, the study explores the utility of bistatic features for distinguishing between open and closed forest canopies, which is of relevance in the context of deforestation and forest degradation monitoring. To assess the predominant information content of TanDEM-X data, the importance of information derived from the bistatic system is compared against the monostatic case, usually available from SAR systems. The

usefulness of the TanDEM-X mission data, i.e. scattering coefficients, derived textural information and interferometric coherence is investigated via a feature selection process. The resulting optimal feature sets representing a monostatic and a bistatic SAR dataset were used in a subsequent classification to assess the added value of the bistatic TanDEM-X features in the separability of land cover classes. The results obtained indicated that especially the interferometric coherence significantly improved the separability of thematic classes compared to a dataset of monostatic acquisition. The bistatic coherence was mainly governed by volume decorrelation of forest canopy constituents and carries information about the canopy structure which is related to canopy cover. In contrast, the bistatic scattering coefficient had no significant contribution to class separability. The classification with coherence and textural information outperformed the classification with the monostatic scattering coefficient and texture by more than 10 % and achieved an overall accuracy of 85 %. These results indicate that TanDEM-X can serve as a valuable and consistent source for mapping and monitoring tropical forests.

4.1 Introduction

Human activities, summarized by the UNFCCC (United Nations Framework Convention on Climate Change) as land use, land-use change and forestry (LULUCF), affect changes in carbon stocks (Intergovernmental Panel on Climate Change IPCC 2003). Their role in the mitigation of climate change has long been recognized. The knowledge of carbon storage at a certain point in time as well as its changes due to deforestation, afforestation, and other land-use transformations are therefore of great importance (Watson et al. 2000). Thus, the mapping and monitoring of tropical forests as a potential significant carbon store are relevant in climate change studies and in the implementation of REDD+ (Reducing Emissions from Deforestation and Degradation; Gibbs et al. 2007).

Synthetic aperture radar (SAR) systems are considered an important tool for mapping and monitoring tropical forests due to their weather independence (e.g. Kuntz 2010). High accuracies in land cover and forest/non-forest classifications have been obtained in the temperate forests of Germany using very high-resolution, multiple polarization, multi-temporal X-band SAR data from the TerraSAR-X mission (Breidenbach et al. 2010) and in Austria in combination with a LiDAR dataset (Perko et al. 2011). However, longer wavelengths, such as L- and P-band are considered more appropriate than X- and C-band in the separation of different forest types and in the detection of secondary or degraded forest due to their increased penetration into the forest canopy (Castro et al. 2003, Saatchi et al. 1997, Stolz &

Mauser 1995). A number of studies show the suitability of space-borne L-band SAR systems for the large scale classification of tropical forest areas. For example, the classification of multi-temporal JERS-1 mosaics (Sgrenzaroli et al. 2004, Simard et al. 2000, Simard et al. 2002) achieved high accuracies, which could even be increased by high resolution dual-polarization ALOS PALSAR data (Hoekman et al. 2010, Longepe et al. 2011, Walker et al. 2010). Even though Morel et al. (2011) also classified plantations and forests with a high accuracy using ALOS PALSAR in a study area in Borneo, they found a significant decrease in the accuracy by adding a logged forest class to the classification. Moreover, there is a significant gap in globally available high resolution SAR coverages, especially since ALOS PALSAR and ENVISAT ended their missions in 2011 and 2012, respectively and the continuation of climate change studies must be ensured without those systems (European Space Agency 2012).

On the other hand, single polarization X-band data show limitations in the separability of forest classes (Castro et al. 2003). Case studies using TerraSAR-X mission data in the tropical forests of Brazil, Uganda, and Central Kalimantan (Otukei et al. 2011, Santos et al. 2010, Ullmann et al. 2012) suggested that the use of multiple polarizations can provide satisfactory results for land cover and forest classifications. For example, Santos et al. (2010) used dual polarimetric TerraSAR-X data in order to classify primary forest, degraded forest, pasture, and bare soil. He emphasized the significance of the entropy obtained from the Cloude decomposition (Cloude & Pottier 1997). Although primary forest was separable from pasture and bare soil in X-band, confusions with degraded forest were found (Santos et al. 2010).

Previous investigations showed that automated mapping with single channel high frequency SAR data does not achieve a sufficient degree of detail and accuracy, especially in the mapping of different forest types or degraded forests (Del Frate et al. 2008, Santos et al. 2010, Sanden & Hoekman 1999). Therefore, very high resolution, different wavelengths or synergetic use with optical data, multiple polarizations and/or multi-temporal analysis are necessary to achieve high accuracies with high frequency radar (Breidenbach et al. 2010, Bruzzone et al. 2004, Erasmi & Twele 2009, Sanden & Hoekman 1999).

Nevertheless, the objective of this investigation is to show that accurate forest monitoring results can be achieved without the necessity to deploy multiple polarizations and multi-temporal data, which may be inconsistent in acquisition modes and timing due to acquisition constraints. Those constraints are caused by the fact that available radar systems providing high resolution and polarimetric or repeatpass capabilities are commercially operated and thus, data acquisition is tasked on demand, making consistent coverages nearly impossible.

The TanDEM-X mission might be an option to overcome these constraints given by incomplete coverage or information content. Starting in 2010, the aim of the TanDEM-X mission is the acquisition of global coverage of bistatic, single-pass interferometric SAR images to produce an accurate digital elevation model (Krieger et al. 2007). For that, the two TanDEM-X sensors acquire Earth's entire land surface several times during the three-year mission duration in high resolution mode. Thus, the mission offers a suitable data source for up-to-date, homogeneous and globally consistent, high resolution land cover survey as baseline for LULUCF monitoring. An initial global coverage was achieved in 2011 and the second coverage will be completed in 2013. The TanDEM-X data are acquired simultaneously from two spatially separated sensors (TerraSAR-X and TanDEM-X). Together, they form a bistatic SAR system and a SAR interferometer in space, where both satellites receive the signal from a common illuminated footprint under different look angles (Krieger et al. 2007, Krieger et al. 2010). Due to the constellation of two closely flying SAR sensors, one sensor is used as transmitter and receiver (monostatic/active), whereas the other sensor is only a receiver (bistatic/passive). According to Willis (1991), this is called bistatic acquisition.

This acquisition results in a combination of two scattering coefficients. The simultaneous multi-angle view enables the detection of objects not visible in monostatic mode (Walterscheid et al. 2006). The angular difference between the two sensors leads to a modification of the received signals depending on the scattering mechanisms and thus provides additional information on the geometric properties of the objects. A number of studies (Dubois-Fernandez et al. 2006, Krieger & Moreira 2006, Krieger et al. 2010) suggest the hypothesis that the availability of mono- and bistatic scattering coefficients will improve not only the segmentation and classification of land cover classes like urban areas which are mainly affected by dihedral scattering and thus are sensitive to aspect angle, but also natural surfaces like agricultural fields or forests. The difference in the received signal is predominant for dihedral scattering observed from man-made objects which is reduced at the passive (receive only) sensor. This in turn results in more homogenous image statistics which is more favorable for the classification of natural surfaces (Walterscheid et al. 2006). Dubois-Fernandez et al. (2006) detected a modification in backscatter even at a very small angle difference between the two sensors. However, they did not use this information in a land cover classification, but identified the need for further analysis.

For the interferometric generation of a high-quality 3-D surface model from the TanDEM-X mission data the most significant advantage of the bistatic acquisition is the reduction of temporal decorrelation and atmospheric disturbances (Krieger et

al. 2007). Therefore, the bistatic interferometric coherence – a measure of the phase decorrelation and the quality of the interferometric derivate (Bamler & Hartl 1998) – reveals special characteristics compared to the repeat-pass constellation normally used. The interferometric coherence is influenced by the baseline, the Doppler centroid frequency, the system noise, the SAR processing, and relevant scene properties like temporal and volume decorrelation (Hanssen 2001, Wegmuller & Werner 1997).

Even for the repeat-pass ERS-1 mission providing only moderate resolution Wegmuller & Werner (1995) demonstrated the benefit of interferometric coherence in land cover classifications, based on the information of the temporal and volume decorrelation. Following the interferometric coherence in combination with the radar backscatter has been used frequently for land-use classifications (e.g. Bruzzone et al. 2004, Engdahl & Hyyppa 2003, Strozzi et al. 2000, Wegmuller & Werner 1995, Wegmuller & Werner 1997). Moreover, the use of ERS interferometric coherence for land cover classifications in Sumatra, Indonesia resulted in an increased separability of forest, plantations and deforested areas, whereas certain vegetation classes could not be distinguished (Stussi et al. 1997). Perko et al. (2011) demonstrated confusions in the repeat-pass interferometric coherence of X-band due to temporal decorrelation of agriculture and forest classes. According to Ribbes et al. (1997), it could be argued that a minimization of the temporal baseline would be beneficial for the use of interferometric coherence in classifications (Ribbes et al. 1997, Stussi et al. 1997). In fact, the two satellites of TanDEM-X have been flying in close formation since October 2010, resulting in a temporal baseline of about a tenth of a second. Thus, temporal decorrelation effects can be neglected (Caicoya et al. 2012), e.g. effects due to differences in moisture content or moving objects.

Therefore, the goal of this research is to investigate and exploit the information content of mono-temporal bistatic TanDEM-X data for land cover and forest mapping in a tropical forest. The TanDEM-X data are used to classify basic land cover classes which are in line with the IPCC good practice guidance for land use, land use change and forestry (IPCC 2003). In addition, the study investigates if the bistatic interferometric coherence improves the separation of open and closed forest, which today is not feasible in deploying monostatic TerraSAR-X data (Santos et al. 2010). The temporal transition from closed to open canopy forest can be seen as an indication of forest degradation and thus, is relevant in the context of REDD+.

4.2 Study site & data

4.2.1 Test site description

The test site covers a peat swamp forest area in Central Kalimantan ($114°\,31^0$E, $2°\,10^0$S) with a flat topography (Hajnsek et al. 2009). The provincial capital Palangkaraya is located about 60 km west of the study area and the Kapuas River is in the western part of the study area (Fig. 4.1). The climate is influenced by a dry southeast monsoon, resulting in a dry season from June to September. The wet season, defined by a wet northeast monsoon, is from October to May. In general, the climate is humid tropic (Jauhiainen et al. 2005).

The peat swamp forests of Indonesia are highly endangered. Large parts of pristine forest were already converted into agriculture and plantations. For that purpose, they are drained by canals. The investigation area is heavily affected by the construction of canals and related deforestation originating from the Mega Rice Project (MRP) initiated by the Indonesian government in 1995. Some canals are visible in the southern part of the amplitude image (Fig. 4.1). The MRP aimed to transform about 1 million hectares of tropical peat lands in rice cultivation, which failed and was abandoned in 1999 (Muhamad & Rieley 2002, Woesten et al. 2008).
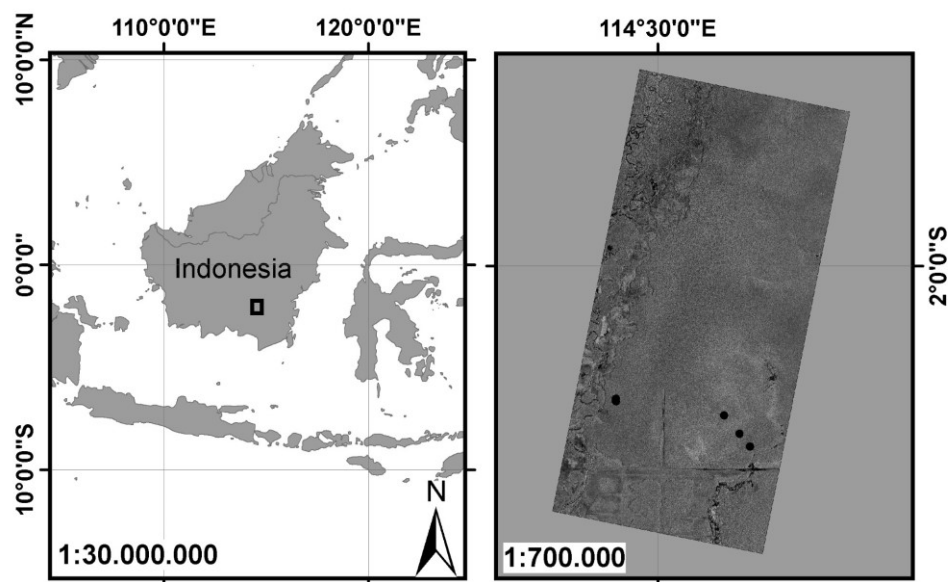
Fig. 4.1: Location of study site in Kalimantan (left) and the corresponding TanDEM-X amplitude image with the location of the field measurements (black dots; right)

The central and the northern parts of the study area are now part of the Mawas conservation area, where the forests are relatively pristine (Aldhous 2004). The

dense forests close to the rivers and at the edge of the peat dome, (located mainly in the eastern part of the amplitude image) are up to 30 m high with aboveground tree biomass values up to 350 t/ha. Towards the center of the peat dome, forest height decreases to 15 m and aboveground biomass to 20 t/ha (Hajnsek et al. 2009). The Mega Rice Project was divided into five spatial blocks with a size of 160,000 to 500,000 ha. Boehm & Siegert (2001) estimated that forest cover decreased from 65 % to 48 % between 1991 and 2000 for the two blocks of the Mega Rice Project within the study area. Drying of the peat due to drainage and illegal logging are still a threat for the forests. On the one hand, increasing decomposition processes releases methane and on the other hand the dried accumulated biomass makes these areas more vulnerable to fire, both resulting in increased greenhouse gas emissions (Aldhous 2004, Hooijer et al. 2010, Page et al. 2002).

4.2.2 Remote sensing & reference datasets

4.2.2.1 TanDEM-X dataset

The SAR data for this study were acquired during the TanDEM-X mission over Central Kalimantan on December 21, 2010. The mode used is called bistatic mode and is applied for the operational TanDEM-X mission acquisitions (Krieger et al. 2007).

Tab. 4.1: Parameters of the TanDEM-X StripMap acquisition

Acquisition parameter	Value
Acquisition date	December 21, 2010
Incidence angle	$47.9° – 49.3°$
Orbit direction	Descending
Look direction	Right
Effective baseline (image center)	163.3 m
Height of ambiguity (image center)	51.2 m
Polarization	HH
Resolution	2.4 m (ground range) x 3.3 m (azimuth)

Both sensors are able to transmit the electromagnetic wave with a phased-array X-band antenna having a carrier frequency of 9.65 GHz (Pitz & Miller 2010), corresponding to a wavelength of ~3.1 cm. The datasets from the operational TanDEM-X mission were acquired in StripMap mode with HH (horizontal)

polarization, resulting in a resolution of approximately 3 m in azimuth and 2 m in range direction. The effective baseline of the available dataset was 163 m (Table 4.1), which is calculated perpendicular to the look direction and is an estimate of the effective distance of both sensors (Hanssen 2001). The data was co-registered, resampled and delivered as CoSSC (co-registered single look slant range complex; Fritz 2012) from the German Aerospace Center (DLR) ground segment.

4.2.2.2 Reference dataset

Field data and aerial photographs were acquired in 2005. Furthermore, georeferenced photos acquired from a low-altitude aircraft were available from 2011 (Table 4.2). Those datasets were used to interpret the training and validation samples (see Section 4.3.1). Overall, 8 transects with a size of 100 m x 10 m were available as reference data. All trees with a diameter at breast height (dbh) greater than 10 cm were recorded within these areas. The average of two field transects was calculated due to spatial adjacency of the measurements, finally resulting in 4 transects (Fig.
4.1). The tree crown cover for the field plots was calculated as the average crown cover per square meter for each field transect which is the product of tree density (trees/m^2) and the average circular tree crown projection area (m^2).

Due to the difficult accessibility of this peat swamp forest, only these 8 transects were available for the study. However, in 2005 during the INDREX-II (Indonesian Radar Experiment) campaign, aerial photos in true color were acquired from an ultra-light aircraft, while the position of the photos and the corresponding altitude of the aircraft were recorded. The average altitude of the aircraft was about 554 m. The images were acquired from January 13 until January 15, 2005 in nadir view, resulting in a total of 343 available photos which cover about 100 km^2. From these photographs a quantitative analysis, like the estimation of the number of trees per area and canopy cover was performed.

Tab. 4.2: Overview of available reference dataset (after Hajnsek & Hoekman 2005)

Dataset	Acquisition year
Field samples (Tree location, tree height, height of first branch, diameter at breast height [dbh], crown extent, and species)	2005
Aerial photographs	2005
Photos from low-altitude aircraft	2011
SPOT 5	2011

ALOS PALSAR	2007 – 2010

In order to select aerial photos over areas which had not changed between 2005 and 2010 we used SPOT 5 and ALOS PALSAR available in fine beam single polarization HH and fine beam dual polarization HH and HV. These remote sensing data were interpreted in combination with the photos from 2005. Aerial photos showing areas of land cover change between major cover types (e.g. from forest to grassland) in comparison to ALOS PALSAR or SPOT were excluded from the analysis. The changes within the forest, such as forest degradation or regrowth, could not be interpreted from those remote sensing datasets. Based on the visual analysis we excluded aerial photos from 2005 for areas that underwent a land cover change.

In addition, more recent photos were available, which had been acquired in a flight campaign by a low altitude aircraft in December, 2011. From this mission, approximately 145 photos in oblique view were used for interpretation of the main land cover classes. However, in contrast to the photos from 2005 a quantitative analysis of tree cover was not possible due to the oblique view.

4.3 Methods

4.3.1 Class definition

The IPCC (2003) provide methods and classes in their good practice guidance for land use, land-use change and forestry (LULUCF) to estimate and report carbon stock changes. These classes, called "main categories" are forest land, cropland, grassland, wetlands, settlements, and other land. Nevertheless, binding definitions of these classes are not given and can be adjusted. Here, forest land, for instance, was determined using the definition by the Food and Agriculture Organization of the United Nations (FAO 2000). The definitions listed in Table 4.3 were used for the interpretation key in order to interpret the aerial photographs. The IPCC (2003) suggests distinguishing forest land into open and closed canopy forest and advised a threshold of 40 % canopy cover. However, this is not a binding definition and can be adjusted. Thus, in this study a threshold of 50 % was used to distinguish between open and closed canopy forests (Table 4.3).

The canopy cover was estimated directly via photo interpretation of the acquisitions from 2005. The nadir view enabled the estimation of the canopy cover from the aerial photographs, each covering an area of about 300,000 m². Quantitative measurements about the number of trees, crown size and derived crown cover within the field transects were used to create a template to extrapolate the knowledge from photos covering the transects to the rest of the aerial photos, where no reference data had been collected. Note that canopy cover (ground projected area of the crowns irrespective to the crown overlap) is assessable by

photo interpretation of the aerial imagery but not the crown cover (the average sum of all crowns, which can exceed 100 % due to overlapping crowns) which had been measured in the field. Therefore the number of trees was used as an additional control variable to relate crown and canopy cover to each other.

Tab. 4.3: Definition of the investigated classes (after FAO 2000, IPCC 2003)

Class	Definition
Forest land	>0.5 ha and >10 % tree canopy cover
Closed forest	Forest with canopy cover >50 %
Open forest	Forest with canopy cover <50 %
Shrubland	Not covered by forest (<10 %) with shrubs dominant
Grassland	Not covered by forest or shrubs (<10 %) with grasses and ferns dominant
Wetlands	Covered or saturated by water at acquisition dates of aerial photos and is not covered by forest land
Water bodies	Bodies of flowing or standing water (e.g. rivers, lakes)

The canopy cover in each photo was estimated via comparison with the template (Nowak et al. 1996). However, due to the multi-layer structure of tropical forest canopies, understory next to dominating trees can be misinterpreted as forest floor and thus lead to underestimation of canopy coverage for example. Therefore, the number of trees per unit area, related to canopy cover, was counted for all selected georeferenced aerial photographs from 2005 to calibrate and confirm the visual interpretation. The photos were then assigned to the respective canopy cover class (Table 4.3).

Fig. 4.2 shows some examples of the defined forest classes in the aerial photographs with their crown cover derived from field data. A decrease in tree crown size is visible in the images from left to right (Fig. 4.2). However, the crowns of the 45 % and 30 % crown cover have a similar appearance. This analysis facilitated the definition of different forest classes namely "forest with more than 50 % canopy cover" and "forest with less than 50 % canopy cover".
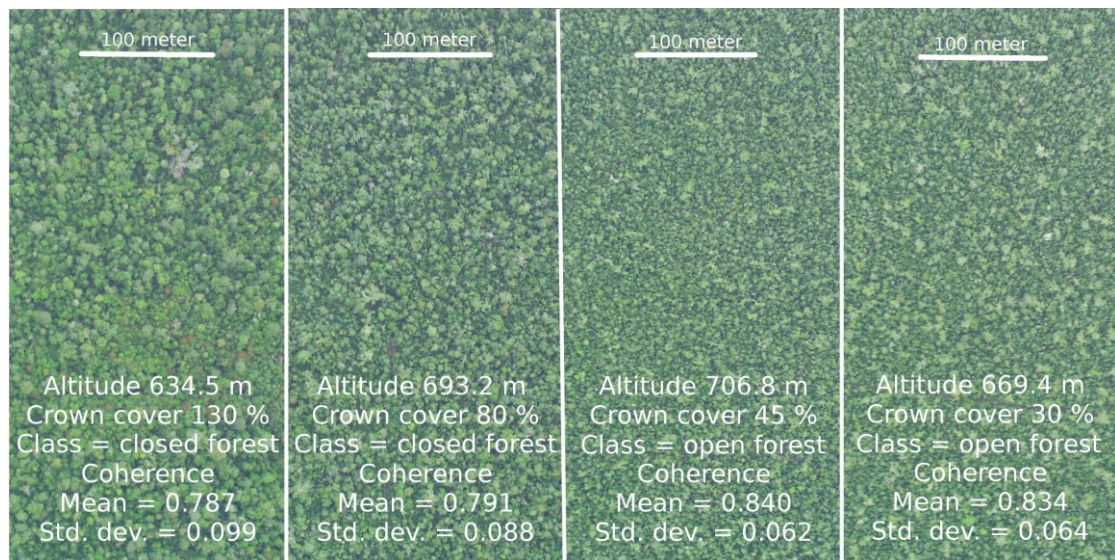
Fig. 4.2: Aerial photographs & crown cover of field transects

The photos from 2011 were used, together with those from 2005, for the assessment of the classes "Water bodies", "Wetlands", "Shrubland" and "Grassland" where oblique view was acceptable for interpretation. In total 361 training samples have been interpreted which are distributed to the defined classes as follows, where the number in parentheses behind each respective class represents the individual number of training samples. Suitable training polygons for the classes "open forest" (88) and "closed forest" (84) were selected based on the interpretation of the aerial photographs from 2005. Training polygons for the classes "grassland" (57), "shrubland" (61), "wetlands" (33) and "water bodies" (38) were selected based on a combination of the aerial photographs from 2011 and 2005.

4.3.2 Feature extraction and segmentation

The active and passive amplitudes were computed from the two complex TanDEMX CoSSC datasets with a multi-looking of 3 in range and 2 in azimuth, respectively. This resulted in a resolution of about 6 m in both directions. To evaluate the difference and information content of active and passive amplitudes, the ratio of the intensities (amplitudes^2) was calculated. A mean value filter with a kernel size of 7 x 7 was applied to both amplitudes in order to reduce the noise of their ratio. The 7 x 7 kernel size was considered to be best by visual interpretation to suppress noise while preserving resolution. The complex interferometric phase was derived via the multiplication of the first complex image with the complex conjugate of the second complex image. The phase of the flat earth was removed. Furthermore, the interferometric coherence was estimated with the following equation:

$$\blacksquare$$

(4.1)

where s_i denote complex image i, the brackets mean ensemble average and vertical lines are for magnitude of complex data (Rosen et al. 2000). All features were geocoded using the orbit parameters and the DEM (digital elevation model) derived from the interferometric analysis of the TanDEM-X data and resampled to a pixel size of 5 m using 4th cubic convolution method. Previous studies showed the geometric accuracy of TerraSAR-X using a high-precision DEM (Reinartz et al. 2011).

Sanden & Hoekman (1999) suggest that the textural information of highresolution X-band images is more useful than backscatter for tropical forest classification. Texture measures were used in this study in order to increase class separability (Dekker 2003). Therefore, the co-occurrence texture measures mean, variance, dissimilarity, homogeneity, contrast, entropy, second moment and correlation, as described by Haralick et al. (1973), were derived from the active amplitude. Additionally, the coefficient of variation was estimated. A kernel size for all texture measurements of 5 x 5 was used. The images were processed in the R environment (R Core Team 2013) with the help of additional packages called "raster" (Hijmans 2013), "rgdal" (Keitt et al. 2013), and "sp" (Bivand et al. 2008).

In order to improve the feature estimates the use of object-based approaches is more appropriate than pixel based processing, bearing in mind that due to the high resolution of the data, details such as logging gaps are still captured. For this, the multi-resolution segmentation (Baatz & Schaepe 2000) within the eCognition software was used. The data were segmented using all derived SAR features and the following parameters: scale parameter 40, shape 0.05 and compactness 0.95. The mean values of the image objects for each feature were exported for further statistical analysis in the R environment.

4.3.3 Feature selection

A separability analysis and feature selection was performed in order to assess the contribution of the derived features to class separability. More specifically, the relevance of the TanDEM-X bistatic SAR parameters in comparison to monostatic parameters, as available from TerraSAR-X, was investigated with this analysis.

The fact that amplitudes, and their derived features, generally do not follow a normal distribution (Gao 2010) and are well correlated leads to the choice of a non-parametric feature selection approach based on a random forest decision tree algorithm (Breiman 2001). The feature importance within the random forest algorithm was calculated by the so called z-score, which is the normalization of the raw importance. However, according to Kursa et al. (2010), the correlation of prediction variables leads to difficulties in the feature selection process within the random forest algorithm. The Boruta algorithm was developed to account for these shortcomings by assessing the importance of the input features compared to

random features (Kursa & Rudnicki 2010, Kursa et al. 2010). Each feature that has a higher importance than a random feature is considered to be important and the algorithm is repeated several times (Kursa et al. 2010).

Tab. 4.4: Overview of the used feature sets (features in classification used in bold)

Monostatic feature set	Bistatic feature set
Active amplitude	**Active amplitude**
	Passive amplitude
	Ratio of active and passive amplitude
Textures of active amplitude	Textures of active amplitude
Coefficient of variation	**Coefficient of variation**
Mean	**Mean**
Variance	Variance
Dissimilarity	Dissimilarity
Homogeneity	Homogeneity
Contrast	Contrast
Entropy	Entropy
Second moment	Second moment
Correlation	**Correlation**
	Interferometric coherence

The feature selection was performed using image object information of the training objects (see Section 4.3.1). Table 4.4 summarizes the monostatic and bistatic feature set constellation, whereas the bistatic feature set included all available variables. The feature selection was conducted for both feature sets respectively. Note that conclusions concerning feature relevance were drawn based on all features as listed in Table 4.4 (Bistatic feature set).

4.3.4 Feature analysis of open and closed forest class

In addition to the automatic feature selection, the separability of the classes "open forest" and "closed forest" was analyzed with the box plot method for the most important features using the training objects of the respective classes. The box-plots can indicate an overlap between classes in specific features. The Jeffries-Matusita Distance between the two forest classes was calculated for each feature in order to statistically evaluate the class overlap and separation. This statistical test describes the similarity of class distributions and reveals the class differences for each feature

(Richards & Jia 2006). It is bounded between 0 and the square root of 2, whereas higher values mean larger separability.

Mean and standard deviation for each field plot within the transects were calculated for each SAR feature. The differences of feature means and their standard deviation have been analyzed with respect to their corresponding field measured crown cover. This facilitated the information, which derived feature is particularly well suited to separate the different canopy cover classes related to the crown cover.

4.3.5 Classification

An object-based classification was conducted with the automatically ranked most important features based on the random forest selection. Two feature sets built the basis for the benchmark of the monostatic and bistatic constellation. The first feature set was composed of the most important monostatic features, active amplitude and the derived textures, such as coefficient of variation, correlation, mean and entropy for the "monostatic classification". The second feature set consisted of the same features as the monostatic constellation apart from entropy which was replaced by the single-pass interferometric coherence which is only available from a bistatic acquisition. The classification using these five features is therefore called "bistatic classification" in the following discussion. Hence, both classifications consisted of five features resulting in the same feature space dimensionality to allow comparison of their accuracies. The features used for the classifications are listed in Table 4.4 in bold.

A parametric maximum likelihood classifier was used for the object based classifications. On one hand maximum likelihood classifier achieves satisfactory results, on the other because it is relatively easy to interpret and simple (Waske & Braun 2009). Furthermore, the impact of the most relevant features on classification accuracies was investigated. Therefore, classifications with all features and with the amplitude and coherence alone were performed in addition to the classifications with the most important features. The training and testing of the classifications were performed on image object level. The same set of training samples was used as input for the feature selection and training of the classifications.

4.3.6 Accuracy analysis

The accuracy of the classifications was assessed using a stratified random sampling approach. Objects selected by this sampling process were interpreted via the aerial photographs. The photos from 2005 were used for evaluating the forest classes. The combined photos from 2005 and 2011 were used for the other classes. A total of 481

objects were analyzed for the accuracy assessment. Training areas were buffered with 100 m and validation objects were distributed outside the buffered areas. Therefore, training areas were spatially separated from the validation objects and thus excluded from the accuracy assessment to avoid any bias. The same sampled objects were used to compare the classifications of monostatic versus bistatic features.

This accuracy assessment resulted in objective and comparable accuracy measures. However, differences in spatial details cannot be evaluated in this way. Therefore, a quantitative analysis using a fuzzy similarity measurement was performed which takes not only the thematic class agreement between maps but also the spatial pattern into consideration. This provides a comparison of differences in spatial patterns of monostatic and bistatic classification as can be delivered by visual interpretation. The method assumes that the examined pixel is affected by its neighbors (Hagen 2003, Hagen-Zanker 2006) and is according to Walker et al. (2010) particularly suitable when the compared maps are based on different sources. This was the case in the comparison of monostatic and bistatic classification due to different feature sets. A two-way comparison was applied to avoid an overestimation of the similarity (Hagen 2003). The similarity measure ranges between 0 % and 100 %, of which 0 % indicates totally different and 100 % indicates totally identical maps. Different kernel sizes (1 x 1, 3 x 3, 5 x 5, 7 x 7, 9 x 9, 11 x 11) for the consideration of the spatial patterns were considered to obtain a kind of a confidence interval (Walker et al. 2010). The application is implemented in the Dinamica EGO software (Soares-Filho et al. 2012).

4.4 Results

4.4.1 Coherence for distinguishing forest classes

Difference in tree canopy structure and crown coverage can be seen in the photographs matching the field plots (Fig. 4.2). The extracted mean value of the interferometric coherence within the field plots was 0.787 at 130 % crown cover. The coherence increased to 0.791 at 80 %, to 0.84 at 45 %, and showed a similar value of 0.834 compared to the latter at 30 %.

The visual analysis of the box-plots of the interferometric coherence showed that there is no overlap between the forest canopy cover classes in the training dataset (Fig. 4.3). In contrast, the active amplitude showed an overlapping area of the two classes at about -9 dB. The coherence had an overall mean of 0.78 within the whole image and a standard deviation of 0.12. The active amplitude had a mean of -9.46

decibels (dB) and standard deviation of 3.51. The statistcal test proved the interpretation of the box-plots. The interferometric coherence achieved a JeffriesMatusita Distance of 1.1, whereas the active amplitude had a distance of 0.45.
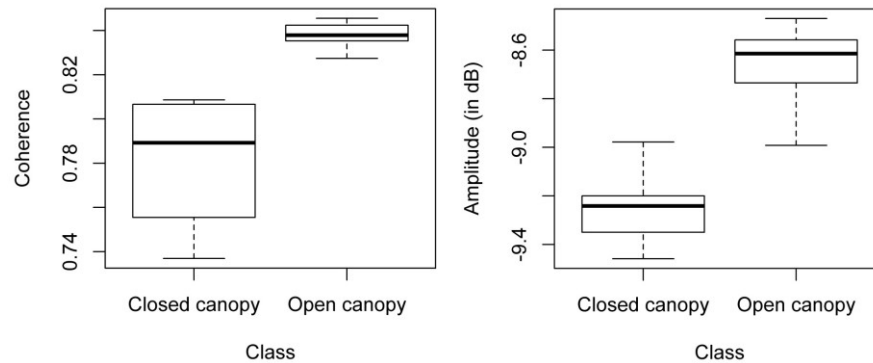
Fig. 4.3: Box plots of forest canopy classes for coherence (left) & active amplitude (right; white boxes = 1st and 3rd quantile; black line = median, outer lines = 1.5 x inner quartile range)

The textures showed, similarly to the amplitude, an overlap between the two canopy classes. The texture features achieved Jeffries-Matusita Distances between 0.35 and 0.6. The amplitude ratio had the lowest Jeffries-Matusita Distance between the two forest canopy cover classes of 0.25. The interferometric coherence achieved the highest distance between the two classes and is therefore the only feature substantially separating open and closed forest classes.

4.4.2 Analysis of feature selection

The applied feature selection (see Section 4.3.3) demonstrated that the interferometric coherence was the most important feature in the separation of all thematic classes. Coherence achieved the highest z-score of 1.6 on average, while texture features considerably increased class separability (Fig. 4.4). The coefficient of variation (CoV) was the most important texture feature and second most important overall with a mean z-score of 1.3.

All selected features proved to be more important than the random features generated by the Boruta algorithm. The active amplitude, the passive amplitude and the ratio scored a feature importance of 1.2, 1 and 0.6, respectively. This indicated that active and passive amplitude and their ratio contributed far less to the class separability than the coherence. The difference in the importance of coefficient of
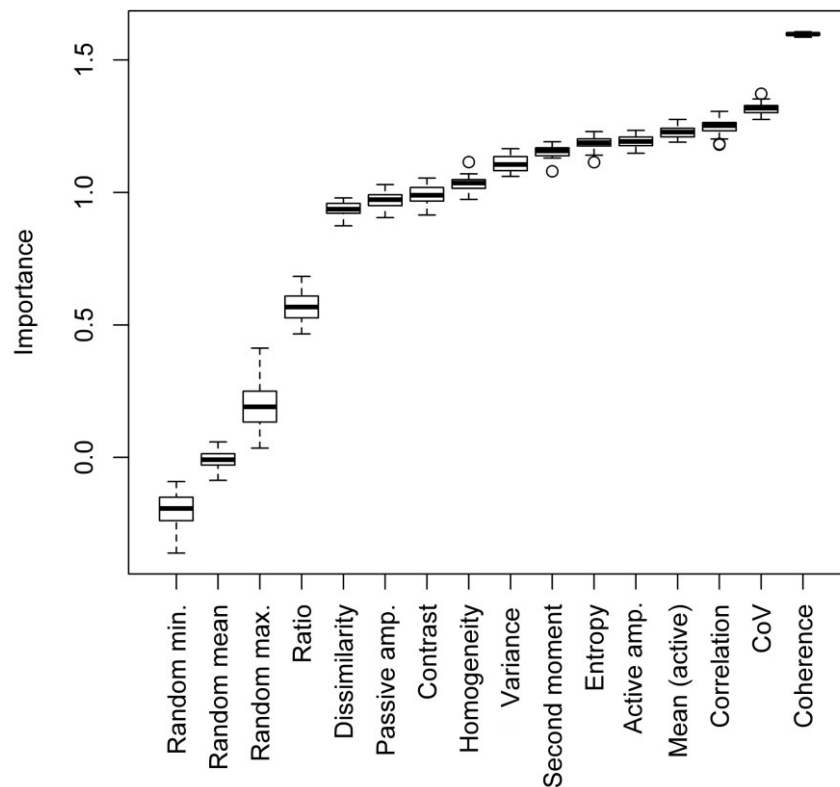
Fig. 4.4: Overview of random forest selection (illustrated by z-score)

variation as 2nd most important and dissimilarity as 12th most important feature was 0.3. This was the same as the distance between the coherence as the most important feature and the 2nd most important feature. This implied that coherence was, by far, the most important. The other features do not differ substantially in their contribution to the class separability, except the ratio, which had the lowest importance.

4.4.3 Classification results

With an overall accuracy of 85 % the bistatic classification was 10 % more accurate than the classification using monostatic features. Considering the categories for Kappa values proposed by Landis & Koch (1977), the bistatic classification achieved a very good result, whereas the monostatic classification achieved a good result. The classification with bistatic features yielded more accurate results in each class than the classification with the monostatic features (Table 4.4) except for the user's accuracy of wetlands (Table 4.5). For forest classes, the commission errors were particularly lower in the bistatic classification, by 14 % and 16 %, respectively. The omission errors were 17 % lower for the open canopy forest than in the monostatic case. This implied that the coherence was suitable to detect two different canopy cover classes in peat forests. Confusion between shrubland and forest (open)

occurred in the monostatic classification, where 11 objects were misclassified as open canopy forest. Therefore, the producer's accuracy of the shrubland class was 59 %.

This could be improved to 94 % by adding the coherence to the classification (Table 4.5).

Tab. 4.5: Comparison of classification accuracies with 95 % confidence interval of

	Forest (open)	Forest (closed)	Grassland	Shrubland	Wetlands	Water bodies	User's racy (in %)
Forest (open)	127 (100)	17 (23)	2 (3)	0 (11)	0 (0)	0 (0)	■
Forest (closed)	9 (32)	130 (126)	0 (1)	0 (0)	0 (2)	0 (0)	94±4 (78±7)
Grassland	3 (7)	0 (0)	57 (55)	1 (2)	1 (1)	0 (0)	92±7 (85±8)
Shrubland	11 (13)	1 (2)	6 (4)	32 (20)	1 (1)	0 (0)	63±13 (50±16)
Wetlands	8 (6)	8 (5)	3 (5)	1 (1)	30 (25)	0 (0)	60±14 (61±14)
Water bodies	0 (0)	0 (0)	1 (1)	0 (0)	0 (0)	32 (31)	97±6 (97±6)
Prodcuer's accuracy (in %)	■	■	■	■	■	■	Overall ■ in % Kappa: 0.84±0.03 (0.73±0.04)

bistatic & monostatic classification (in brackets).

accu-

acc.

The image segmentation resulted in objects with a minimum size of an image object of 300 m², whereas the mean size of the image objects was 5,000 m². In general, both classification results showed a similar land cover distribution (Fig. 4.5). The fuzzy similarity analysis to quantify the difference between the results demonstrated that the spatial pattern of the two classifications had an agreement of 72.7 % using 1 x 1 kernel to 75.5 % using 11 x 11 kernel. The classification using bistatic features was less noisy compared to the monostatic case and, showed at the same time a higher level of detail. The bistatic classification result clearly indicated degradation patterns within the closed canopy forest which was classified correctly as open canopy forest (at approximately $2°10^0$ S, $114°28^0$E, Fig. 4.5 subset). These

were classified as closed forest in the monostatic classification with randomly scattered small scale patches of open forest canopy.

A classification with two features (active amplitude and coherence) achieved an accuracy of 71 %, which was improved to 85 % by the addition of the textures coefficient of variation, mean, and correlation. This considerable improvement in classification accuracy suggests that texture can add additional information content complementing the bistatic feature set. More generally it confirms that textural information is useful in the classification of tropical forests (Sanden & Hoekman 1999). In comparison a classification with all derived features resulted in an accuracy of 81 %.
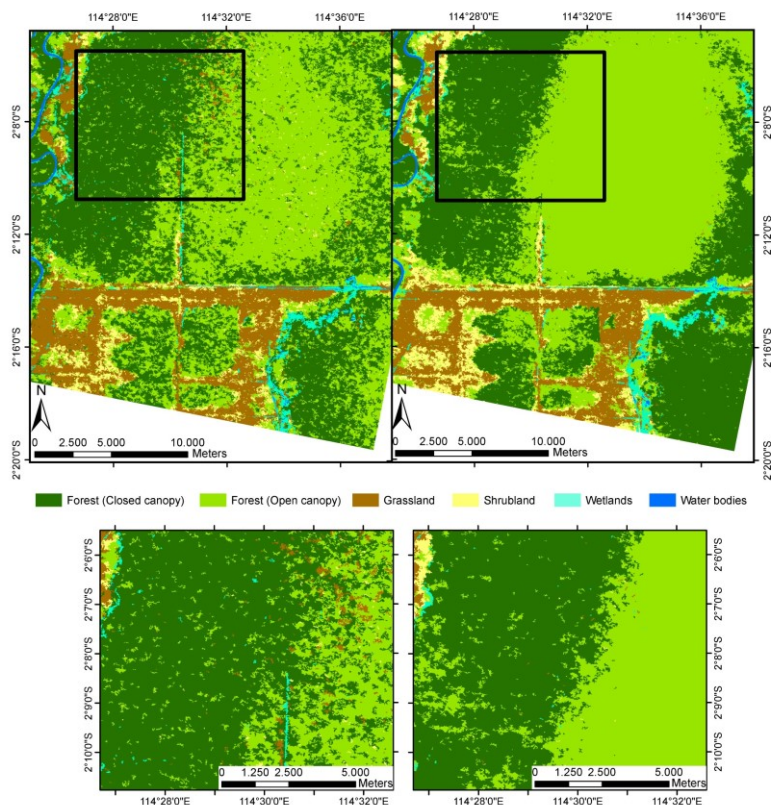
Fig. 4.5: Detailed overview of classification results with monostatic (left) & bistatic features (right)

4.5 Discussion

4.5.1 Feature importance

The quasi simultaneous acquisition of TanDEM-X image pairs result in neglectable temporal decorrelation. Thus, TanDEM-X coherence is mainly governed by volume decorrelation and noise, which in turn is influenced by the height of volume scatterers (like trees in forests) and their structure. Therefore, Caicoya et al. (2012) demonstrated the possibility of tree height derivation from TanDEM-X coherence

via inversion of the Random Volume over Ground Model (RVoG, Papathanassiou & Cloude 2001) in boreal forests. However, RVoG model inversion requires appropriate assumptions, as it is designed to describe volume decorrelation using PolInSAR (polarimetric interferometry) features, while for operational TanDEM-X acquisition only HH polarization is available. Appropriate assumptions were derived by comparison of modeled versus LiDAR height measurements (Caicoya et al. 2012).

In this study, the interpretation of coherence with field data indicates that there is a relationship between interferometric coherence and crown cover. This suggests that the coherence is also useful in describing the forest structure apart from tree height. Forest structure information can be used directly in land cover and forest surveys. This analysis supports the assumption that the coherence decreases with higher crown coverage, since the electromagnetic waves interact with a denser volume (i.e. more leaves in tree crowns) and, thus, volume decorrelation occurs. If the crown coverage is low, then the probability that the wave interacts with branches, twigs and stems due to side looking geometry is higher compared to cases of higher coverage. This results in a higher proportion of direct and multiple returns compared to volume interaction and thus less volume decorrelation. This suggests the conclusion that the bistatic coherence contains information about the vegetation structure. However, the sensitivity is limited as the coherence ranges between 0.79 and 0.84 whereas crown coverages differ by 100 %.

Several studies have examined the use of coherence from repeat pass constellations to improve class separability and achieved higher classification accuracies compared to classifications without the interferometric coherence. Most of these studies used the coherence only for the separation of vegetation and other land cover classes or forest/non-forest (Bruzzone et al. 2004, Perko et al. 2011, Strozzi et al. 2000). Differentiation between vegetation classes is not successful with repeat-pass X-band coherence due to the temporal decorrelation (Perko et al. 2011). The X-band coherence over vegetation is generally very low and does not show differences in vegetation type since it is dominated by temporal decorrelation. Therefore, it is only possible to separate between vegetation and non-vegetation in the best case (Perko et al. 2011).

Our results suggest that the single-pass interferometric coherence is suitable to substantially distinguish between at least two different canopy cover degrees in peat forests. Furthermore, it is assumed that this feature is helpful in separating the shrubland and grassland class from forest classes due to the lower volume decorrelation of grasses and shrubs in comparison to trees, thus improving the classification accuracy. The feature selection shows that the interferometric

coherence is the most important feature. This is confirmed by the classification results benchmarking a feature set using coherence against one without coherence.

The bistatic features, passive amplitude and ratio, had a low contribution to the separability in contrast to the coherence. Thus, it could be assumed that the angular difference of the two satellites in the operational TanDEM-X acquisition is not sufficient to achieve an improvement in classification when using bistatic scattering coefficients as proposed by Dubois-Fernandez et al. (2006) using an angular difference of 0.1°. This could be expected since the angular difference of an operational TanDEM-X acquisition is approximately only a tenth up to a hundredth of that used in Dubois-Fernandez et al. (2006). Therefore, the improvement in information content using the bistatic scattering coefficient is marginal. In contrast, texture measurements improved the separability and the overall accuracy substantially. They contribute information for class separability and some were ranked with a higher importance in a feature selection than the amplitude. Especially when using highresolution monostatic SAR data texture was proved to be very important to improve class separability. However, the classification with monostatic constellation showed that the texture measurements were not able to distinguish the forest classes substantially. Even considering that quantitative evaluation (e.g. box plots) did not show the difference in class separation between bistatic coherence and other features so clearly, visual analysis of the classification result exhibits that small scale degraded areas can only be detected using the coherence. The degraded patches were subordinate to the noise of small scale misclassifications in the monostatic constellation including the textures.

The classification with all derived features achieved an accuracy of 81 % and therefore, was 4 % less accurate compared to the classification with the most important features from the bistatic set (85 %). Hence, it could be argued that some derived features contained disinformation which decreases the separability of the classes and the resulting accuracy.

4.5.2 Classification results

The 10 % higher classification accuracy indicates the importance of the interferometric coherence compared to the classification without coherence and its contribution to improved class separability. Due to the fact that temporal decorrelation is neglectable for operational TanDEM-X bistatic acquisitions the coherence is mainly influenced by volume decorrelation and noise in flat terrain areas. This study suggests that volume decorrelation is influenced by the structure and height of the volume and tree canopy coverage. However, a similar classification in strong relief could be more vulnerable to misclassifications whereas this study

area is flat (Hajnsek et al. 2009), and thus other sources of decorrelation as layover or shadow could be avoided. Furthermore, the coherence is also dependent on the effective baseline. A shorter baseline results in a high level of coherence, even over forest areas, which limit the sensitivity to the canopy coverage and differences in land cover. Larger baselines result in a larger range of coherence values which is advantageous for classification purposes, whereas too large baselines can result in total decorrelation (Krieger et al. 2010).

The use of aerial photographs from 2005 for the generation of the training areas for the classes open and closed forests and their validation, could lead to inconsistencies due to the time difference to the TanDEM-X acquisition. The field transects could not cover the whole range of canopy cover and understory could cause misinterpretations. Furthermore, the estimation of the number of trees per unit area and the interpretation of the appearance of the crowns via the aerial photos can be misleading. Trees hidden by larger trees cannot be differentiated in the photos and omission errors arise when smaller trees are growing close to large trees and thus cannot be detected as an individual tree. However, the photo interpretation may be considered as sufficient for classifying the photos into two classes and not continuous canopy cover values.

Besides these sources of possible uncertainty, our results show that the X-band single-pass interferometric coherence can discriminate substantially open or degraded forest from closed undisturbed forest. In contrast, Santos et al. (2010) were not only able to separate forest from pasture and bare soil with dual-polarimetric TerraSAR-X data, but have also observed confusion between primary forest and degraded forest and have achieved an overall accuracy of 76 % and a kappa of 0.67 in the Brazilian Amazon. Even when using L-band from ALOS PALSAR Morel et al. (2011) found confusion between degraded and intact forest on Borneo. Longepe et al. (2011) also reported confusion between regrowth, plantations and intact forest with ALOS PALSAR on Sumatra.

Confusion between disturbed or peat swamp forest regrowth with primary peat swamp forest and with agriculture was observed in classifications with the optical Landsat sensor in other studies (e.g. Wijedasa et al. 2012). Although overall accuracies of 77 % - 86 % were achieved in classifications of peat swamp forests in Sundaland, the user's accuracy for the disturbed peat swamp forest class only achieved 53 % - 59 % (Wijedasa et al. 2012). The use of coarser scale data such as MODIS to map peat swamp forests of Indonesia achieved an accuracy of 82 % 85 % (Miettinen et al. 2008, Miettinen et al. 2012). Nevertheless, Wijedasa et al. (2012) suggested that smaller peat swamp forest fragments can be overlooked due to the moderate resolution of the MODIS data. In addition, using optical sensors can result

in data gaps caused by the high degree of cloud cover in the tropical area (Nezry et al. 1993). Creating composites by multi-temporal images could indeed reduce the gaps in the data, but it can lead to inconsistencies through possible changes between the acquisitions. Even with the use of composite mosaics, consisting of up to 4 or more images, there were still gaps of 7.8 % - 10.3 % of the study area (Wijedasa et al. 2012). Another possibility is the synergetic use of optical and SAR data (Erasmi & Twele 2009, Lehmann et al. 2012).

However such an approach consumes a lot of resources regarding data and processing time. TanDEM-X on the other hand, exhibits the advantage of weather and day/night independence. Profiting from the on-going TanDEM-X mission objectives aiming to produce a homogeneous and globally consistent, high resolution DEM, the interferometric TanDEM-X data could be used as a consistent data source for mapping and monitoring tropical forests.

4.6 Conclusions

The bistatic features from the TanDEM-X mission can significantly improve the separability of forest cover and forest density, namely forest classes with more and less than 50 % canopy cover. From all parameters investigated, the single-pass interferometric coherence proved to be the most important feature for class separability. A non-parametric random forest feature selection confirmed this result.

Due to the correlation of interferometric coherence with canopy cover, it is possible to derive more spatial detail at a higher accuracy, which is important, for example, in forest degradation mapping. In addition, the classification including bistatic features is less noisy compared to monostatic features only. This leads to an increase in the overall classification accuracy by more than 10 %, resulting in an overall accuracy of 85 %. The accuracies from a classification including coherence were superior in every class compared to a classification without coherence. Improvements have been observed especially in the differentiation between the forest cover classes as well as between shrublands and forest land. In contrast, the passive amplitude and ratio of active and passive amplitude did not improve the classification results. This suggests the conclusion that the angular difference between the two sensors is not suitable to increase the information content and class separability via a bistatic scattering coefficient.

The IPCC (2003) recommends, in its good practice guidance for LULUCF the separation of forest land in open and closed canopy forest. Distinguishing between these two forest classes is relevant in the monitoring of forest degradation. It is of

key importance for national carbon accounting and REDD projects to reduce the uncertainty in the estimation of carbon stock changes (GOFC-GOLD 2012). Therefore, the globally available high resolution bistatic dataset from the TanDEMX mission is considered an important contribution for baseline mapping for the years 2011 - 2013 in LULUCF and in REDD measurement, reporting and verification concepts.

Acknowledgments

References

Aldhous, P. (2004). Borneo is burning. *Nature*, 432, 144–146.

Baatz, M. & Schaepe, A. (2000). Multiresolution segmentation - An optimization approach for high quality multi-scale image segmentation. In: Strobl, J., Blaschke, T. & Griesebner, G. (Eds.): *Angewandte geographische Informationsverarbeitung XII. Beitraege zum AGIT-Symposium Salzburg 2000* . Wichman: Heidelberg, 12–
23.

Bamler, R. & Hartl, P. (1998). Synthetic aperture radar interferometry. *Inverse Problems* (4), 14, R1–R54.

Bivand, R. S., Pebesma, E. J. & Gomez-Rubio, V (2008). *Applied spatial analysis with R*. Springer: New York.

Boehm, H.-D. & Siegert, F. (2001). Ecological impact of the onemillion hectare rice project in Central Kalimantan, Indonesia, using remote sensing and GIS. Land use change and (Il)-legal logging in Central Kalimantan, Indonesia. In: *22nd Asian Conference on Remote Sensing, 5-9 November 2001*.

Breidenbach, J., Ortiz, S. M. & Reich, M. (2010). Forest monitoring with TerraSARX: first results. *European Journal of Forest Research*, 129, 813–823.

Breiman, L. (2001). Random Forests. *Machine Learning* (1), 45, 5–32.

Bruzzone, L., Marconcini, M., Wegmuller, U. & Wiesmann, A. (2004). An advanced system for the automatic classification of multitemporal SAR images. *IEEE Transactions on Geoscience and Remote Sensing* (6), 42, 1321–1334.

Caicoya, A. T., Kugler, F., Hajnsek, I. & Papathanassiou, K. (2012). Boreal forest biomass classification with TanDEM-X. In: *IEEE International Geoscience and Remote Sensing Symposium (IGARSS), 2012,*3439–3442.

Castro, K. L., Sanchez-Azofeifa, G. A. & Rivard, B. (2003). Monitoring secondary tropical forests using space-borne data: Implications for Central America. *International Journal of Remote Sensing* (9), 24, 1853–1894.

Cloude, S. R. & Pottier, E. (1997). An entropy based classification scheme for land applications of polarimetric SAR. *IEEE Transactions on Geoscience and Remote Sensing* (1), 35, 68–78.

Dekker, R. (2003). Texture analysis and classification of ERS SAR images for map updating of urban areas in The Netherlands. *IEEE Transactions on Geoscience and Remote Sensing* (9), 41, 1950–1958.

Del Frate, F., Pacifici, F. & Solimini, D. (2008). Monitoring Urban Land Cover in Rome, Italy, and Its Changes by Single-Polarization Multitemporal SAR Images. *IEEE Journal of Selected Topics in Applied Earth Observations and Remote Sensing* (2), 1, 87–97.

Dubois-Fernandez, P., Cantalloube, H., Vaizan, B., Krieger, G., Horn, R., Wendler, M. & Giroux, V. (2006). ONERA-DLR bistatic SAR campaign: planning, data acquistiton, and first analysis of bistatic scattering behaviour of natural and urban targets. *IEE Proceedings - Radar, Sonar and Navigation* (3), 153, 214– 223.

Engdahl, M. & Hyyppa, J. (2003). Land-cover classification using multitemporal ERS-1/2 InSAR data. *IEEE Transactions on Geoscience and Remote Sensing* (7), 41, 1620–1628.

Erasmi, S. & Twele, A. (2009). Regional land cover mapping in the humid tropics using combined optical and SAR satellite data - a case study from Central Sulawesi, Indonesia. *International Journal of Remote Sensing* (10), 30, 2465– 2478.

European Space Agency (2012). *ESA declares end of mission for ENVISAT*. http://www.esa.int/Our Activities/Observing the _Earth/Envisat/ ESA declares _end of _mission for _Envisat: Last access: March 02, 2013.

FAO (2000). *FRA 2000. On definitions of forest and forest change. Forest Resources Assessment Programme Working Paper 33*. FAO: Rome.

Fritz, T. (2012). *TanDEM-X. Ground Segment. TanDEM-X Experimental Product Description. Issue: 1.2*. Deutsches Zentrum fuer Luft- und Raumfahrt (DLR): Oberpfaffenhofen.

Gao, G. (2010). Statistical modeling of SAR images: A survey. *Sensors* (1), 10, 775– 795.

Gibbs, H. K., Brown, S., Niles, J. O. & Foley, J. A. (2007). Monitoring and estimating tropical forest carbon stocks: making REDD a reality. *Environmental Research Letters*, 2, 1–13.

GOFC-GOLD (2012). *A sourcebook of methods and procedures for monitoring and reporting an-thropogenic greenhouse gas emissions and removals associated with deforestation, gains and losses of carbon stocks in forests remaining forests, and forestation. GOFC-GOLD Report version COP18-1*. Wageningen University: Wageningen.

Hagen, A. (2003). Fuzzy set approach to assessing similarity of categorical maps. *International Journal of Geographical Information Science* (3), 17, 235–249.

Hagen-Zanker, A. (2006). Map comparison methods that simultaneously address overlap and structure. *Journal of Geographical Systems* (2), 8, 165–185.

Hajnsek, I. & Hoekman, D. H. (2005). *Final Report, INDREX II - Indonesian Radar Experiment Campaign over Tropical Forest in L- and P-band, Version 1, 14 June 2006, ESA Contract RFQ/3-11077/04/NL/CB, Report ESA*. DLR and Wageningen University: Wageningen.

Hajnsek, I., Kugler, F., Lee, S.-K. & Papathanassiou, K. (2009). Tropical-ForestParameter Estimation by Means of Pol-InSAR: The INDREX-II Campaign. *IEEE Transactions on Geoscience and Remote Sensing* (2), 47, 481–493.

Hanssen, R. (2001). *Radar interferometry: data interpretation and error analysis*. Kluwer Academic: Dordrecht.

Haralick, R., Shanmugam, K. & Dinstein, I. (1973). Textural Features for Image Classification. *IEEE Transactions on Systems, Man and Cybernetics* (6), 6, 610–621.

Hijmans, R. J. (2013). *raster: Geographic data analysis and modeling*. http://CRAN.R-project.org/package=raster: R package version 2.1-66.

Hoekman, D., Vissers, M. A. M. & Wielaard, N. (2010). PALSAR Wide-Area Mapping of Borneo: Methodology and Map Validation. *IEEE Journal of Selected Topics in Applied Earth Observations and Remote Sensing* (4), 3, 605–617.

Hooijer, A., Page, S., Canadell, J. G., Silvius, M., Kwadijk, J., Wosten, H. & Jauhiainen, J. (2010). Current and future CO_2 emissions from drained peatlands southeast Asia.. *Biogeosciences* (5), 7, 1505–1514.

IPCC (2003). *Good Practice Guidance for Land Use, Land-Use Change and Forestry*. IGES: Kanagawa.

Jauhiainen, J., Takahashi, H., Heikkinen, J. E. P., Martikainen, P. J. & Vasander, H. (2005). Carbon fluxes from a tropical peat swamp forest floor. *Global Change Biology* (10), 11, 1788–1797.

Keitt, T. H., Bivand, R., Pebesma, E. & Rowlingson, B. (2013). *rgdal: Bindings for the Geospatial Data Abstraction Library*. http://CRAN.Rproject.org/package=rgdal: R package version 0.8-14.

Krieger, G. & Moreira, A. (2006). Spaceborne bi- and multistatic SAR: potential and challenges. *IEEE Proceedings - Radar, Sonar and Navigation* (3), 153, 184– 198.

Krieger, G., Moreira, A., Fiedler, H., Hajnsek, I., Werner, M., Younis, M. & Zink, M. (2007). TanDEM-X: A Satellite Formation for High-Resolution SAR Interferometry. *IEEE Transactions on Geoscience and Remote Sensing* (11), 45, 3317–3341.

Krieger, G., Hajnsek, I., Papathanassiou, K., Younis, M. & Moreira, A. (2010). Interferometric Synthetic Aperture Radar (SAR) Missions Employing Formation Flying. *Proceedings of the IEEE* (5), 98, 816–843.

Kuntz, S. (2010). Potential of spaceborne SAR for monitoring the tropical environments. *Tropical Ecology*, 51, 3–10.

Kursa, M. B., Jankowski, A. & Rudnicki, W. R. (2010). Boruta–a system for feature selection. *Fundamenta Informaticae* (4), 101, 271–285.

Kursa, M. B. & Rudnicki, W. R. (2010). Feature Selection with the Boruta Package. *Journal of Statistical Software* (11), 36, 1–13.

Landis, J. R. & Koch, G. G. (1977). The measurement of observer agreement for categorical data.. *Biometrics* (1), 33, 159–174.

Lehmann, E. A., Caccetta, P. A., Zhou, Z.-S., McNeill, S. J., Wu, X. & Mitchell, A. L. (2012). Joint Processing of Landsat and ALOS-PALSAR Data for Forest Mapping and Monitoring. *IEEE Transactions on Geoscience and Remote Sensing* (1), 50, 55–67.

Longepe, N., Rakwatin, P., Isoguchi, O., Shimada, M., Uryu, Y. & Yulianto, K. (2011). Assessment of ALOS PALSAR 50 m Orthorectified FBD Data for Regional Land Cover Classification by Support Vector Machines. *IEEE Transactions on Geoscience and Remote Sensing* (6), 49, 2135–2150.

Miettinen, J., Wong, C. M. & Liew, S. C. (2008). New 500A m spatial resolution landˆ cover map of the western insular Southeast Asia region. *International Journal of Remote Sensing* (20), 29, 6075–6081.

Miettinen, J., Shi, C., Tan, W. J. & Liew, S. C. (2012). 2010 land cover map of insular Southeast Asia in 250-m spatial resolution. *Remote Sensing Letters* (1), 3, 11–20.

Morel, A. C., Saatchi, S. S., Malhi, Y., Berry, N. J., Banin, L., Burslem, D., Nilus, R. & Ong, R. C. (2011). Estimating aboveground biomass in forest and oil palm plantation in Sabah, Malaysian Borneo using ALOS PALSAR data. *Forest Ecology and Management* (9), 262, 1786 –1798.

Muhamad, N. Z. & Rieley, J. O. (2002). Management of tropical peatlands in Indonesia: Mega reclamation project in Central Kalimantan. In: Rieley, J. O., Page, S. E. & Setiadi, B. (Eds.): *Proceedings of the International Symposium on Tropical Peatland* . BPPT and Indonesian Peat association: Jakarta, 155–162.

Nezry, E., Mougin, E., Lopes, A. & Gastellu-Etchegorry, J. (1993). Tropical vegetation mapping with combined visible and SAR spareborne data. *International Journal of Remote Sensing*, 14, 2165–2184.

Nowak, D. J., Rowntree, R. A., McPherson, E., Sisinni, S. M., Kerkmann, E. R. & Stevens, J. C. (1996). Measuring and analyzing urban tree cover. *Landscape and Urban Planning* (1), 36, 49 –57.

Otukei, J. R., Blaschke, T., Collins, M. & Maghsoudi, Y. (2011). Analysis of ALOS PALSAR and TerraSAR-X data for protected area mapping: A case of the Bwindi Impenetrable National Park-Uganda. In: *IEEE International Geoscience and Remote Sensing Symposium (IGARSS), 2011*,348–351.

Page, S. E., Siegert, F., Rieley, J. O., Boehm, H.-D. V., Jaya, A. & Limin, S. (2002). The amount of carbon released from peat and forest fires in Indonesia during 1997. *Nature* (6911), 420, 61–65.

Papathanassiou, K. & Cloude, S. (2001). Single-baseline polarimetric SAR interferometry. *IEEE Transactions on Geoscience and Remote Sensing* (11), 39, 2352– 2363.

Perko, R., Raggam, H., Deutscher, J., Gutjahr, K. & Schardt, M. (2011). Forest Assessment Using High Resolution SAR Data in X-Band. *Remote Sensing* (4), 3, 792–815.

Pitz, W. & Miller, D. (2010). The TerraSAR-X Satellite. *IEEE Transactions on Geoscience and Remote Sensing* (2), 48, 615 –622.

R Core Team (2013). *R: A Language and Environment for Statistical Computing*. R Foundation for Statistical Computing: Vienna.

Reinartz, P., Muller, R., Schwind, P., Suri, S. & Bamler, R. (2011). Orthorectification of VHR optical satellite data exploiting the geometric accuracy of TerraSAR-X data. *ISPRS Journal of Photogrammetry and Remote Sensing* (1), 66, 124 –132.

Ribbes, F., Le Toan, T., Bruniquel, J., Floury, N., Stussi, N., Liew, S. & Wasrin, U. R. (1997). Forest mapping in tropical region using multitemporal and interferometric ERS-1/2 data. In: *Proceedings of 3rd ERS Symposium, 17-21 March, 1997*,vol. 3, 351–356.

Richards, J. A. & Jia, X. (2006). *Remote sensing digital image analysis: An introduction*. Springer: Berlin.

Rosen, P., Hensley, S., Joughin, I., Li, F., Madsen, S., Rodriguez, E. & Goldstein, R. (2000). Synthetic aperture radar interferometry. *Proceedings of the IEEE* (3), 88, 333 –382.

Saatchi, S. S., Soares, J. V. & Alves, D. S. (1997). Mapping deforestation and land use in amazon rainforest by using SIR-C imagery. *Remote Sensing of Environment* (2), 59, 191 –202.

Sanden, J. J. van der & Hoekman, D. H. (1999). Potential of Airborne Radar To Support the Assessment of Land Cover in a Tropical Rain Forest Environment. *Remote Sensing of Environment*, 68, 26 –40.

Santos, J. R., Mura, J. C., Kux, H. J. H., Garcia, C. E., Kuntz, S., Brown, I. F. & Pantoja, N. V. (2010). Classification of TerraSAR-X imagery for the characterization of Amazon tropical forests. In: *30th EARSeL Symposium: Remote Sensing for Science, Education and Culture,*vol. 31, 329–334.

Sgrenzaroli, M., Baraldi, A., De Grandi, G., Eva, H. & Achard, F. (2004). A novel approach to the classification of regional-scale Radar mosaics for tropical vegetation mapping. *IEEE Transactions on Geoscience and Remote Sensing* (11), 42, 2654–2669.

Simard, M., Saatchi, S. & De Grandi, G. (2000). The use of decision tree and multiscale texture for classification of JERS-1 SAR data over tropical forest. *IEEE Transactions on Geoscience and Remote Sensing* (5), 38, 2310–2321.

Simard, M., Grandi, G. D., Saatchi, S. & Mayaux, P. (2002). Mapping tropical coastal vegetation using JERS-1 and ERS-1 radar data with a decision tree classifier. *International Journal of Remote Sensing* (7), 23, 1461–1474.

Soares-Filho, B. S., Rodrigues, H. & Costa, W. (2012). *Modeling Environmental Dynamics with Dinamica EGO*. Sensoriamento Remoto/Universidade Federal de Minas Gerais: Belo Horizonte.

Stolz, R. & Mauser, W. (1995). First evaluations of Shuttle SIR-C and X-SAR data for landcover classifications. In: *International Geoscience and Remote Sensing Symposium, 1995. IGARSS '95. 'Quantitative Remote Sensing for Science and Applications',*vol. 2, 1058–1060.

Strozzi, T., Dammert, P., Wegmuller, U., Martinez, J.-M., Askne, J., Beaudoin, A. & Hallikainen, N. (2000). Landuse mapping with ERS SAR interferometry. *IEEE Transactions on Geoscience and Remote Sensing* (2), 38, 766 –775.

Stussi, N., Liew, S., Lim, H., Nichol, J. & Goh, K. C. (1997). Landcover classification using ERS SAR/INSAR data over coastal region of central Sumatra. In:
*Proceedings of 3rd ERS Symposium, 17-21 March, 1997,*vol. 3, 391–396.

Ullmann, T., Lumsdon, P., Poncet, F. v., Esch, T., Lang, O., Tinz, M., Kuntz, S. & Dech, S. (2012). Application of quadpolarimetric TerraSAR-X data for landcover characterization in tropical regions - A case study in South Kalimantan, Indonesia. In: *IEEE International Geoscience and Remote Sensing Symposium (IGARSS), 2012,*5133–5136.

Walker, W., Stickler, C., Kellndorfer, J., Kirsch, K. & Nepstad, D. (2010). LargeArea Classification and Mapping of Forest and Land Cover in the Brazilian Amazon: A Comparative Analysis of ALOS/PALSAR and Landsat Data Sources. *IEEE Journal of Selected Topics in Applied Earth Observations and Remote Sensing* (4), 3, 594–604.

Walterscheid, I., Ender, J., Brenner, A. & Loffeld, O. (2006). Bistatic SAR Processing and Experiments. *IEEE Transactions on Geoscience and Remote Sensing* (10), 44, 2710 –2717.

Waske, B. & Braun, M. (2009). Classifier ensembles for land cover mapping using multitemporal SAR imagery. *ISPRS Journal of Photogrammetry and Remote Sensing* (5), 64, 450 –457.

Watson, R. T., Noble, I. R., Bolin, B., Ravindranath, N. H., Verardo, D. J. & Dokken, D. J. (2000). *Land use, land use change and forestry*. Cambridge Univ. Press: Cambridge.

Wegmuller, U. & Werner, C. (1997). Retrieval of vegetation parameters with SAR interferometry. *IEEE Transactions on Geoscience and Remote Sensing* (1), 35, 18 –24.

Wegmuller, U. & Werner, C. (1995). SAR interferometric signatures of forest. *IEEE Transactions on Geoscience and Remote Sensing* (5), 33, 1153 –1161.

Wijedasa, L. S., Sloan, S., Michelakis, D. G. & Clements, G. R. (2012). Overcoming Limitations with Landsat Imagery for Mapping of Peat Swamp Forests in Sundaland. *Remote Sensing* (9), 4, 2595–2618.

Willis, N. (1991). *Bistatic Radar*. SciTech Publishing: Raleigh.

Woesten, J. H. M., Clymans, E., Page, S. E., Rieley, J. O. & Limin, S. H. (2008). Peat-water interrelationships in a tropical peatland ecosystem in Southeast Asia. *Catena* (2), 73, 212–224.

5 TanDEM-X data for aboveground biomass retrieval in a tropical peat swamp forest

M. Schlund[a,b], F. von Poncet[a], S. Kuntz[a], C. Schmullius[b] & D. H. Hoekman[c]

[a] *Airbus Defence and Space, Claude-Dornier-Str., 88090 Immenstaad, Germany* [b] *Department of Earth Observation, Friedrich-Schiller University, 07743 Jena, Germany* [c] *Dept. of Environmental Sciences,Wageningen University, Droevendaalsesteeg 4, 6708 PB Wageningen, The Netherlands*

Abstract

Forests play an important role in the global carbon cycle as a carbon sink. Deforestation and degradation of forests lead to carbon emissions, which should be prevented or minimized by protecting forests. Radar remote sensing has proven to be particularly useful to monitor forests especially in the tropics due to weather and daytime independence. Radar data from the TanDEM-X mission provide a potential opportunity to monitor large areas of tropical forests due to the multi-temporal global coverage and the high resolution.

Tropical peat swamp forests are difficult to access and thus high effort to conduct field measurements is necessary. Therefore, aboveground biomass was estimated from a limited amount of in-situ measurements of relatively undisturbed peat swamp forest and a LiDAR based canopy height model to achieve a representative amount of biomass estimates for radar analysis. The LiDAR and field measurements resulted in an identical estimate of mean biomass and thus provided a reliable

source to correlate with SAR (synthetic aperture radar) features from the TanDEM-X mission and ultimately up-scale the found relation to the entire study site.

The relationship of interferometric coherence of the bistatic TanDEM-X data showed a moderate to high correlation with the biomass (R^2 = 0.5) and RMSE of 53 t/ha corresponding to a biomass range from 183 to 495 t/ha. Thus, it could be used to indicate forest degradation areas, which are characterized by larger opening of the canopy cover and thus lower biomass. The results indicate that interferometric coherence is useful for quantification of aboveground biomass in tropical peat swamp forest. TanDEM-X coherence can at minimum serve as a stratification to assess spatial distribution of qualitative biomass classes in the context of REDD+ monitoring, reporting, and verification schemes and for the identification of forest degradation areas.

5.1 Introduction

Forests act as natural carbon storage and thus play an important role in the global carbon cycle and for climate change mitigation (Gibbs et al. 2007, Olander et al. 2008, Werf et al. 2009). The stored carbon is directly linked with the biomass of forests and can be converted to carbon stock using a factor of 50 % or less (Martin & Thomas 2011). Quantifying biomass and its change over time is a prerequisite to implement programs like REDD+ (Reducing Emission from Deforestation and Degradation). This program aims to incentivize the reduction of carbon emissions from deforestation and forest degradation and enhancement of carbon stocks in order to mitigate climate change. Tropical forests, especially peat swamp forests, and their soils store high amounts of carbon (Page et al. 2002, Page et al. 2011, Werf et al. 2009). According to Werf et al. (2009), the emissions from tropical peat swamp forests and their soils equal approximately 1/4 of the emissions of the total tropical forests. This demonstrates the significance of these ecosystems despite their relatively small extent compared to the overall tropical forest cover. Nevertheless, they are threatened by more frequent and stronger droughts due to climate change, deforestation and degradation, which can turn them to a tremendous source of carbon emissions (Page et al. 2002, Page et al. 2011).

Field measurements alone have limitations assessing biomass over large areas. Thus, for implementing REDD+ field work alone may not be feasible in many tropical countries due to the difficult accessibility, the large spatial extent and the variation of biophysical parameters in tropical forests. Thus, combinations of remote sensing and field measurements are recommended for REDD+, because of their ability to up-

3forest

scale the field measurements on a larger scale (Asner et al. 2009b, Gibbs et al. 2007). For instance, LiDAR (Light detection and ranging) sensors and algorithms based on those sensors for estimating biomass are successfully used in combination with field measurements (Asner et al. 2009b, Boehm et al. 2013, Gonzalez et al. 2010, Lefsky et al. 2005, St-Onge et al. 2008). However, LiDAR sensors are mostly airborne and thus relatively expensive compared to space borne data. Consequently, they will have a small spatial coverage compared to space borne sensors, resulting in limited consistency regarding large area surveillance and estimation of the biomass (Koch 2010, Koehl et al. 2011).

SAR (synthetic aperture radar) systems are an alternative for mapping and monitoring tropical forests consistently because of their weather and day/night independence (e.g. Kuntz 2010). The received signals from SAR sensors are not a direct measurement of aboveground biomass (Woodhouse et al. 2012). Instead it is found that the SAR signal correlates with biomass, since the electromagnetic wave penetrates the vegetation canopy and interacts with the vegetation constituents such as leaves, twigs, branches, and stems (Balzter 2001, Dobson et al. 1995, Le Toan et al. 1992, Saatchi et al. 2011b). Therefore, it has been shown that backscatter increases with the biomass up to signal saturation depending on wavelength (Balzter et al. 2007, Englhart et al. 2011, Mitchard et al. 2011). Systems with longer wavelengths such as L- and P-band sensors are considered more appropriate to determine biomass due to their greater penetration into the canopy, compared to X- and C-band sensors (Castro et al. 2003, Kasischke et al. 1997, Luckman et al. 2000, Saatchi et al. 1997). With L-band systems a saturation of the signal at biomass values around 100 to 150 t/ha is frequently observed (Kasischke et al. 1997, Luckman et al. 1998, Luckman et al. 2000, Mitchard et al. 2011). A saturation of C-band ERS sensors was found at about 30 to 50 t/ha (Castro et al. 2003, Gama et al. 2010, Luckman et al. 2000). A lower saturation threshold or no correlation was demonstrated with X-band data due to the shorter wavelength (Gama et al. 2010). Nevertheless, Englhart et al. (2011) found a saturation threshold of X-band amplitude data in tropical peat swamp forest of 80 t/ha.

However, not only radar backscatter can be correlated to aboveground tree biomass, but also the interferometric coherence can be regarded as a significant indicator of biophysical characteristics in forests (Luckman et al. 2000, Santoro et al. 2007, Schlund et al. 2014a). The interferometric coherence is a measure of the phase decorrelation and the quality of the interferometric estimates derived from two SAR acquisitions (Bamler & Hartl 1998). It is influenced by the baseline, the Doppler centroid frequency, the system noise, the SAR processing, and relevant

scene properties like temporal and volume decorrelation (Hanssen 2001, Wegmuller & Werner 1997). The coherence decreases with increasing biomass due to increased volume and potentially temporal decorrelation, which in turn are influenced by the spatial and temporal separation of the acquisitions (Balzter 2001). The interferometric coherence is correlated to biophysical parameters and thus enables modeling of biophysical forest parameters (Askne et al. 1997).

L-band coherence proofed to be related to growing stock volume in boreal forests (Eriksson et al. 2003). But also shorter wavelengths such as C-band have frequently been used to estimate growing stock volume using ERS data (Askne et al. 2003, Santoro et al. 2002, Santoro et al. 2007). Empirical models were applied with linear or exponential functions (Fransson et al. 2001, Wagner et al. 2003) as well as semiempirical models such as the water cloud model for the derivation of growing stock volume in boreal forests (Cartus et al. 2011, Santoro et al. 2002, Santoro et al. 2007). However, the relationship partially depends on weather conditions (e.g. moisture, frozen or thaw) and thus optimal acquisition conditions are necessary in order to achieve high accuracies, whereas the typically utilized ERS tandem data were inconsistent in their availability for large-scale applications (Cartus et al. 2011). In contrast to conventional spaceborne SAR missions, the bistatic TanDEM-X mission acquires multiple globally consistent single-pass interferometric datasets to create a highly accurate global digital elevation model (Krieger et al. 2007). The two SAR sensors of the TanDEM-X mission acquired data of the entire land mass several times during the lifetime of the mission, allowing a homogenous, large scale analysis at high spatial resolution.

In general, repeat-pass interferometric coherence of X-band sensors is low in vegetation (Perko et al. 2011) and thus not correlated with volume or biomass (Gama et al. 2010). The main reason is the temporal decorrelation. However, the temporal decorrelation can be minimized using the across-track interferometer TanDEM-X, which is one of the most significant advantages of the mission (Krieger et al. 2007). Initial analysis shows that TanDEM-X data are very useful to create highly accurate land cover mapping with different vegetation type classes. Classifications with TanDEM-X data achieved an accuracy of 85 % (Schlund et al. 2014a). The high accuracy is mainly based on the single-pass interferometric coherence, which can be used in classifications or quantitative estimations.

Caicoya et al. (2012) and Kugler et al. (2014) showed the potential to derive mean forest stand height based on the interferometric coherence from operational TanDEM-X mission and a LiDAR dataset by inverting the Random Volume over Ground model (RVoG). Nevertheless, the volume decorrelation and thus the

5*forest*

coherence are not only influenced by the height of the volume, but also by the structure of the volume. The size of the volume, which is equivalent to the height of the forest, and the structure are related to the biomass. Therefore, it can be concluded that the coherence can be directly correlated with the biomass. The correlation of the biomass with the interferometric coherence from TanDEM-X and the resulting potential for improvement in context of forest mapping and monitoring will be investigated in this study. Englhart et al. (2011) suggested a correlation with X-band backscatter for low biomass values. Thus, the backscatter of TanDEM-X in order to derive biomass will be investigated as well. Field measurements in combination with LiDAR data will be used in order to increase the number of observations to be correlated with the SAR measurements.

5.2 Data & study site

5.2.1 Study site

The study site in Central Kalimantan exhibits a flat terrain and is covered by tropical peat swamp forest limited through the Kapuas River in the West (Fig. 5.1). The provincial capital Palangkaraya is located about 60 km west of the study area. In general, the climate is humid tropic divided into a dry season from June to September and a wet season from October to May (Jauhiainen et al. 2005).
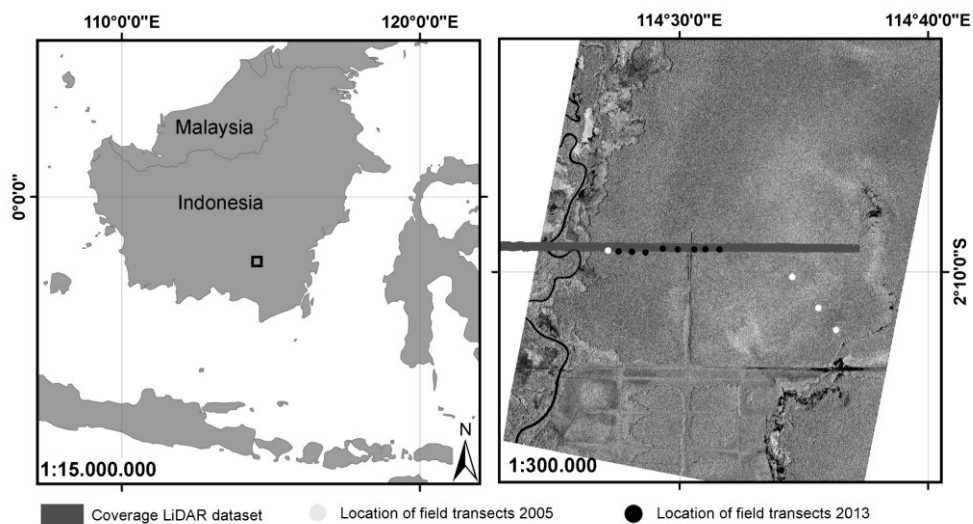
Fig. 5.1: TanDEM-X acquisition, LiDAR coverage and location of field measurements from 2005 (white dots) and 2013 (black dots; right) located in Central Kalimantan, Indonesia (left)

The peat swamp forests of Indonesia are highly endangered. Large parts of pristine forest were already converted into agriculture and plantations. For that

purpose, the peat swamp areas are drained by canals. The study area is heavily affected by the construction of canals and related deforestation, which is visible in the southern part of the SAR amplitude image (Fig. 5.1). These canals and the related deforestation originated from the Mega Rice Project (MRP), which was initiated by the Indonesian government in 1995. The main objective of the MRP was to transform about 1 million hectares of tropical peat lands in rice cultivation. The MRP was divided into five spatial blocks with a size of 160,000 to 500,000 ha. Boehm & Siegert (2001) estimated that forest cover decreased from 65 % to 48 % between 1991 and 2000 for the two blocks of the MRP within the study area. The project failed and was abandoned in 1999 (Muhamad & Rieley 2002, Woesten et al. 2008), but drying of the peat due to drainage and illegal logging is still a threat for the forests. On the one hand, increasing decomposition processes release methane and carbon. On the other hand, the dried accumulated biomass makes these areas more vulnerable to fire, both resulting in increased greenhouse gas emissions (Aldhous 2004, Hooijer et al. 2010, Jauhiainen et al. 2005, Page et al. 2002). Nevertheless, large forested regions in the central, eastern and northern parts of the study area belong to the Mawas conservation area and thus are undisturbed since the end of the 1990s. The dense forests close to the rivers and at the edge of the peat dome are up to 30 m high. Towards the center of the peat dome, forest height decreases to 15 m (Boehm et al. 2010, Hajnsek et al. 2009).

5.2.2 TanDEM-X datasets

The bistatic TanDEM-X datasets were acquired in repeat-pass in December 21, 2010 and April 21, 2011 over Central Kalimantan, Indonesia. The TanDEM-X mission operates two X-band SAR satellites, acquiring interferometric SAR data. Both sensors are able to transmit the electromagnetic wave with a phased-array X-band antenna havinga carrier frequency of 9.65 GHz (Pitz & Miller 2010), corresponding to a wavelength of ~3.1 cm.

The data were acquired in the horizontal polarization (HH) using the bistatic acquisition mode. One sensor acted as transmitter and receiver (monostatic/active) while the other only received (bistatic/passive) the electromagnetic waves in this mode. This acquisition configuration was enabled by the close formation flight of the two satellites. Therefore, the temporal baseline was about a tenth of a second resulting in negligible temporal decorrelation caused e.g. by different moisture content, wind or moving objects. The effective baseline describing the effective distance between the two sensors (Hanssen 2001) constituted 163 m and 123 m, respectively (Table 5.1). The bistatic mode in HH polarization is also the operational

7forest

acquisition mode of the TanDEM-X mission used to create the global digital elevation model (Krieger et al. 2007). The data were acquired in StripMap mode, resulting in a resolution of about 3 m (Table 5.1). The data were co-registered, resampled and delivered as CoSSC (co-registered single-look slant range complex; Fritz 2012).

Tab. 5.1: Overview of TanDEM-X dataset

Properties	Value	Value
Acquisition date	December 21, 2010	April 21, 2011
Incidence angle	$47.9° - 49.3°$	$47.9° - 49.3°$
Resolution (azimuth)	3.3 m	3.3 m
Resolution (ground range)	2.4 m	2.4 m
Orbit direction	Descending	Descending
Look direction	Right	Right
Polarization	HH	HH
Effective baseline (image center)	163.3 m	123.3 m

The acquisition dates took place in the middle and end of the rainy season. Since the moisture of the illuminated objects has major influence on the backscatter due to the associated dielectric constant, the rainfall for days previous to the acquisition and at acquisition was investigated. For this purpose the one-degree daily product of the Global Precipitation Climatology Project (GPCP 1DD; Huffman et al. 2001) was purchased for the months of December, 2010 and April, 2011. This product was created using infrared and microwave space borne sensors and provides information on the daily precipitation of a $1°$ by $1°$ cell. The analysis showed relatively dry conditions at the day of the SAR acquisition April 21, 2011 (0 mm/day) and the week before with an average rainfall of 5 mm/day despite the rainy season. The week before the acquisition of December, 2010 had an average rainfall of about 9 mm/ day. However, the two days before data acquisition were dry without any recorded precipitation. Therefore, the influence of moisture within the trees could be neglected.

5.2.3 Reference datasets

5.2.3.1 LiDAR & other remote sensing data

Full-waveform LiDAR data were acquired on August 05, 2007 on a sunny and cloudfree day with a Riegl LMS-Q560 instrument (Table 5.2). The helicopter had an

altitude of 500 m aboveground. The acquisition date was in the dry season in order to avoid inaccurate derivation of the DTM due to high water levels on the ground. A terrain-adaptive bare earth algorithm was used for classifying the laser beams into ground and over ground classes. Delaunay triangulation was utilized to create a triangular irregular network (TIN) which was the basis for the extraction of square grid pixels with a linear interpolation (Boehm et al. 2013, Liesenberg et al. 2013). The extraction of the DSM and DTM was performed by an IDL software package used by company Milan (Boehm et al. 2013). The final dataset had a horizontal resolution of one meter and a vertical resolution of 0.15 m. A digital surface model (DSM) and a digital terrain model (DTM) were derived and delivered as a final product as well as the full-waveform for a strip in the study area. The LiDAR acquisition covered a whole peat dome in the Mawas area with a riverine forest in the west to mixed swamp forest and low pole forest located in the center and east of the LiDAR strip (Fig. 5.1; Boehm et al. 2010, Boehm et al. 2013, Page et al. 1999). Therefore, this dataset covered a large range of tree heights and aboveground tree biomass values related to these forest types. The LiDAR dataset covered about 31 km^2 of the TanDEM-X acquisition.

A Pleiades image was acquired on March 21, 2012 for additional interpretation and plausibility analysis of degradation patterns found in SAR imagery. The spatial resolution of the acquisition was 2 m with a spectral resolution of four bands in the wavelengths of blue, green, red, and near infrared. In addition, Pleiades acquired a

Tab. 5.2: Properties of the airborne LiDAR system LMS-Q560 (Riegl)

Property	Value
Scan angle	±30°
Swath width	~500 m
Scan frequency	66 to 100 kHz
Vertical laser beam accuracy	≤0.1 m
Horizontal laser beam accuracy	≤0.5 m (for x- & y-direction)
Laser beam (mrad)	0.5 (footprint up to 30 cm)
Laser wavelength	1.5 μm (near-infrared)
Point density	1.4 points/m^2

panchromatic image with 0.5 m resolution as well, which was used to pan-sharpen the multispectral bands. Therefore, the final product was resampled to a resolution of 0.5 m and was delivered as an ortho-rectified product (Astrium GEO-Information Services 2012). The image was used for visual interpretation and thus the

9*forest*

pansharpening did not hinder any quantitative analysis of the image, whereas improved the interpretability. The image was acquired with a very low incidence angle of 1.5° which was close to nadir view. Therefore, the interpretation of openings in the forests was feasible. The cloud cover of the acquisition was estimated with 11 %.

5.2.3.2 Field data

Field measurements were collected in January 2005 at eight transects in addition to the remote sensing data. The field measurements were conducted in transects with a size of 100 m by 10 m. However, two transects were averaged due to their spatial adjacency resulting finally in four field transects with a size of 100 m ∗ 20 m. Additional field measurements were conducted in June 2013, where eight transects with a size of 50 m by 20 m were conducted. The smaller size was chosen assuming no drastic change of the forest within the length of transects (50 m vs. 100 m), in order to sample more field transects in this difficult to access peat swamp forest. The field transects were located with GPS. All trees with a diameter at breast height (dbh) larger than 10 cm were measured in both campaigns and tree species were recorded. In total, 12 transects with tree measurements were available (Table 5.3). A clinometer was used for the tree height measurements. The dbh was estimated by the division of the measured girth with π. The stems of peat swamp forest trees are relatively thin (in average 15 cm) and most of them were regular. Irregular cross sections of stems were not handled individually.

The location of the field measurements was systematically distributed along the peat dome of the study area. Hence, a great range and variability of the aboveground tree biomass values and vegetation zones of a tropical peat swamp forest Tab. 5.3: Field measurements and according mean, minimum and maximum of all measured trees

Measurement	Mean	Minimum	Maximum
Tree height (in m)	15.6	2.2 m	37.8 m
Height of first green branch (in m)	9.8	0.5	26.9
Diameter of crowns (in m)	4	0.8	10.7
DBH (in cm)	15.2	10	63.3
Average number of trees/ha	1075.8	-	-

with different vertical structures were covered between the transects despite the difficult accessibility of the area. The field measurements covered a range of

0*forest*

aboveground biomass between 160 t/ha and 440 t/ha. However, only seven transects with a biomass range between 230 t/ha and 440 t/ha were located within the LiDAR dataset due to the restricted accessibility of this peat swamp forest. The aboveground biomass values were calculated by allometric equations as described in Section 5.3.2.

5.3 Methods

5.3.1 Feature extraction from TanDEM-X

The active and passive amplitudes were computed from the complex TanDEM-X CoSSC datasets. A multi-looking with a factor of 3 in range direction and 2 in azimuth direction was applied, in order to suppress speckle noise. This resulted in a (slant range) resolution of about 6 m in both directions. The amplitudes were calibrated to beta nought values in decibels (β_{dB}^0) with the following formula (Fritz & Eineder 2013):

$$\beta_{dB}^0 = 10 * log_{10}(k_s * |DN|^2) \tag{5.1}$$

where k_s means calibration and processing scaling factor, and DN is the modulus of the complex values represented as digital number for each pixel.

A frost filter with 5 by 5 and 9 by 9 moving window size was applied in addition to the multi-looking in order to suppress speckle noise thus increasing the accuracy of the observations. The choice of the frost adaptive speckle filter aimed at reducing the speckle noise while preserving edges, spatial resolution and radiometric properties (Huang & Liu 2007). According to Hajnsek et al. (2009) the area is flat, which could be confirmed by the LiDAR dataset. Therefore, an incidence angle correction was not applied, in order to avoid errors related to the DEM inaccuracies caused for example by volume decorrelation.

The multi-look interferogram of the TanDEM-X CoSSC datasets was calculated with the same multi-looking factors used in the amplitude processing. The interferogram was calculated as follows:

$$\blacksquare \tag{5.2}$$

where s_1 denotes complex dataset 1 and $\blacksquare$ means complex conjugate of dataset 2. This was equivalent to the subtraction of the two phase information from both datasets, thereby obtaining only the phase difference (Bamler & Hartl 1998). Systematic phase changes occurred in range direction in the interferogram due to

1*forest*

the side looking acquisition geometry and the associated changes in the distance from the target to the sensors. These phase changes were removed by an interferometric processing step called interferogram flattening (Cloude 2009).

The interferometric coherence is the modulus of complex cross correlation between two SAR acquisitions and is defined as (Bamler & Hartl 1998):

$$\blacksquare \tag{5.3}$$

where E is the expectation value, s_i denote complex image i and vertical lines are for magnitude of complex data.

However, the expectation value is an unknown and is estimated via spatial averaging (Bamler & Hartl 1998, Hanssen 2001). The interferometric coherence was thus calculated using the following formula after application of the interferogram flattening:

$$\blacksquare \tag{5.4}$$

where s_i denotes complex image i, the brackets mean ensemble average and vertical lines are for magnitude of complex data resulting in a range for the coherence from 0 to 1, whereas 1 means completely coherent (Rosen et al. 2000). Kernel sizes of 3 by 3, 5 by 5, and 7 by 7 were used.

The amplitudes and interferometric coherences were geocoded using the orbit parameters with the digital elevation model obtained from the interferometric analysis of the datasets and were resampled to a pixel size of 3 m with 4th cubic convolution. Previous studies showed the high geometric accuracy of TerraSAR-X using a high precision DEM (Reinartz et al. 2011), and thus localization errors between TanDEM-X, LiDAR, and field measurements could be minimized. However, the GPS measurements for the field transects have a limited accuracy of a few meter. But it can be assumed that the forest changes not drastically within a few meters and thus possible errors should be small (Mascaro et al. 2011).

5.3.2 Biomass estimation via field measurements and LiDAR

The aboveground tree biomass density in tons per hectare for each transect was calculated according to different allometric equations based on stand tables and volume data. In total, six different approaches for biomass estimation were compared. The choice was in favor of global or pan-tropical models (Brown & Iverson 1992, Brown & Lugo 1992, Chave et al. 2005, Hajnsek & Hoekman 2005), because these are based on a large number of destructive measurements (Brown &

2*forest*

Iverson 1992, Brown & Lugo 1992, Brown et al. 1989, Chave et al. 2005, Reyes et al. 1992). Regional or local models exhibit a higher risk of biased predictions due to the small sample size (Chave et al. 2005).

The results differed in their aboveground biomass values. The mean value of the different models ranged from 117.91 to 294.21. Therefore, a comparison with other studies in peat swamp forests was conducted and the equation which resulted in similar aboveground biomass values compared to literature values was finally used (see Section 5.5.3). It is worth noting that some models, Brown et al. (1989) for example, resulted in significant lower aboveground biomass values compared to other studies in peat swamp forests. The aboveground tree biomass density used as field reference for each transect was calculated according following allometric equations resulting in similar biomass values compared to other studies (Brown & Lugo 1992, Hajnsek & Hoekman 2005):

$$biomass = vob * wd * bef(t/ha) \tag{5.5}$$

where *vob* is the volume over bark, *wd* is volume-weighted average wood density which was determined as 0.57 t/m representing the arithmetic mean for Asian forests (Reyes et al. 1992). The *bef* is the biomass expansion factor in order to include leaves, twigs, and branches.

The volume over bark was calculated as the sum of bole volume (*bv*):

$$bole\ volume = basal\ area * total\ tree\ height * shape\ factor \tag{5.6}$$ with a shape

factor of 0.7. The biomass expansion factor for bole volume equal

or greater than 190 t/ha was determined as 1.74.

The biomass expansion factor for a bole volume lower than 190 t/ha was calculated (Brown & Lugo 1992):

$$bef = exp(3.213 - 0.506 * ln(bv)) \tag{5.7}$$

In order to increase the number of observations for correlations between biomass and SAR features, the biomass was estimated with the LiDAR canopy height model. The DSM and DTM of the LiDAR acquisition were subtracted and resulted in the canopy height model (CHM) representing the vegetation height and the surface of the canopy (Koch et al. 2006). This approach was chosen since a number of studies proved the feasibility of deriving aboveground biomass with LiDAR CHM metrics (Boehm et al. 2013, Koch 2010, Kronseder et al. 2012, St-Onge et al. 2008). Subsequently, metrics such as mean, percentiles in steps of 5, and standard

deviation of the CHM were calculated for each field transect located within the LiDAR coverage. These estimations were considered as accurate predictors for forest parameters (Kronseder et al. 2012, St-Onge et al. 2008). Those metrics were correlated with the total aboveground biomass of the field transect measurements. An inversion model based on the metrics of the LiDAR canopy height model and related field transect measurements was developed using a multiple linear regression approach with a least square fitting (Dandois & Ellis 2013, Kronseder et al. 2012). The model yielded a R^2 of 0.49 and a root mean square error of 33.6 t/ha for the aboveground biomass estimation. The biomass model was based on the field transects which were consistent with the LiDAR dataset. Field transects from 2007 having a size of 0.1 ha and one field transect from 2005 having a size of 0.2 ha were used. The field transect from 2005 was split into $2 * 0.1$ ha in order to keep spatial consistency. Therefore, a total of eight 0.1 ha areas were consequently used to apply the biomass model to a 0.1 regular grid over the whole LiDAR coverage.

However, Asner et al. (2010) suggested that the error decreases with the spatial resolution. Mascaro et al. (2011) demonstrated a decrease in error up to 40 % with decreasing spatial resolution of the estimation from 0.36 ha to 1 ha. Therefore, the 0.1 ha grid used for biomass estimation from LiDAR data was bilinear resampled to 1 ha in order to reduce potential estimation and localization errors. Furthermore, a hectare unit was considered as a reasonable unit for biomass estimation in line with minimum mapping unit used in science, management and policy (Asner et al. 2013, GOFC-GOLD 2012, Maniatis & Mollicone 2010, Mascaro et al. 2011). In total, 926 biomass estimates of 1 ha size were derived from the LiDAR dataset, ranging from 119 t/ha to 510 t/ha.

5.3.3 Empirical analysis of relationship between biomass and SAR features

The mean value of interferometric coherence and amplitude for each 1 ha sampling grid cell was calculated. Each 1 ha grid cell contained about 1111 pixel with a pixel spacing of 3 m and thus noise in the amplitude and coherence images were appropriately suppressed. The aboveground biomass value for each grid cell was correlated with the corresponding mean value of the coherence and amplitude. A linear model was developed via least squares regression (Seber & Lee 2003) for the interferometric coherence and for the amplitude with the response variable aboveground biomass. In addition, a non-linear power function was tested to describe the coherence and biomass relationship:

$$y = a * x^b \tag{5.8}$$

4forest

An exponential function was applied for the amplitude as well as for coherence and biomass relationship in addition to linear and power regressions with least-square estimates (Bates & Watts 1988):

$$y = a * exp(x * b) \tag{5.9}$$

where *a* and *b* were parameters of the functions and *x* represented the variable which was in that case the amplitude value in dB or the coherence. This equation was used, because it achieved higher R^2 compared to other non-linear relationships without consideration of theoretical reasons.

The analysis was focused on 1 ha grid cells covered by forest, undisturbed since the end of the 1990s. Woodhouse et al. (2012) questioned establishing relations based on data sets mixed across forest types, because the resulting relation of aboveground biomass and SAR intensity is formed by clusters representing different forest types. This phenomenon should be even more pronounced when considering different land cover types. Therefore, a previously conducted accurate classification was used (Schlund et al. 2014a) to exclude areas classified as grassland, shrub land, water, and wetlands. Thus, it was ensured with high accuracy of 91 % that only forest biomass was considered without any surfaces with low or no biomass. This stratification resulted in a total of 926 LiDAR derived forest biomass estimates which were randomly divided into 2/3 for model development (*n* = 617) and 1/3 (*n* = 309) for independent model validation.

The predictive accuracy of the model was described by comparing the modeled biomass via coherence or amplitude and actual aboveground biomass from LiDAR estimation. The root mean square (*RMSE*), coefficient of determination (R^2), and the relative volume error (*V E_{rel}*) were considered in order to evaluate the model. The R^2 is the fraction of variance explained by the model and defined as (Seber & Lee 2003):

$$\tag{5.10}$$

where y_i is the actual value of i and $\hat{y}_i$ the predicted value of i, and $\bar{y}$ is the mean of actual values. The relative volume error was calculated as follows:

$$\tag{5.11}$$

5*forest*

where y_i is the actual value of i and $\hat{y}_i$ the predicted value of i and thus positive values indicated a systematic underestimated biomass in the models whereas negative values indicated a systematic overestimation of the prediction. According to Krause et al. (2005) the volume error is an appropriate indicator for a systematic over- or underestimation of a model.

The SAR based biomass inversion model was applied to the entire coverage of the coherence and amplitude to provide an overview of the distribution of aboveground biomass in the study area for visual evaluation purposes. In addition, the five field measurements not used for biomass up-scaling with LiDAR were used as independent validation for the inversion model. The total biomass of these field measurements was calculated per 1 ha grid cell. The image processing and statistical analysis was conducted in the R environment (R Core Team 2013) with the help of additional packages called "raster" (Hijmans 2013), "rgdal" (Keitt et al. 2013), and "sp" (Bivand et al. 2008).

5.4 Results

5.4.1 SAR features vs. LiDAR estimated biomass

The coherence had a substantially higher coefficient of determination with the actual aboveground tree biomass compared to the amplitude (Fig. 5.2). Nevertheless, the deviations from the linear fitted line were highest at greater biomass values at about 350 t/ha and higher. Therefore, it was concluded that the relationship of coherence and biomass saturated at those aboveground biomass values. The application of the exponential and power functions to the biomass estimation with coherence resulted in lower R^2 compared to linear models with 0.43 and 0.42. The R^2 of 0.31 for the unfiltered amplitude was significantly lower than the coherence. The application of the best non-linear model resulted in an even lower R^2 compared to the linear model of 0.3. The application of speckle filters did not improve the coefficient of determination substantially and resulted in a R^2 of 0.32 for both filtered amplitude images. The interferometric coherence and amplitude resulted in similar R^2 for both acquisitions (Fig. 5.2). The R^2 decreased with kernel size in the coherence calculation from 0.5 (3 by 3), 0.46 (5 by 5) to 0.4 (7 by 7). However, the R^2 was still substantially higher for each used kernel size than for the amplitude.

In total, the actual aboveground biomass values ranged from 119 t/ha to 510 t/ha with an average of 282.7 t/ha, with a standard deviation of 74.3 t/ha. The dynamic range of the single-pass interferometric coherence from April 2011 is between 0.75

6forest

and 0.9, whereas the values of the amplitude range between -11.5 dB and -8.5 dB. In contrast, the amplitude values of December 2010 were increased compared to April 2011 between -9.6 dB and -7.4 dB, whereas the interferometric coherence range decreased to 0.65 and 0.86. The overall observed mean values for the coherence images were 0.81 for December 2010 and 0.86 for April 2011, whereas Fig. 5.2: Linear relationship of coherence (left) & active amplitude (right) from acquisitions from December 21, 2010 (top) & April 21, 2011 (bottom) with biomass estimated from LiDAR (n = 617)

the respective standard deviation constituted about 0.04 and 0.03. The overall observed mean values for the amplitudes were -8.5 dB (2010) and -10.3 dB (2011) with a respective standard deviation of 0.36 and 0.46. The passive amplitudes showed a similar relationship compared to the active amplitudes, indicating that the bistatic angle was not large enough to result in a different correlation.

5.4.2 Inverting the models to full extent

The application of the models with the highest R^2 for the amplitude and coherence to the full extent of the respective acquisition showed substantial differences between the coherence and amplitude. The acquisition from April 21, 2011 resulted in the highest R^2 for the interferometric coherence as well as for the amplitude and thus these images were used for the model (Fig. 5.3). The coherence derived estimates resulted in a larger overall range of estimated biomass values. Higher biomass values of 300 to 500 t/ha were more frequent in the coherence compared to the amplitude. Those were observed mainly in the vicinity of rivers in the west and southeast of the map (Fig. 5.3). Furthermore, the biomass gradient from the lowland river regions with high biomass decreasing towards the top of the peat dome was well represented in the coherence based biomass map (Fig. 5.4). This observation was in line with general descriptions of tropical peat swamp forests regarding their ecology, species composition, and spatial structure (Boehm et al. 2013, Page et al. 1999, Phillips 1998, Sorensen 1993). In general, the result of the interferometric coherence was less noisy. The result of the amplitude inversion generally showed lower biomass values.

7*forest*
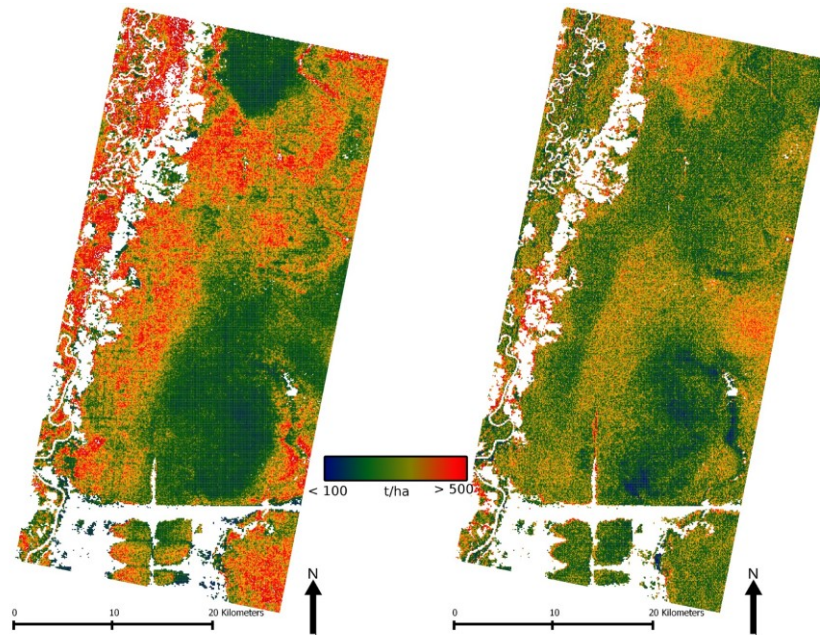
Fig. 5.3: Biomass estimation via up-scaling from field measurements to LiDAR to TanDEM-X coherence (left) and amplitude (right) from April 21, 2011

In addition, the coherence contained more information about biomass degradation as a consequence of anthropogenic disturbances of the forests in the past decades. Former logging tracks were observed in the interferometric coherence and its biomass derivate. Those tracks were constructed in preparation of the Mega Rice Project and prior to the declaration as conservation area in 2003 to selectively log trees with high timber values. The tracks were also visible in the very high resolution Pleiades image where the decrease of near-infrared reflection (compared to the surroundings) was interpreted as forest degradation areas (Fig. 5.4). These areas were not detectable by investigating neither the unfiltered nor the filtered amplitude images.
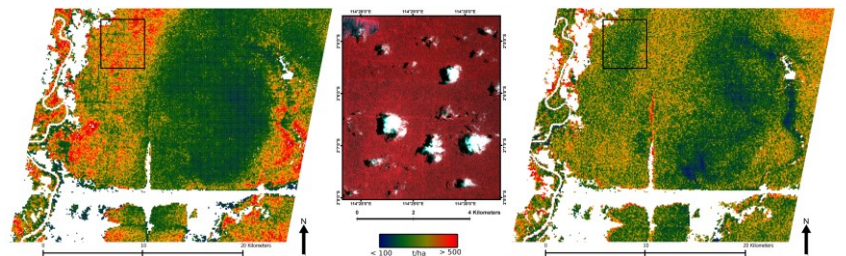
Fig. 5.4: Detailed view of biomass estimation fromTanDEM-X coherence (left), amplitude (right), and comparison to Pleiades false-color image (center; R=near-infrared, G=red, B=green)

The model evaluation with the randomly selected validation samples from the LiDAR data showed a *RMSE* of 53 t/ha in the interferometric coherence model.

8*forest*

This represented about 14 % of the value range of the actual biomass from LiDAR (Fig. 5.5). The R^2 of validation samples was slightly higher than in the model development. The spatial distribution and the scatter plot of the biomass derivation showed that the biomass of the model was underestimated at higher actual biomass levels (center & west; Fig. 5.5). In contrast, the model overestimated the predicted biomass at lower actual aboveground biomass (east; Fig. 5.5). A moderate systematic overestimation of the model was documented with the relative volume error of -0.3 %. As expected, the independent validation of the biomass derived from the amplitude model had a higher *RMSE* of 72 t/ha and a higher relative volume error of -0.32 %. However, the relative volume error was not substantially higher, but it also indicated a systematic overestimation of the model. Similarly to the correlation with the samples for model development, the prediction achieved a low R^2 of 0.3 in the validation.
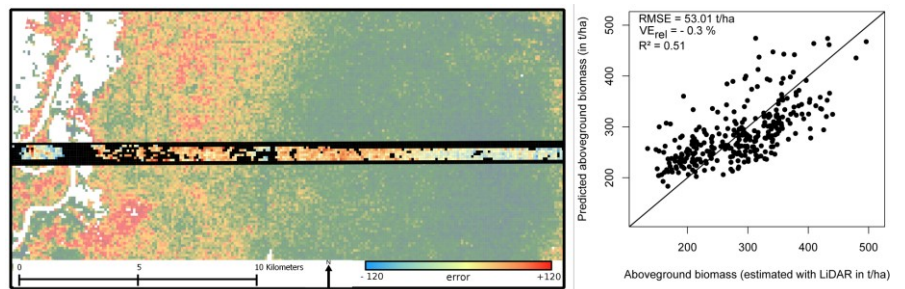
Fig. 5.5: Spatial distribution of errors from biomass derived from interferometric coherence estimation against LiDAR estimated biomass with all samples (left) & scatterplot of independent validation samples with 1:1 line (n= 309)

The evaluation of the predicted results with the five field measurements, which were not used for up-scaling of the LiDAR data set, also showed a lower *RMSE* of 86.6 t/ha for the interferometric coherence compared to 102.2 t/ha for the amplitude. The relative volume errors of -12 % and -13 % indicated also a systematic overestimation of both SAR inversion models compared to the actual biomass from field measurements. Nonetheless, this volume error was significantly higher compared to the LiDAR evaluation which was attributable to the lower number of observations and at the sampling range of a lower total biomass in the validation dataset. Therefore, deviations resulted in a larger impact. The comparison of SAR based biomass model with the five independent field samples could be used only as indication. Nevertheless, these results confirmed that the interferometric coherence had a closer correlation with the biomass and resulted in improved estimates compared to the amplitude.

A comparison of the resulting descriptive values for aboveground biomass from field measurements, LiDAR, and interferometric coherence estimation showed simTab. 5.4: Comparison of aboveground biomass values from field measurements, LiDAR and TanDEM-X interferometric coherence estimation

	Field measurements (all; in t/ha)	Field measurements (used for up-scaling; in t/ha)	LiDAR estimated aboveground biomass (independent validation set; in t/ha)	Coherence estimated aboveground biomass (independent validation set; in t/ha)
Mean	282.7	308.0	282.7	277.3
Standard deviation	82.4	61.3	73.5	51.5
Minimum	161.4	230.0	119.3	183.2
Maximum	439.8	439.8	511.1	495.2
n	12	7	309	309

ilar mean values for all estimations (Table 5.4). The LiDAR estimated mean value was equal to the field measured mean value of all transects. The aboveground biomass mean value based on interfometric coherence differed 5 t/ha compared to field measured and LiDAR estimated mean value. In addition, the standard deviations as well as the ranges varied not substantially.

5.5 Discussion

5.5.1 Coherence as a function of biomass

The results imply that the volume decorrelation and thus the interferometric coherence are correlated to the forest structure and the aboveground tree biomass. Schlund et al. (2013); Schlund et al. (2014a) suggested that the interferometric coherence of the single-pass system TanDEM-X is - among other factors - dependent on canopy cover, which was used to differentiate the forest in a high accurate land cover classification.

In addition, other studies suggested that the coherence is related to forest structure as well as to the forest height (Kugler et al. 2013, Kugler et al. 2014, Caicoya et al. 2012). Volume decorrelation occurs when the electromagnetic wave interacts with volume scatterers. The volume consists of vertical components, which

0*forest*

contribute to the backscatter and are projected in the resolution cell. Differences in the projection of the vertical components within a resolution cell of the interferometric image pairs result in a decorrelation (Krieger et al. 2010, Rosen et al. 2000). The forests act as a volume and the vertical height and the density of the volume influences the interferometric coherence. This phenomenon is described for example in the random volume over ground model (RVoG) in order to derive tree heights (Cloude & Papathanassiou 1998, Cloude & Papathanassiou 2003, Papathanassiou & Cloude 2001). Operational TanDEM-X data together with a LiDAR dataset (Caicoya et al. 2012) or experimental TanDEM-X data with different baselines and polarizations (Kugler et al. 2014, Kugler et al. 2013) enable potentially to derive tree heights using the RVoG. A coefficient of determination of 0.5 (without external DTM) and 0.97 (with external DTM) was achieved between RVoG model results and actual tree heights in the Mawas tropical peat swamp forests resulting in RMSE values of 6 m to 2 m (Kugler et al. 2014). Nevertheless, the RVoG was developed for lower frequency and multi-polarized SAR data and thus, different assumptions of the earth phase had to be made when applying the model to TanDEM-X data (Cloude & Papathanassiou 1998, Kugler et al. 2014, Papathanassiou & Cloude 2001, Caicoya et al. 2012).

The biomass is a function of different structure parameters such as forest height and canopy cover. Consequently the interferometric coherence was directly related to the aboveground biomass and achieved a R^2 of about 0.5 (Figs. 5.3; 5.4). In comparison to the presented results, the estimation of growing stock volume with C-band coherence in Boreal forests at optimal acquisition conditions reached a coefficient of determination of about 0.5 and errors of 15-25 % compared to field measurements (Cartus et al. 2011, Santoro et al. 2002, Santoro et al. 2007).

The coherence decreases with increasing biomass due to higher volume decorrelation caused by larger vertical height and more closed canopy. The interferometric measurement is thus related to multiple forest structure parameters such as the vertical height, vertical structure and canopy cover. The up-scaling from LiDAR to TanDEM-X showed a marginal difference of 5 t/ha estimating the mean biomass (277 t/ha; Table 5.4). Therefore, the information derived by X-band coherence could be used as complementary information to traditional biomass estimations using long-wavelength SAR backscatter data. A suitable and efficient combination of long-wavelength backscatter biomass estimation (e.g. in Mitchard et al. 2011, Englhart et al. 2011) and estimations derived from short-wavelength interferometric information potentially improves biomass estimation results substantially. In addition, forest degradation leads to less biomass and more

1*forest*

openings in the canopy, which can result in more direct scattering interactions with trunks and branches. The probability of volume scattering and volume decorrelation is higher with a more closed canopy resulting in lower interferometric coherence. Nevertheless, the relationship between forest structure and interferometric coherence suggests a sensitivity limitation. The derived coherence is only an estimation of the real coherence, whereas lower coherence values have a lower estimation accuracy of the real coherence and thus can result in lower accuracy of biophysical derivations (Askne et al. 1997, Santoro et al. 2002). The slight decrease of the correlation with increasing window size could be due to coarser spatial coherence estimation. The sensitivity is also dependent on the interferometric baseline (Balzter 2001). A similar projection of the vertical component within the resolution cell, resulting in less volume decorrelation, is more probable with a smaller baseline. This is evident in the slightly increase of the coherence values with decreasing baseline. However, the interferometric coherence from baselines compared in this study (163 m versus 123 m) did not show substantial differences in their correlation to aboveground biomass and the related sensitivity to biomass, which is an important fact regarding transferability of results. Nevertheless, the parameters of the linear functions differed slightly, which limits the exact transfer of one model to different acquisition properties.

However, the coherence and the derived aboveground biomass can provide an indication of information about the spatial distribution of the biomass, different forest structure types, conditions of forests and forest degradation despite possible inaccuracies in absolute aboveground biomass estimation (Fig. 5.4). This information can be used for instance in REDD+ sampling schemes for stratification purposes.

5.5.2 SAR amplitude in a peat swamp forest

The results of the amplitude (in dB) showed a decrease with increasing aboveground biomass in contrast to other studies in a peat swamp forest (Englhart et al. 2011). The amplitude increases typically with increasing aboveground biomass due to higher volume backscattering (Balzter et al. 2007, Mitchard et al. 2011). However, the X-band wave is very short and mostly interacts with near-surface elements of the canopy and thus longer wavelengths are considered more appropriate for aboveground biomass correlation (Castro et al. 2003, Luckman et al. 2000, Saatchi et al. 1997). The observed increased backscattering at forest with less biomass could be due to more direct or double bounce interactions. The trees are more distant, the forest canopy is open and therefore the wave interacts more likely

with trunks and branches due to the side-looking acquisition geometry. This results in no or less volume scattering. Direct, dihedral or trihedral backscattering is generally higher than volume scattering.

In this study, the amplitude of a X-band SAR shows a weak relation with the biomass in this tropical peat swamp forest. Unlike other studies (e.g. Englhart et al. 2011, Luckman et al. 2000, Mitchard et al. 2011), the backscatter is decreasing with the biomass and the relation is close to a linear function. Woodhouse et al. (2012) addressed that different forest types with their respective biomass are analyzed together in most studies. The biomass differs even more among land cover types and thus exhibits a large range of biomass values correlated with different scattering mechanism of open and vegetation covered surfaces. Therefore, conclusions of an individual land cover type have limited validity. Therefore, only the biomass within the forest area was investigated, exceeding the saturation limit in X-band of 80 t/ha reported by Englhart et al. (2011). Thus, it could be concluded that the amplitude is not correlated to the biomass of tropical peat swamp forest in the Mawas area, investigated in our study.

5.5.3 Up-scaling of biomass measurements to LiDAR dataset

A number of studies proofed the ability of LiDAR metrics to accurately estimate biomass of tropical forests (e.g. Asner et al. 2009b, Asner et al. 2013, Boehm et al. 2013, Mascaro et al. 2011). The application of LiDAR CHM showed relatively high accuracies for biomass estimation also in peat swamp forests with an error budget of about 20 % (Boehm et al. 2013) and comparable results to Kronseder et al. (2012) and Englhart et al. (2011) in the Sebangau Catchment were reported (Boehm et al. 2013). Consequently it was inferred that LiDAR based biomass estimates provide a reliable reference to compensate for the small number of available field samples for SAR inversion model development. According to Asner et al. (2009b) only few field measurements are necessary to transform LiDAR metrics to biomass, if the field measurements are distributed over the entire range of biomass. The biomass of the used field transects ranged from 230 t/ha to 440 t/ha. Field transects in the very low biomass regions were not sampled within the LiDAR strip due to the very limited accessibility of these areas. Therefore, additional field measurements especially in low biomass regions could potentially improve the LiDAR based biomass estimation. Nevertheless, the LiDAR based estimate of the mean biomass achieved an identical mean as calculated from all field samples (Table 5.4) and thus confirmed that LiDAR CHM based biomass estimation can serve as suitable mean for following SAR feature analysis and inversion modeling.

3*forest*

Furthermore, one might argue that the different acquisition dates of the field measurements and LiDAR dataset could result in inconsistencies. However, the area of interest is part of a conservation area where the forests are relatively undisturbed after the abandonment of the Mega Rice Project in the year 1999 (Aldhous 2004). Moreover, investigations showed that the biomass increases only marginally in undisturbed peat swamp forests of Central Kalimantan as well as in the study area (Boehm et al. 2012, Boehm et al. 2013, Englhart et al. 2013, Sweda et al. 2012). Therefore, it can be concluded that inconsistencies between the different acquisition dates are minimal and may not affect the results substantially.

Other sources of error to consider in the up-scaling from field measurements to LiDAR are related to the field sampling like GPS localization inaccuracies and in the transformation of field measurements to biomass with allometric equations. The biomass values of our study were compared with other studies in tropical peat swamp forests of south-east Asia, in order to evidence the quality of biomass estimation. The statistical distribution of dbh and tree height measured in peat swamp forests within other studies (Page et al. 1999, Nishimua et al. 2007, Boehm et al. 2013) was similar to the values measured in our investigation and thus it was assumed that related biomass estimates are comparable to other studies.

Several allometric equations were tested in order to choose the most appropriate for biomass estimation in peat swamp forest. Mainly global or pan-tropical models with a large sample size were used in order to avoid potential biases of local or regional models with very small sample sizes (Chave et al. 2005). It was assumed that the advantage of using a local model will not compensate the potential bias. The results of the used allometric equations differed significantly (see Section 5.3.2) and thus the choice was guided by the goal to attain similar values as other studies conducted in peat swamp forests.

The chosen equation resulted in a mean of 282.73 t/ha for the estimation of aboveground biomass from field data (as well as from LIDAR data) ranging from 161.4 t/ha to 439.8 t/ha (Table 5.4). A number of studies investigated aboveground biomass in the peat swamp forest of Sebangau national park, Central Kalimantan and found values ranging between 1 t/ha and 369 t/ha (Boehm et al. 2013, Englhart et al. 2011, Kronseder et al. 2012). Kronseder et al. (2012) classified the forest into three disturbance classes, which had values of about 228 t/ha for unlogged forest, 160 t/ha for logged forest, and 15 t/ha for burned forests. Waldes & Page (2002) measured slightly higher biomass of 248-311 t/ha in six field plots compared to Kronseder et al. (2012) in the peat swamp forests of Sebangau. LiDAR estimated biomass values above 300 t/ha are also confirmed by Boehm et al. (2013) for the

Sebangau area. Verwer & Meer (2010) reported an aboveground biomass of relatively undisturbed peat swamp forest between 264 and 397.4 t/ha. Thus the estimated biomass from field data and LiDAR corresponds well to the measurements from Central Kalimantan.

In contrast, Morel et al. (2011) measured biomass in Malaysian Borneo peat swamp forests of 104 t/ha for secondary forest, 66 t/ha for forest with medium and 128 t/ha with low disturbances. Kaneko (1992) measured considerably higher aboveground biomass in the range of 287-491 t/ha in peat swamp forests in Thailand. Koh et al. (2011), Koh et al. (2012) and Murdiyarso et al. (2010) provide a carbon stock value of 179.7 ± 38.2 t/ha corresponding to a mean biomass of 359.6 ± 76.4 t/ha (Martin & Thomas 2011) for peat swamp forest on Java, Borneo and Peninsular Malaysia.

The differences in those estimates could of course be related to the different geographical locations and the associated conditions as well as different allometric equations used for biomass calculation. However, the initiated preparation and partly drainage of the area for the abandoned Mega Rice Project (Aldhous 2004), resulted in forest degradation which is still interpretable in the Pleiades image and interferometric coherence. Logging patterns are still visible in the imagery. This could explain the slightly lower biomass compared to e.g. Kaneko (1992). Nevertheless, the values of the biomass estimation derived from the field measurements and LiDAR are in the range of other studies in peat swamp forests of south-east Asia. Therefore, it can be concluded that the biomass values used in this study are representative and can be used for the purpose of this study.

5.6 Conclusions

The results of the study show that TanDEM-X data can provide an important contribution to the mapping of the aboveground tree biomass of tropical regions. This is especially the case in areas frequently covered by clouds and difficult to access, resulting normally in a small number of field measurements. It was shown that the up-scaling approach of a few field measurements to LiDAR data and ultimately to TanDEM-X for large-scale applications can achieve reliable results. The SAR features were not directly linked to the limited number of field measurements for model development, but the LiDAR data were used to estimate aboveground biomass in order to increase the number of observations and were subsequently sampled for model development and error assessment.

5*forest*

The investigations were mainly focused on relatively undisturbed tropical peat swamp forest and not on other land cover classes with low aboveground biomass. As expected, the relationship between biomass and interferometric coherence was significantly stronger compared to the amplitude of the high frequency X-band system with its 3 cm wavelength. This was demonstrated by a higher R^2 of 0.5 compared to 0.3. Similarly, these results could be confirmed by the application of coherence based biomass inversion model and independent validation. The biomass estimation using the interferometric coherence was less noisy and included more spatial details, indicating forest degradation. Thus, the bistatic interferometric coherence can be used to provide at least the geographical distribution and dynamics of the biomass, the status of forests and forest degradation, despite of any possible error in the direct absolute biomass derivative. The provided wall-to-wall biomass stratification can be used as a prerequisite for efficient forest carbon inventories.

These are of key importance for national carbon accounting and REDD+ projects to reduce the uncertainty in the estimation of carbon stock changes (GOFC-GOLD 2012). Therefore, the globally available high resolution interferometric dataset from the TanDEM-X mission should be considered as an important contribution for stratification or biophysical estimation purposes in REDD+ measurement, reporting and verification concepts.

Acknowledgments

References

Aldhous, P. (2004). Borneo is burning. *Nature*, 432, 144–146.

Askne, J., Santoro, M., Smith, G. & Fransson, J. (2003). Multitemporal repeat-pass SAR interferometry of boreal forests. *IEEE Transactions on Geoscience and Remote Sensing* (7), 41, 1540–1550.

6forest

Askne, J., Dammert, P., Ulander, L. & Smith, G. (1997). C-band repeat-pass interferometric SAR observations of the forest. *IEEE Transactions on Geoscience and Remote Sensing* (1), 35, 25–35.

Asner, G. P., Flint Hughes, R., Varga, T. A., Knapp, D. E. & Kennedy-Bowdoin, T. (2009b). Environmental and Biotic Controls over Aboveground Biomass Throughout a Tropical Rain Forest. *Ecosystems* (2), 12, 261–278.

Asner, G. P., Powell, G. V. N., Mascaro, J., Knapp, D. E., Clark, J. K., Jacobson, J., Kennedy-Bowdoin, T., Balaji, A., Paez-Acosta, G., Victoria, E., Secada, L., Valqui, M. & Hughes, R. F. (2010). High-resolution forest carbon stocks and emissions in the Amazon. *Proceedings of the National Academy of Sciences* (38), 107, 16738–16742.

Asner, G. P., Mascaro, J., Anderson, C., Knapp, D. E., Martin, R. E., KennedyBowdoin, T., Breugel, M. van, Davies, S., Hall, J. S., Muller-Landau, H. C., Potvin, C., Sousa, W., Wright, J. & Bermingham, E. (2013). High-fidelity national carbon mapping for resource management and REDD+. *Carbon Balance and Management* (7), 8, 1–14.

Astrium GEO-Information Services (2012). *Pleiades imagery - user guide. Version 2.0.*. Astrium GEO-Information Services: Toulouse.

Balzter, H. (2001). Forest mapping and monitoring with interferometric synthetic aperture radar (InSAR). *Progress in Physical Geography* (2), 25, 159–177.

Balzter, H., Rowland, C. & Saich, P. (2007). Forest canopy height and carbon estimation at Monks Wood National Nature Reserve, UK, using dual-wavelength SAR interferometry. *Remote Sensing of Environment* (3), 108, 224–239.

Bamler, R. & Hartl, P. (1998). Synthetic aperture radar interferometry. *Inverse Problems* (4), 14, R1–R54.

Bates, D. M. & Watts, D. G. (1988). *Nonlinear regression analysis and its applications*. Wiley & Sons: New Jersey.

Bivand, R. S., Pebesma, E. J. & Gomez-Rubio, V (2008). *Applied spatial analysis with R*. Springer: New York.

Boehm, H. D. V., Liesenberg, V. & Frank, J. (2010). Relating tree height variations to peat dome slope in Central Kalimantan, Indonesia using small-footprint airborne LiDAR data. *Proceedings of 10th international conference of LiDAR applications for assessing forest ecosystems.-SilviLaser, 2010*, 1, 216–228.

Boehm, H. D. V., Liesenberg, V. & Limin, S. H. (2013). Multi-Temporal Airborne LiDAR-Survey and Field Measurements of Tropical Peat Swamp Forest to Monitor Changes. *IEEE Journal of Selected Topics in Applied Earth Observations and Remote Sensing* (3), 6, 1525–1530.

7*forest*

Boehm, H.-D. & Siegert, F. (2001). Ecological impact of the onemillion hectare rice project in Central Kalimantan, Indonesia, using remote sensing and GIS. Land use change and (Il)-legal logging in Central Kalimantan, Indonesia. In: *22nd Asian Conference on Remote Sensing, 5-9 November 2001*.

Boehm, H. D., Liesenberg, V., Sweda, T., Tsuzuki, H. & Limin, S. (2012). Multitemporal airborne LiDAR-surveys in 2007 and 2011 over tropical peat swamp forest environments in Central Kalimantan, Indonesia. In: *Proceedings of the 14th international peat congress, Stockholm, Sweden, 3-8 June 2012.*

Brown, S., Gillespie, A. J. R. & Lugo, A. E. (1989). Biomass estimation methods for tropical forests with applications to forest inventory data. *Forest Science*, 35, 881–902.

Brown, S. & Iverson, L. R. (1992). Biomass estimates for tropical forests. *World Resources Review*, 4, 366–384.

Brown, S. & Lugo, A. E. (1992). Aboveground biomass estimates for tropical moist forests of the Brazilian Amazon. *Interciencia*, 17, 8–18.

Caicoya, A. T., Kugler, F., Hajnsek, I. & Papathanassiou, K. (2012). Boreal forest biomass classification with TanDEM-X. In: *IEEE International Geoscience and Remote Sensing Symposium (IGARSS), 2012*,3439–3442.

Cartus, O., Santoro, M., Schmullius, C. & Li, Z. (2011). Large area forest stem volume mapping in the boreal zone using synergy of ERS-1/2 tandem coherence and MODIS vegetation continuous fields. *Remote Sensing of Environment* (3), 115, 931–943.

Castro, K. L., Sanchez-Azofeifa, G. A. & Rivard, B. (2003). Monitoring secondary tropical forests using space-borne data: Implications for Central America. *International Journal of Remote Sensing* (9), 24, 1853–1894.

Chave, J., Andalo, C., Brown, S., Cairns, M., Chambers, J., Eamus, D, Folster, H, Fromard, F., Higuchi, N., Kira, T (2005). Tree allometry and improved estimation of carbon stocks and balance in tropical forests. *Oecologia* (1), 145, 87– 99.

Cloude, S. (2009). *Polarisation: Applications in Remote Sensing*. Oxford University Press: Oxford.

Cloude, S. & Papathanassiou, K. (1998). Polarimetric SAR interferometry. *IEEE Transactions on Geoscience and Remote Sensing* (5), 36, 1551–1565.

Cloude, S. & Papathanassiou, K. (2003). Three-stage inversion process for polarimetric SAR interferometry. *IEE Proceedings - Radar, Sonar and Navigation* (3), 150, 125–134.

8*forest*

Dandois, J. P. & Ellis, E. C. (2013). High spatial resolution three-dimensional mapping of vegetation spectral dynamics using computer vision. *Remote Sensing of Environment*, 136, 259–276.

Dobson, M., Ulaby, F., Pierce, L., Sharik, T., Bergen, K., Kellndorfer, J., Kendra, J., Li, E., Lin, Y., Nashashibi, A., Sarabandi, K. & Siqueira, P. (1995). Estimation of forest biophysical characteristics in Northern Michigan with SIR-C/X-SAR. *IEEE Transactions on Geoscience and Remote Sensing* (4), 33, 877–895.

Englhart, S., Keuck, V. & Siegert, F. (2011). Aboveground biomass retrieval in tropical forests - The potential of combined X- and L-band SAR data use. *Remote Sensing of Environment*, 115, 1260–1271.

Englhart, S., Jubanski, J. & Siegert, F. (2013). Quantifying Dynamics in Tropical Peat Swamp Forest Biomass with Multi-Temporal LiDAR Datasets. *Remote Sensing* (5), 5, 2368–2388.

Eriksson, L., Santoro, M., Wiesmann, A. & Schmullius, C. (2003). Multitemporal JERS repeat-pass coherence for growing-stock volume estimation of Siberian forest. *IEEE Transactions on Geoscience and Remote Sensing* (7), 41, 1561– 1570.

Fransson, J. E. S., Smith, G., Askne, J. & Olsson, H. (2001). Stem volume estimation in boreal forests using ERS-1/2 coherence and SPOT XS optical data. *International Journal of Remote Sensing* (14), 22, 2777–2791.

Fritz, T. (2012). *TanDEM-X. Ground Segment. TanDEM-X Experimental Product Description. Issue: 1.2*. Deutsches Zentrum fuer Luft- und Raumfahrt (DLR): Oberpfaffenhofen.

Fritz, T. & Eineder, M. (2013). *TerraSAR-X Ground Segment. Basic Product Specification Document. Issue: 1.9*. Deutsches Zentrum fuer Luft- und Raumfahrt (DLR): Oberpfaffenhofen.

Gama, F. F., Dos Santos, J. R. & Mura, J. C. (2010). Eucalyptus Biomass and Volume Estimation Using Interferometric and Polarimetric SAR Data. *Remote Sensing* (4), 2, 939–956.

Gibbs, H. K., Brown, S., Niles, J. O. & Foley, J. A. (2007). Monitoring and estimating tropical forest carbon stocks: making REDD a reality. *Environmental Research Letters*, 2, 1–13.

GOFC-GOLD (2012). *A sourcebook of methods and procedures for monitoring and reporting an-thropogenic greenhouse gas emissions and removals associated with deforestation, gains and losses of carbon stocks in forests remaining forests, and forestation. GOFC-GOLD Report version COP18-1*. Wageningen University: Wageningen.

Gonzalez, P., Asner, G. P., Battles, J. J., Lefsky, M. A., Waring, K. M. & Palace, M. (2010). Forest carbon densities and uncertainties from Lidar, QuickBird, and field

9*forest*

measurements in California. *Remote Sensing of Environment* (7), 114, 1561–1575.

Hajnsek, I. & Hoekman, D. H. (2005). *Final Report, INDREX II - Indonesian Radar Experiment Campaign over Tropical Forest in L- and P-band, Version 1, 14 June 2006, ESA Contract RFQ/3-11077/04/NL/CB, Report ESA*. DLR and Wageningen University: Wageningen.

Hajnsek, I., Kugler, F., Lee, S.-K. & Papathanassiou, K. (2009). Tropical-ForestParameter Estimation by Means of Pol-InSAR: The INDREX-II Campaign. *IEEE Transactions on Geoscience and Remote Sensing* (2), 47, 481–493.

Hanssen, R. (2001). *Radar interferometry: data interpretation and error analysis.* Kluwer Academic: Dordrecht.

Hijmans, R. J. (2013). *raster: Geographic data analysis and modeling.* http://CRAN.R-project.org/package=raster: R package version 2.1-66.

Hooijer, A., Page, S., Canadell, J. G., Silvius, M., Kwadijk, J., Wosten, H. & Jauhiainen, J. (2010). Current and future CO2 emissions from drained peatlands southeast Asia.. *Biogeosciences* (5), 7, 1505–1514.

Huang, S. & Liu, D. (2007). Some uncertain factor analysis and improvement in spaceborne synthetic aperture radar imaging. *Signal Processing* (12), 87, 3202–2317.

Huffman, G. J., Adler, R. F., Morrissey, M. M., Bolvin, D. T., Curtis, S., Joyce, R., McGavock, B. & Susskind, J. (2001). Global precipitation at one-degree daily resolution from multisatellite observations. *Journal of Hydrometeorology* (1), 2, 36–50.

Jauhiainen, J., Takahashi, H., Heikkinen, J. E. P., Martikainen, P. J. & Vasander, H. (2005). Carbon fluxes from a tropical peat swamp forest floor. *Global Change Biology* (10), 11, 1788–1797.

Kaneko, N. (1992). Comparison of forest structure of tropical peat swamp forests in Southern Thailand and Malaysia. In: Kyuma, K., Vijarnsorn, P. & Zakaria, A. (Eds.): *Coastal lowland ecosystems in Southern Thailand and Malaysia*: Kyoto.

Kasischke, E. S., Melack, J. M. & Dobson, M. C. (1997). The use of imaging radars for ecological applications: A review. *Remote Sensing of Environment* (2), 59, 141–156.

Keitt, T. H., Bivand, R., Pebesma, E. & Rowlingson, B. (2013). *rgdal: Bindings for the Geospatial Data Abstraction Library*. http://CRAN.Rproject.org/package=rgdal: R package version 0.8-14.

Koch, B. (2010). Status and future of laser scanning, synthetic aperture radar and hyperspectral remote sensing data for forest biomass assessment. *ISPRS Journal of Photogrammetry and Remote Sensing*, 65, 581–590.

00*forest*

Koch, B., Heyder, U. & Weinacker, H. (2006). Detection of individual tree crowns in airborne Lidar data. *Photogrammetric Engineering & Remote Sensing* (72), 4, 357–363.

Koehl, M., Lister, A., Scott, C., Baldauf, T. & Plugge, D. (2011). Implications of sampling design and sample size for national carbon accounting systems. *Carbon Balance and Management* (1), 6, 1–20.

Koh, L., Miettinen, J., Liew, S. & Ghazoula, J. (2011). Remotely sensed evidence of tropical peatland conversion to oil palm. *Proceedings of the National Academy of Science of the United States of America (PNAS)* (12), 108, 5127–5132.

Koh, L., Gibbs, H., Potapov, P. & Hansen, M. (2012). REDDcalculator.com: A webbased decision-support tool for implementing Indonesia's forest moratorium. *Methods in Ecology and Evolution*, 3, 310–316.

Krause, P., Boyle, D. P. & Baese, F. (2005). Comparison of different efficiency criteria for hydrological model assessment. *Advances in Geosciences*, 5, 89–97.

Krieger, G., Moreira, A., Fiedler, H., Hajnsek, I., Werner, M., Younis, M. & Zink, M. (2007). TanDEM-X: A Satellite Formation for High-Resolution SAR Interferometry. *IEEE Transactions on Geoscience and Remote Sensing* (11), 45, 3317– 3341.

Krieger, G., Hajnsek, I., Papathanassiou, K., Younis, M. & Moreira, A. (2010). Interferometric Synthetic Aperture Radar (SAR) Missions Employing Formation Flying. *Proceedings of the IEEE* (5), 98, 816–843.

Kronseder, K., Ballhorn, U., Boehm, V. & Siegert, F. (2012). Above ground biomass estimation across forest types at different degradation levels in Central Kalimantan using LiDAR data. *International Journal of Applied Earth Observation and Geoinformation* (0), 18, 37–48.

Kugler, F., Hajnsek, I. & Papathanassiou, K. (2013). Pol-InSAR techniques for forest characterizationwith TanDEM-X. In: *Proceedings of PolInSAR 2013, 2013-0128-2013-02-01, Frascati (Rome), Italy*.

Kugler, F., Schulze, D., Hajnsek, I., Pretzsch, H. & Papathanassiou, K. (2014). TanDEM-X Pol-InSAR Performance for Forest Height Estimation. *IEEE Transactions on Geoscience and Remote Sensing* (10), 52, 6404–6422.

Kuntz, S. (2010). Potential of spaceborne SAR for monitoring the tropical environments. *Tropical Ecology*, 51, 3–10.

Le Toan, T., Beaudoin, A., Riom, J. & Guyon, D. (1992). Relating forest biomass to SAR data. *IEEE Transactions on Geoscience and Remote Sensing* (2), 30, 403–411.

Lefsky, M. A., Harding, D. J., Keller, M., Cohen, W. B., Carabajal, C. C., Del Bom Espirito-Santo, F., Hunter, M. O. & Oliveira, R. de (2005). Estimates of forest canopy height

01*forest*
and aboveground biomass using ICESat. *Geophysical Research Letters* (22), 32, 1–4.

Liesenberg, V., Boehm, H. D., Joosten, H. & Limin, S. (2013). Spatial and temporal variation of above ground biomass in tropical dome-shaped peatlands measured by airborne LiDAR. *Proceedings of international symposium on wild fire and carbon management in peat-forest in Indonesia*, 1, 99–117.

Luckman, A., Baker, J. & Wegmueller, U. (2000). Repeat-Pass Interferometric Coherence Measurements of Disturbed Tropical Forest from JERS and ERS Satellites. *Remote Sensing of Environment* (3), 73, 350–360.

Luckman, A., Baker, J., Honzak, M. & Lucas, R. (1998). Tropical Forest Biomass Density Estimation Using JERS-1 SAR: Seasonal Variation, Confidence Limits, and Application to Image Mosaics. *Remote Sensing of Environment* (2), 63, 126–139.

Maniatis, D. & Mollicone, D. (2010). Options for sampling and stratification for national forest inventories to implement REDD+ under the UNFCCC. *Carbon Balance and Management*, 5, 1–9.

Martin, A. R. & Thomas, S. C. (2011). A Reassessment of Carbon Content in Tropical Trees. *PLoS ONE* (8), 6, 1–9.

Mascaro, J., Detto, M., Asner, G. P. & Muller-Landau, H. C. (2011). Evaluating uncertainty in mapping forest carbon with airborne LiDAR. *Remote Sensing of Environment* (12), 115, 3770–3774.

Mitchard, E., Saatchi, S., Lewis, S., Feldpausch, T., Woodhouse, I., Sonke, B., Rowland, C. & Meir, P. (2011). Measuring biomass changes due to woody encroachment and deforestation/degradation in a forest-savanna boundary region of central Africa using multi-temporal L-band radar backscatter. *Remote Sensing of Environment* (11), 115, 2861–2873.

Morel, A. C., Saatchi, S. S., Malhi, Y., Berry, N. J., Banin, L., Burslem, D., Nilus, R. & Ong, R. C. (2011). Estimating aboveground biomass in forest and oil palm plantation in Sabah, Malaysian Borneo using ALOS PALSAR data. *Forest Ecology and Management* (9), 262, 1786 –1798.

Muhamad, N. Z. & Rieley, J. O. (2002). Management of tropical peatlands in Indonesia: Mega reclamation project in Central Kalimantan. In: Rieley, J. O., Page, S. E. & Setiadi, B. (Eds.): *Proceedings of the International Symposium on Tropical Peatland* . BPPT and Indonesian Peat association: Jakarta, 155–162.

Murdiyarso, D., Hergoualc'h, K. & Verchot, L. (2010). Opportunities for reducing greenhouse gas emissions in tropical peatlands. *Proceedings of the National*

02*forest*

Academy of Science of the United States of America (PNAS) (46), 107, 19655–19660.

Nishimua, T. B., Suzuki, E., Kohyama, T. & Tsuyuzaki, S. (2007). Mortality and Growth of Trees in Peat-swamp and Heath Forests in Central Kalimantan After Severe Drought. *Vegetatio* (2), 188, 165–177.

Olander, L. P., Gibbs, H. K., Steininger, M., Swenson, J. J. & Murray, B. C. (2008). Reference scenarios for deforestation and forest degradation in support of REDD: a review of data and methods. *Environmental Research Letters*, 3, 1–11.

Page, S. E., Rieley, J. O. & Banks, C. J. (2011). Global and regional importance of the tropical peatland carbon pool. *Global Change Biology* (2), 17, 798–818.

Page, S. E., Rieley, J. O., Shotyk, O. W. & Weiss, D. (1999). Interdependence of peat and vegetation in a tropical peat swamp forest. *Philosphoical Transaction of the Royal Society*, 354, 1885–1897.

Page, S. E., Siegert, F., Rieley, J. O., Boehm, H.-D. V., Jaya, A. & Limin, S. (2002). The amount of carbon released from peat and forest fires in Indonesia during 1997. *Nature* (6911), 420, 61–65.

Papathanassiou, K. & Cloude, S. (2001). Single-baseline polarimetric SAR interferometry. *IEEE Transactions on Geoscience and Remote Sensing* (11), 39, 2352– 2363.

Perko, R., Raggam, H., Deutscher, J., Gutjahr, K. & Schardt, M. (2011). Forest Assessment Using High Resolution SAR Data in X-Band. *Remote Sensing* (4), 3, 792–815.

Phillips, V. D. (1998). Peatswamp ecology and sustainable development in Borneo. *Biodiversity & Conservation* (5), 7, 651–671.

Pitz, W. & Miller, D. (2010). The TerraSAR-X Satellite. *IEEE Transactions on Geoscience and Remote Sensing* (2), 48, 615 –622.

R Core Team (2013). *R: A Language and Environment for Statistical Computing*. R Foundation for Statistical Computing: Vienna.

Reinartz, P., Muller, R., Schwind, P., Suri, S. & Bamler, R. (2011). Orthorectification of VHR optical satellite data exploiting the geometric accuracy of TerraSAR-X data. *ISPRS Journal of Photogrammetry and Remote Sensing* (1), 66, 124 –132.

Reyes, G., Brown, S., Chapman, J. & Lugo, A. E. (1992). *Wood densities of tropical tree species*. USDA Forest Service: New Orleans.

Rosen, P., Hensley, S., Joughin, I., Li, F., Madsen, S., Rodriguez, E. & Goldstein, R. (2000). Synthetic aperture radar interferometry. *Proceedings of the IEEE* (3), 88, 333 –382.

03*forest*

Saatchi, S. S., Soares, J. V. & Alves, D. S. (1997). Mapping deforestation and land use in amazon rainforest by using SIR-C imagery. *Remote Sensing of Environment* (2), 59, 191 –202.

Saatchi, S., Marlier, M., Chazdon, R. L., Clark, D. B. & Russell, A. E. (2011b). Impact of spatial variability of tropical forest structure on radar estimation of aboveground biomass. *Remote Sensing of Environment* (11), 115, 2836–2849.

Santoro, M., Askne, J., Smith, G. & Fransson, J. E. (2002). Stem volume retrieval in boreal forests from ERS-1/2 interferometry. *Remote Sensing of Environment* (1), 81, 19 –35.

Santoro, M., Shvidenko, A., McCallum, I., Askne, J. & Schmullius, C. (2007). Properties of ERS-1/2 coherence in the Siberian boreal forest and implications for stem volume retrieval. *Remote Sensing of Environment* (2), 106, 154 –172.

Schlund, M., Poncet, F. v., Kuntz, S. & Hoekman, D. H. (2013). Relationship of canopy cover with TanDEM-X features in a tropical peat swamp forest. In: Jekel, T., Car, A., Strobl, J. & Griesebner, G. (Eds.): *GI Forum 2013. Creating the GISociety* . VDE: Offenbach, 109–113.

Schlund, M., Poncet, F. von, Hoekman, D. H., Kuntz, S. & Schmullius, C. (2014a). Importance of bistatic SAR features from TanDEM-X for forest mapping and monitoring. *Remote Sensing of Environment*, 151, 16–26.

Seber, G. A. F. & Lee, A. J. (2003). *Linear regression analysis*. Wiley & Sons: New Jersey.

Sorensen, K. W. (1993). Indonesian peat swamp forests and their role as a carbon sink. *Chemosphere* (6), 27, 1065 –1082.

St-Onge, B., Hu, Y. & Vega, C. (2008). Mapping the height and aboveground biomass of a mixed forest using lidar and stereo Ikonos images. *International Journal of Remote Sensing* (5), 29, 1277–1294.

Sweda, T., Tsuzuki, H., Maeda, Y., Boehm, V. & Limin, S. (2012). Above- and belowground carbon budget of degraded tropical peatland revealed by multitemporal airborne laser altimetry. In: *Proceedings of the 14th international peat congress, Stockholm, Sweden, 3-8 June 2012*.

Verwer, C. & Meer, P. van der (2010). *Carbon pools in tropical peat forests - Towards a reference value for forest biomass carbon in relatively undisturbed peat swamp forests in Southeast Asia*. Wageningen University and Research Center (Alterrareport 2108): Wageningen.

Wagner, W., Luckman, A., Vietmeier, J., Tansey, K., Balzter, H., Schmullius, C., Davidson, M., Gaveau, D., Gluck, M., Le Toan, T. (2003). Large-scale mapping of boreal forest in SIBERIA using ERS tandem coherence and JERS backscatter data. *Remote Sensing of Environment* (2), 85, 125–144.

04*forest*

Waldes, N. J. L. & Page, S. E. (2002). Forest structure and tree diversity of a peat swamp forest in Central Kalimantan, Indonesia. In: *Proceedings of International Symposium on Tropical Peatlands, Jakarta (Indonesia), 22-08-2002-23-08-2002, BPPT*.

Wegmuller, U. & Werner, C. (1997). Retrieval of vegetation parameters with SAR interferometry. *IEEE Transactions on Geoscience and Remote Sensing* (1), 35, 18 –24.

Werf, G. R. van der, Morton, D. C., DeFries, R. S., Olivier, J. G. J., Kasibhatla, P. S., Jackson, R. B., Collatz, G. J. & Randerson, J. T. (2009). CO2 emissions from forest loss. *Nature Geoscience*, 2, 737–738.

Woesten, J. H. M., Clymans, E., Page, S. E., Rieley, J. O. & Limin, S. H. (2008). Peat-water interrelationships in a tropical peatland ecosystem in Southeast Asia. *Catena* (2), 73, 212–224.

Woodhouse, I. H., Mitchard, E. T. A., Brolly, M., Maniatis, D. & Ryan, C. M. (2012). Radar backscatter is not a 'direct measure' of forest biomass. *Nature Climate Change*, 2, 556–557.

6 WorldDEM^{TM} data for canopy height and aboveground biomass retrieval in a tropical peat swamp forest

M. Schlund[a,b], F. von Poncet[a], S. Kuntz[a], H.-D. V. Boehm[c], D. H. Hoekman[d] & Schmullius[b]

[a] *Airbus Defence and Space, Claude-Dornier-Str., 88090 Immenstaad, Germany* [b] *Department of Earth Observation, Friedrich-Schiller University, 07743 Jena, Germany* [c] *Kalteng Consultants, Kirchstockacher Weg 2, 85635 Hoehenkirchen, Germany* [d] *Dept. of Environmental Sciences,Wageningen University, Droevendaalsesteeg 4, 6708 PB Wageningen, The Netherlands*

Abstract

Forests have significance as natural carbon storage. Especially tropical peat swamp forests play an important role in the global carbon cycle despite their relatively small extent. Radar data has proven to be useful to estimate aboveground biomass due to their interferometric capability. Therefore, the potential of the globally available digital elevation model WorldDEM™ was investigated for aboveground biomass estimation in a tropical peat swamp forest. Existing field samples were used to up-scale field measured biomass to larger areas via canopy height models. These canopy height models were derived from an intermediate TanDEM-X DEM (iDEM; as a precursor for WorldDEM™) and LiDAR measurements.

The analysis showed high accuracies (RMSE = 5 m) for canopy height models based on iDEM and reliable estimation of aboveground biomass. The iDEM canopy height model, exclusively based on TanDEM-X, achieved a R^2 of 0.2, nonetheless resulted in a cross-validated RMSE of 54 t/ha (16 %). This is comparable to other aboveground biomass estimations in tropical peat swamp forests. A canopy height model retrieved from the difference of iDEM and an accurate LiDAR terrain model

achieved a considerably higher correlation with aboveground biomass ($R^2 = 0.68$) and low cross-validated RMSE of 24.5 t /ha (7.5 %). High accurate terrain models are not available on global scale. Therefore, the results suggest that an approach exclusively based on WorldDEM^{TM} could be used in areas where no accurate terrain model is available. Even though this will result in moderately lower accuracies it can be applied globally consistent.

6.1 Introduction

Forests have the ability to sequester carbon and thus are important in the global carbon cycle and for climate change mitigation (Werf et al. 2009, Gibbs et al. 2007, Olander et al. 2008). Using a conversion factor of approximately 50 % or less the stored carbon correlates with the biomass of the trees (Martin & Thomas 2011). Therefore, it is a prerequisite to estimate the aboveground biomass and its change over time to implement programs like REDD+ (Reducing Emissions from Deforestation and Degradation), where the reduction of carbon emission from deforestation and degradation and the enhancement of carbon stocks are incentivized. The REDD+ program is mainly intended for tropical countries due to their large forest cover and the high amount of carbon stored in tropical forests (Werf et al. 2009). Tropical peat swamp forests and their soils play a significant role in the global carbon cycle because their carbon emissions equal 1/4 of total emissions from tropical forests despite their relatively small extent compared to the overall tropical forests (Page et al. 2002, Page et al. 2011, Werf et al. 2009, Lawson et al. 2014).

Field measurements can be an important source to estimate aboveground biomass. Nevertheless, field measurements have their limits in inaccessible regions and/or over large areas. Therefore, it is recommended to use field measurements in sampling based schemes in combination with remote sensing due to their ability to up-scale the field measurements to a larger scale (Gibbs et al. 2007, Asner et al. 2009b). According to Koch (2010) exists two basic methods to estimate aboveground biomass with remote sensing, which can be called direct or indirect methods. Estimating aboveground biomass via direct methods means to relate the signal response with the biomass and establish a regression between those parameters (Koch 2010). Optical and SAR (Synthetic Aperture Radar) sensors are mainly used for the direct method. However, passive optical sensors have limited applicability due to the low correlation of the signal with the biomass (Schlerf et al. 2005, Rahman et al. 2008, Koch 2010). Their estimations are often not accurate

enough or saturate at biomass levels even lower than typically found in dense tropical forests.

SAR sensors seem more promising for directly assessing aboveground biomass since microwaves can penetrate into the forest canopy and interact with vegetation constituents (Balzter 2001, Dobson et al. 1995, Le Toan et al. 1992). Therefore, it is found that the SAR signal correlates with the biomass (Dobson et al. 1995, Le Toan et al. 1992). This is the case for SAR backscatter as well as interferometric coherence (Luckman et al. 2000, Saatchi et al. 1997, Dobson et al. 1995, Le Toan et al. 1992, Eriksson et al. 2003, Askne et al. 2003). Compared to C- and X-band, systems with longer wavelengths such as L- and P-band are considered more appropriate for backscatter based biomass estimations due to the ability to penetrate deeper into the canopy (Castro et al. 2003, Kasischke et al. 1997, Luckman et al. 2000, Saatchi et al. 1997). However, saturation levels of 100 to 150 t/ha were found for L-band SAR backscatter (Kasischke et al. 1997, Luckman et al. 1998, Luckman et al. 2000, Mitchard et al. 2011). Even lower saturation levels were reported using shorter wavelengths such as C-band (30 to 50 t/ha; Castro et al. 2003, Luckman et al. 2000, Gama et al. 2010) or X-band (no correlation to 80 t/ha; Gama et al. 2010, Englhart et al. 2011). In contrast, the interferometric coherence from L-, C- and X- band is frequently used to estimate growing stock volume or aboveground biomass showing higher saturation levels (Fransson et al. 2001, Wagner et al. 2003, Santoro et al. 2002, Santoro et al. 2007, Schlund et al. 2015). For example, Schlund et al. (2015) estimated a saturation level of approximately 350 t/ha for X-band coherence in a tropical peat swamp forest.

However, indirect methods for aboveground biomass estimation can even overcome the saturation limitation. Indirect methods estimate biomass via forest parameters like forest height, crown closure and stand type, which are used to estimate the biomass (Koch 2010, Lefsky et al. 2005). A frequently used method is to produce a digital surface model (DSM) and derive a canopy height model (CHM) by subtracting a digital terrain model (DTM). The CHM represents the vegetation height as well as the canopy surface (Koch et al. 2006) and is therefore used to estimate the biomass in combination with field measured data (Boehm et al. 2013, St-Onge et al. 2008, Dandois & Ellis 2013, Solberg et al. 2010, Drake et al. 2002). A number of studies proved the capability of LiDAR sensors in this approach (Boehm et al. 2013, St-Onge et al. 2008, Dandois & Ellis 2013, Drake et al. 2002). However, LiDAR campaigns today are mostly airborne and thus cost-intensive compared to space borne systems (Koehl et al. 2011, Koch 2010). Consequently, aboveground biomass estimations via LiDAR sensors are applicable mainly for small spatial coverage or should be integrated in sampling schemes for large area applications

(Asner et al. 2009b). Space borne systems can acquire large areas consistently but only with moderate resolutions. Optical as well as SAR sensor can be used to derive digital elevation models, allowing the CHM estimation. However, only SAR sensors can consistently acquire data over tropical forests because of their weather and day/night independence.

The potential of InSAR (interferometric synthetic aperture radar) for canopy height and aboveground biomass estimation has long been recognized. The method is based on the assumption that short wavelength SAR will penetrate marginally into the canopy. Thus, the resulting digital elevation model can be considered as surface model (DSM). SRTM (Shuttle Radar Topography Mission) C- and X-band were frequently used to estimate canopy height in combination with an external DTM (Sexton et al. 2009, Solberg et al. 2010, Weydahl et al. 2007). Sexton et al. (2009), for instance, found a RMSE of 4.7 m and 3.9 m estimating canopy height from SRTM and airborne LiDAR. Solberg et al. (2010) used SRTM X-band heights and LiDAR to determine a canopy height model, which resulted in a R^2 of 0.72 and 0.52 for biomass estimations with relative errors of 19 %. In order to yield stable estimates of SRTM height Kellndorfer et al. (2004) suggested a minimum mapping unit of 1.8 ha. Accuracy of canopy height model derivation with single-pass InSAR of X- and L-band from airborne sensors with high spatial resolution was assessed with a RMSE of 3.5 m in temperate woodlands (Balzter et al. 2007). The potential of X- and P-band InSAR for canopy height estimation was evaluated in tropical forests (Rombach & Moreira 2003, Gama et al. 2010, Neeff et al. 2005). For instance, Neeff et al. (2005) demonstrated the potential of airborne InSAR with X- and P-band for canopy height (R^2 = 0.83, RMSE = 4.1 m) and biomass estimation (R^2 = 0.89, cross-validated RMSE = 46.1 t/ha) in the tropical forest of the Amazon basin.

In contrast to airborne system, the TanDEM-X mission aims to create a global digital elevation model (DEM) on basis of interferometric SAR exploitation (Krieger et al. 2007). Digital elevation models derived from TanDEM-X InSAR dataset were used to estimate canopy height and biomass of boreal forests resulting in a relative error of 43 % on plot level and 19 % on stand level (Solberg et al. 2013, Rahlf et al. 2014, Solberg et al. 2015). The final product, which is called WorldDEM^(TM), consists of multiple TanDEM-X InSAR datasets resulting in specified vertical accuracies of 2 m (relative) and 4 m (absolute) on 12 m horizontal resolution (Airbus Defence and Space 2014).

However, REDD+ is focusing on tropical environments. Likewise the biomass estimation in tropical peatlands is becoming more important since their carbon content is not well studied, despite their importance in the global carbon cycle (Lawson et al. 2014, Werf et al. 2009). Therefore, the potential of the TanDEM-X

mission with its final surface model product called WorldDEM™ is evaluated in a tropical peat swamp forest. Canopy height models from WorldDEM™ are calculated and used for aboveground biomass estimation. However, main challenge of this approach is the availability of a digital terrain model representing the bare earth height. A number of studies show different approaches to retrieve canopy height from InSAR data via using a LiDAR DTM (Sexton et al. 2009, Solberg et al. 2010, Solberg et al. 2013, Rahlf et al. 2014), interferometric SAR exploitation of long wavelengths (Balzter et al. 2007, Sexton et al. 2009, Gama et al. 2010) or other data sources like topographic maps (Weydahl et al. 2007, Kellndorfer et al. 2004, Hyde et al. 2006). Therefore, the derivation of a canopy height model using the X-band elevation model and an airborne LiDAR DTM is evaluated in this study. Furthermore, a digital terrain model is extracted via interpolation and manual processing from the WorldDEM™. The accuracy and potential of WorldDEM™ for the retrieval of the canopy height model is evaluated and compared to LiDAR. Finally, the different canopy height models are used to estimate aboveground biomass via correlation with field measurements in a tropical peat swamp forest.

6.2 Study area

The study area is located in Central Kalimantan and is about 60 km west of the provincial capital Palangkaraya. In general, the climate is humid tropic divided into an averaged dry season from June to September and a wet season from October to May (Jauhiainen et al. 2005). The study area exhibits a flat terrain and is covered by tropical peat swamp forest, which is limited through the Kapuas River in the west (Fig. 6.1).
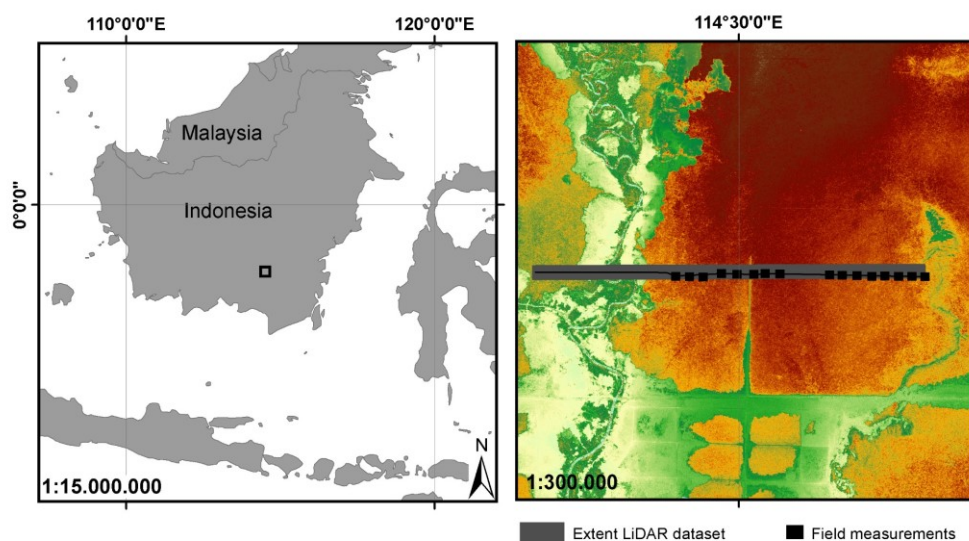
Fig. 6.1: Location of study area in Central Kalimantan, Indonesia (left) and iDEM of study area with location of field plots, LiDAR transect (grey) and profile from figure 2 and 6 (black line; right)

Tropical peat swamp forests differ significantly from tropical dryland forests (Lawson et al. 2014). Peat lands develop usually in low drainage areas with a high water table almost throughout the whole year resulting in a deficit of nutrients and accumulation of organic material (Phillips 1998, Page et al. 1999, Hooijer et al. 2010, Lawson et al. 2014). The study area has a convex topography, which results in a dome shaped terrain, visible in the digital terrain models (Fig. 6.2). This dome shape is typical for many peat lands (Phillips 1998).

The largest peat layer is at the top of the peat dome with decreasing peat thickness towards the edge of the dome (Sorensen 1993, Phillips 1998, Page et al. 1999). The
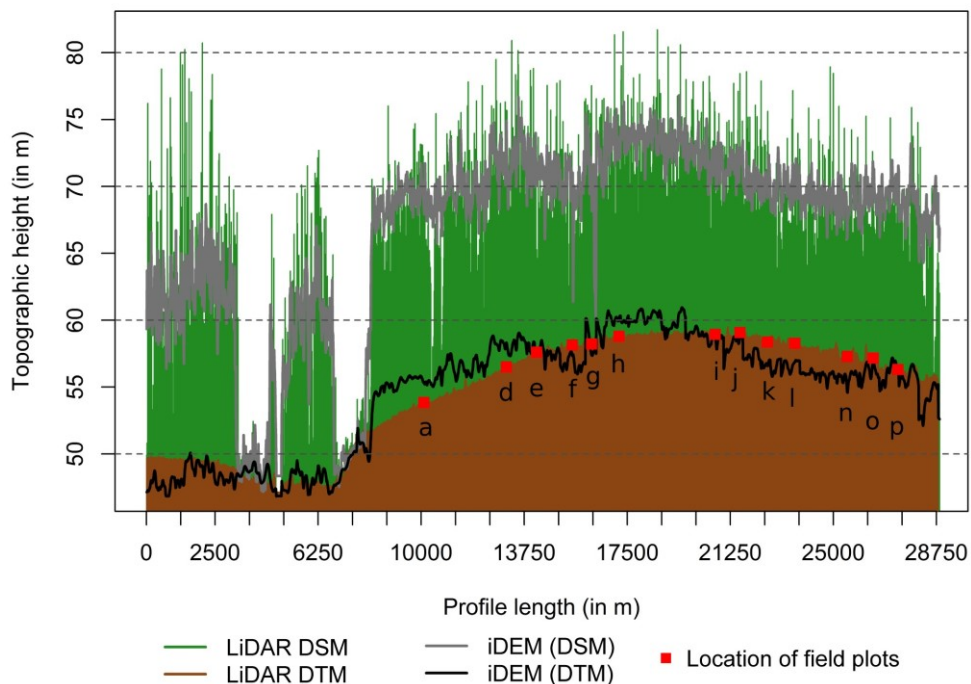
Fig. 6.2: Profile of LiDAR as well as iDEM DSM and DTM over peat dome (from west to east) with location of field transects

nutrients are elutriated from the top and thus the nutrient level decreases from the edges towards the top of the peat dome (Phillips 1998, Sorensen 1993, Page et al. 1999). This nutrient distribution results in a typical species composition and forest structure. Forests with high trees up to 35 m and high biomass are located towards the edge of the peat dome close to the river (Fig. 6.2, Fig. 6.3). The height and biomass of the trees decreases towards the top of the peat dome, whereas the tree density increases (Fig. 6.2, Fig. 6.3, Sorensen 1993, Page et al. 1999). Physiognomic

and structural profiles were created from field measurements (see Section 6.3.3) showing the transition from tall trees to smaller and thin trees, whereas increase in number of trees within the field transect. Field plots (a) to (d) are heterogeneous with dominating large trees resulting in high biomass, whereas (j) to (p) exhibit small trees with a homogenous height (Fig. 6.3).

6.3 Data description

6.3.1 Interferometric height models

The potential of a globally available digital elevation model based on interferometric estimations was evaluated. This digital elevation model was created by using a close formation of the two German SAR satellites, TerraSAR-X and TanDEM-X. Both SAR sensors of the TanDEM-X mission acquired interferometric data of the

Fig. 6.3: Physiognomic - structural profiles of the 16 field plots allocated along the transect

entire land mass several times between 2010 and 2014. Both sensors are able to transmit the electromagnetic wave with a phased-array X-band antenna having a carrier frequency of 9.65 GHz (Pitz & Miller 2010), corresponding to a wavelength of ∼3.1 cm. The data for the creation of the global digital elevation model were acquired in the horizontal polarization (HH) using the so-called bistatic acquisition in StripMap mode (i.e. one satellite transmits the SAR signal and both receive the signal simultaneously from slightly different orbit positions resulting in negligible temporal decorrelation effects).

However, it is worth noting that the interferometric exploitation is a demanding task in dense tropical forests due to higher volume decorrelation compared to other land cover with low volume scattering or even bare soil. Therefore, for this investigation WorldDEM™ data was not yet available in the study area, as the processing at present focuses first on temperate regions. Nevertheless, a TanDEM-X intermediate DEM (iDEM) was available for the test site in Central Kalimantan in order to assess the potential of the WorldDEM™ coming soon. The iDEM was created using only one baseline configuration out of several interferometric acquisitions of the mission's first year. The final WorldDEM™ will be created out of multiple acquisitions and baseline configurations in order to fulfill the specified vertical accuracy (Krieger et al. 2007, Airbus Defence and Space 2014). Thus the accuracy of this intermediate product (iDEM) may be lower than the WorldDEM™. However, it can be argued that the assessment of its potential for aboveground biomass estimations is already useful with the iDEM. This is due to the similar data source and processing differing only in the multiple-baseline phase unwrapping, affecting mainly mountainous regions (Wessel et al. 2013). The iDEM tile used in this study was created with TanDEM-X acquisitions from December 21, 2010 to January 15, 2012 covering a 1° by 1° cell. In a semi-automated process a digital terrain model representing the bare earth terrain was created on basis of the iDEM. Firstly, objects were delineated and their height estimated. Secondly, this estimated height was subtracted from the respective objects. Finally, small objects were removed and the terrain height interpolated. Both interferometric height models had a posting of about 12 m (0.4" by 0.4", Wessel et al. 2013, Airbus Defence and Space 2014). Since the iDEM is an intermediate product its accuracy as well as the accuracy of the derived DTM was not specified in the product description. In contrast, the final WorldDEM™ is specified with an absolute vertical accuracy of 4 m and a relative vertical accuracy of 2 m at slopes with ≤ 20 % and 4 m at slopes with > 20 %, respectively (Airbus Defence and Space 2014).

6.3.2 LiDAR height models

Full-waveform LiDAR data were acquired on August 05, 2007 on a sunny and cloudfree day with a Riegl LMS-Q560 instrument (Table 6.1). The Riegl LMS-Q560 instrument was mounted on a helicopter and flown in an altitude of 500 m above ground. The acquisition date was in the dry season in order to avoid inaccurate derivation of the DTM due to high water levels on the ground. The laser beams were classified with a terrain-adaptive bare earth algorithm into ground and over ground classes. Delaunay triangulation was utilized in order to create a triangular irregular network (TIN), which was the basis for the extraction of square grid pixels with a

linear interpolation (Boehm et al. 2013, Liesenberg et al. 2013). The DTM were extracted from the DSM by an IDL software package used by company Milan (Boehm et al. 2013). The final dataset had a horizontal resolution of half meter and a vertical resolution of 0.15 m. The LiDAR dataset covered about 34 km^2 of the iDEM.

Tab. 6.1: Properties of the airborne LiDAR system LMS-Q560 (Riegl)

Property	Value
Scan angle	±30°
Swath width	~500 m
Scan frequency	66 to 100 kHz
Vertical laser beam accuracy	≤0.1 m
Horizontal laser beam accuracy	≤0.5 m (for x- & y-direction)
Laser beam (mrad)	0.5 (footprint up to 30 cm)
Laser wavelength	1.5 μm (near-infrared)
Point density	1.4 points/m^2

6.3.3 Field data

Field measurements were conducted in 2013 and 2014. A transect along west-east direction in the study area covering the whole peat dome from riverine forest to low pole forest were used to sample field plots systematically every kilometer (Fig. 6.1). Hence, a large range of aboveground tree biomass values and variability of vegetation zones of a tropical peat swamp forest with different vertical structures were covered despite the difficult accessibility of the area. In total, 16 sample plots with a size of 50 m by 20 m were measured. The small size of field plots was chosen assuming no drastic change of the forest within the length of the plots in order to sample more field plots in this peat swamp forest, which is quite difficult to assess on ground. All field plots were located with GPS. Within a plot all trees with a diameter at breast height (dbh) larger than 10 cm were measured and tree species recorded (Table 6.2).

In total, 16 field plots with tree measurements were located within iDEM and 13 within LiDAR coverage. The field measurements covered a range of aboveground biomass between 250 t/ha and 450 t/ha. The aboveground biomass values were calculated by allometric equations as described in Section 6.4.2. A clinometer was used for the tree height measurements. The stems of the measured peat swamp forest trees were relatively thin (in average 14.4 cm; Tab. 6.2) and most of them were regularly shaped. Irregular cross sections of stems were not handled individually.

Tab. 6.2: Field measurements and according mean, minimum and maximum of all measured trees

Measurement	Mean	Minimum	Maximum
Tree height (in m)	15.6	5.3 m	37.8 m
Height of first green branch (in m)	9.6	1.5	26.9
DBH (in cm)	14.4	10	63.3
Average number of trees/ha	1329.4	-	-

6.4 Methods

6.4.1 Verification of height models

The accuracy of the iDEM and the derived DTM was assessed by comparison with the respective LiDAR DSM and DTM. For this purpose, the LiDAR elevation models were resampled to similar pixel-size as the iDEM (12 m). Different canopy height models were calculated by subtracting the LiDAR DTM from LiDAR DSM (CHM$_{LiDAR}$), the LiDAR DTM from iDEM (CHM$_{iDEM/LiDAR}$) as well as the iDEM from iDEM DTM (CHM$_{iDEM}$; Table 6.3).

Tab. 6.3: Overview of available canopy height models

Canopy height model	Input DSM	Input DTM	Original spatial resolution	Number of used field transects
CHM$_{iDEM}$	iDEM DSM	iDEM DTM	12 m	16
CHM$_{iDEM/LiDAR}$	iDEM DSM	LiDAR DTM	12 m	13
CHM$_{LiDAR}$	LiDAR DSM	LiDAR DTM	0.5 m	13

In order to evaluate the different height models quantitatively, a statistical analysis was carried out using statistical quality criterions on pixel basis. The root mean square error (RMSE) and linear error of 90 % (LE 90) were used as absolute accuracy measures. The RMSE was calculated with the following formula:

$$\text{█████████████████████████████} (in\ \%) = \text{███████████} \tag{6.1}$$

The LE 90 is a commonly used criterion to evaluate a DEM in vertical dimensions. This value describes the vertical distance in which 90 % of the control points and corresponding model values should be found from each other. The mean error (ME), standard error (SE), and a ratio of both errors (k) were used to calculate the LE 90:

$$\blacksquare \tag{6.2}$$

$$\blacksquare \tag{6.3}$$

$$\blacksquare$$

$$LE90 = ME + (k * SE) \tag{6.5}$$

The relative volume error ($V\ E_{rel}$) was calculated in order to estimate the systematic over- or underestimation of the model:

$$\blacksquare \tag{6.6}$$

Positive values indicate a systematic underestimation of the model versus the reference whereas negative values indicate a systematic overestimation of the model against the reference. Additionally the coefficient of determination (R^2) was calculated as follows:

$$\blacksquare \tag{6.7}$$

, where y_i is the actual value of i and $\hat{y}_i$ the predicted value of i, and $\bar{y}$ is the mean of actual values. The iDEM DSM heights were hardly comparable to LiDAR DSM heights considering differing penetration depths of the used signals. Therefore, the accuracy of the DSM was assessed over ground cover types with and without vegetation. Areas without vegetation cover were delineated assuming no penetration effects where the LiDAR CHM was below 2 m. In addition, the CHM$_{iDEM}$ as well CHM$_{iDEM/LiDAR}$ were verified against CHM$_{LiDAR}$ in order to assess the error propagation into canopy height models for biomass estimation.

6.4.2 Biomass estimation & verification

The aboveground tree biomass density in tons per hectare for each field plot was calculated using different allometric equations based on stand tables and volume data. Lawson et al. (2014) suggested that standard allometric equations have to be tested in peat forests since they were not developed for peat forests. Nevertheless, the choice was in favor of global or pan-tropical models (Brown & Lugo 1992, Brown et al. 1989, Chave et al. 2005, Hajnsek & Hoekman 2005, Chave et al. 2014), because

these are based on a large number of destructive measurements (Brown & Iverson 1992, Brown & Lugo 1992, Brown et al. 1989, Chave et al. 2005, Reyes et al. 1992, Manuri et al. 2014). Regional or local models exhibit a higher risk of biased predictions due to the small sample size (Chave et al. 2005, Manuri et al. 2014). In total, nine different approaches for biomass estimation were compared. The resulting aboveground biomass values differed substantially. The mean value of the different models ranged between 129 t/ha to 340 t/ha. Therefore, a comparison with other studies in peat swamp forests was conducted and the equation which resulted in similar aboveground biomass values compared to literature values was finally used (see Section 6.6.3). The aboveground tree biomass density used as field reference for each field plot was calculated according to following allometric equations (Brown & Lugo 1992, Hajnsek & Hoekman 2005):

$$biomass = vob * wd * bef (t/ha) \qquad (6.8)$$

where *vob* is the volume over bark, *wd* is volume-weighted average wood density which was determined as 0.57 t/m^3 representing the arithmetic mean for Asian forests (Reyes et al. 1992). The *bef* is the biomass expansion factor in order to include leaves, twigs, and branches. The volume over bark was calculated as the sum of bole volume (*bv*):

$$bole\ volume = basal\ area * total\ tree\ height * shape\ factor \qquad (6.9)$$ with a shape factor of 0.7. The biomass expansion factor for bole volume equal or larger than 190 t/ha was determined as 1.74. The biomass expansion factor for a bole volume below 190 t/ha was calculated (Brown & Lugo 1992):

$$bef = exp(3.213 - 0.506 * ln(bv)) \qquad (6.10)$$

Mean values of the different canopy height models were extracted for each field plot. Each 0.1 ha grid cell contained about 10 pixels with a pixel spacing of 12 m for iDEM models. It can be assumed that this yielded stable results due to the high accuracy specified for WorldDEM^{TM}, which was also achieved in this iDEM sample (see Section 6.5.1). The aboveground biomass value for each plot was correlated with the corresponding mean value of the CHM from iDEM (CHM$_{iDEM}$ as well as CHM$_{iDEM/LiDAR}$) and CHM$_{LiDAR}$. A linear model via least squares regression fitting (Seber & Lee 2003) was applied for the different canopy height models with the response variable aboveground biomass. However, not all field plots were located within the LiDAR dataset. Therefore, those field plots were not used for any model

based on LiDAR DTM or DSM resulting in a smaller number of field observation with 13 samples (Table 6.3).

An explicit validation data set was not available due the difficult accessibility of the area resulting in the low number of field plots. Therefore, a k-fold crossvalidation was applied in order to estimate the goodness of the models (Breiman et al. 1984, Kohavi 1995), where k was set to 10. The 10-fold cross-validation was frequently used and recommended for such purposes (Molinaro et al. 2005, Kohavi 1995, Breiman & Spector 1992, Breiman 1996).

6.5 Results

6.5.1 Goodness of the height models

The iDEM DSM achieved a RMSE of 0.74 m and a LE90 of 0.79 m compared to LiDAR measurements in areas without vegetation cover without any significant over or underestimation (VE_{rel} = 0.1 %, Fig. 6.5). Thus the accuracy of this iDEM even exceeded the value specified for WorldDEM™. The main topologic features were clearly visible in both models. The forest edge in the western part of the height models had a similar shape and extent. The canal from north to south was also visible in both DSMs (Fig. 6.4). When including areas with vegetation cover, the accuracy decreased to a RMSE of 5.1 m and a LE90 of 7.48 m. The observed VE_{rel} of -3 %. revealed a small systematic overestimation. The investigations confirmed that the value variations were much smaller in the iDEM DSM compared to LiDAR DSM (Fig. 6.2, Fig. 6.5).

In contrast to the DSM, the variations in the iDEM DTM were larger compared to LiDAR DTM. The iDEM DTM represented the terrain topography in general, with minor overestimations where taller trees and underestimations where smaller trees were present (Fig. 6.2). However, the iDEM DTM achieved also very high accuracies even underneath forest cover with a RMSE of 1.39 m and LE90 of 1.49 m (Fig. 6.5). The iDEM DTM showed no systematic over- or underestimation with a relative volume error of 0.1 %.

Overall, the iDEM DSM ranged between 47 m and 79 m, whereas the corresponding DTM had a value range of 46 m and 62 m. The LiDAR DTM suggested a similar value range of about 47 m and 65 m. This confirmed the flatness of the area. The LiDAR DSM resulted in a similar minimum value of 47 m, but had a higher maximum of about 90 m. As expected, the errors from both models propagated to the CHM_{iDEM}. Nevertheless, the canopy height model derived exclusively from
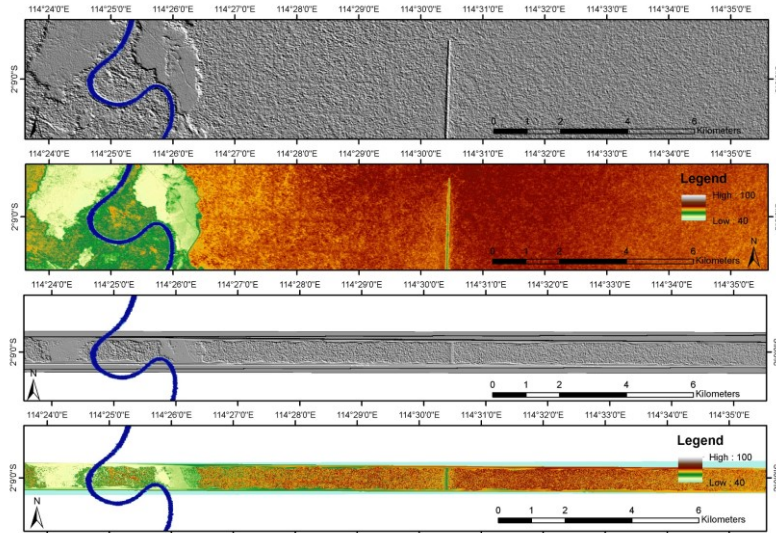
Fig. 6.4: Comparison of iDEM DSM (and corresponding shaded relief; top) & LiDAR DSM (and corresponding shaded relief, bottom)

Fig. 6.5: Color density representation of scatterplots from iDEM DSM (left) and iDEM DTM (right) validation under vegetation cover (top) and without vegetation cover (bottom)

iDEM achieved a moderate RMSE of 5.2 m and LE90 of 7.6. The lower variations of the DSM and the overestimation of DTM at taller trees and underestimation at smaller trees resulted in a lower spatial variability of the forest canopy height compared to LiDAR. The CHM$_{iDEM}$ were homogenous over all forest areas, whereas

the CHM$_{LiDAR}$ indicated trends of lower and higher vegetation. This was clearly visible in the east of the height profile (Fig. 6.6 top). In contrast, the CHM$_{iDEM/LiDAR}$ represented differences in vegetation height quite well compared to CHM$_{LiDAR}$ (Fig. 6.6 lower part). Nevertheless, CHM$_{iDEM/LiDAR}$ achieved similar accuracies compared to CHM$_{iDEM}$ with a RMSE of 5.1 m and LE90 7.5 m. The value range of the CHM$_{iDEM}$ was substantially lower compared to LiDAR. The CHM based on iDEM had a range from 0 m to 25 m, whereas the CHM$_{LiDAR}$ ranged between 0 m and 37 m.
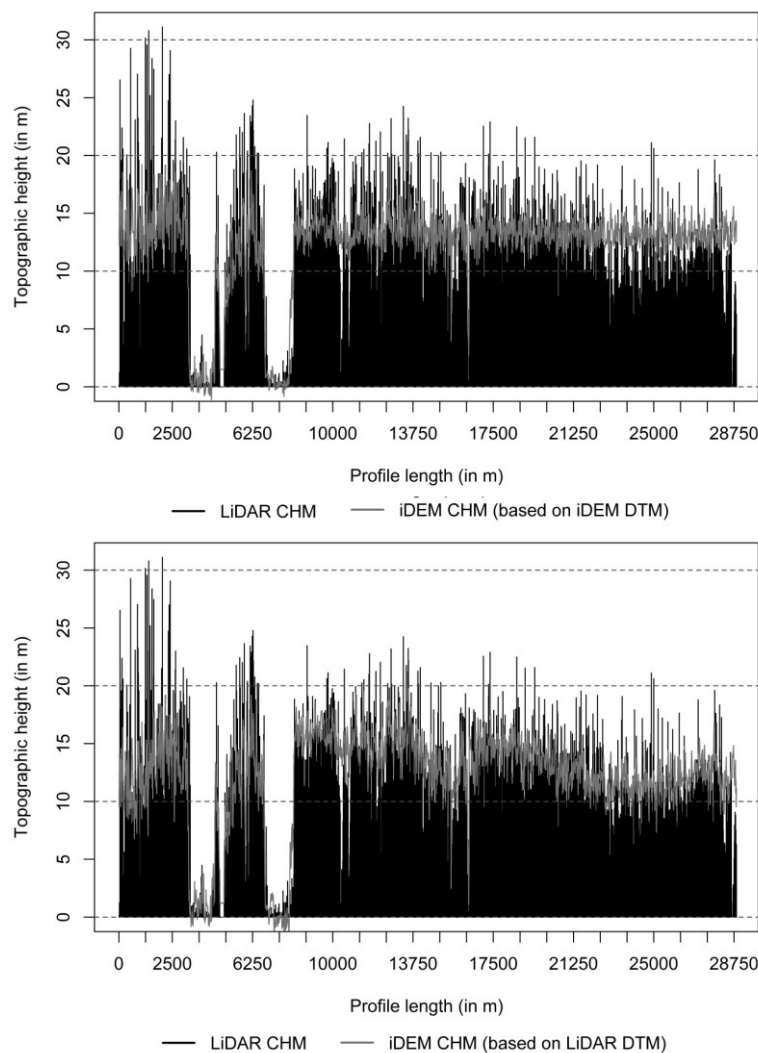
Fig. 6.6: Profile of CHM$_{LiDAR}$ (black) and two different iDEM CHMs (CHM$_{iDEM}$ = up, CHM$_{iDEM/LiDAR}$ = low)

6.5.2 Biomass estimation

The CHM$_{iDEM/LiDAR}$ and field measured aboveground biomass showed a high coefficient of determination with 0.68 (Fig. 6.7). The CHM$_{iDEM}$ resulted in a substantially lower R^2 of 0.18. The CHM$_{iDEM}$ ranged between 12 m and 14 m for the

field plots, whereas the biomass ranged between 258 t/ha and 440 t/ha. In contrast, the

CHM$_{iDEM/LiDAR}$ had a larger range of 9.9 m and 14.8 m compared to the CHM$_{iDEM}$, although the derived biomass range was almost similar (258 t/ha - 410 t/ha). The CHM$_{LiDAR}$ ranged between 6.3 m and 12.9 m and resulted in a R^2 of 0.75 (Fig. 6.7).
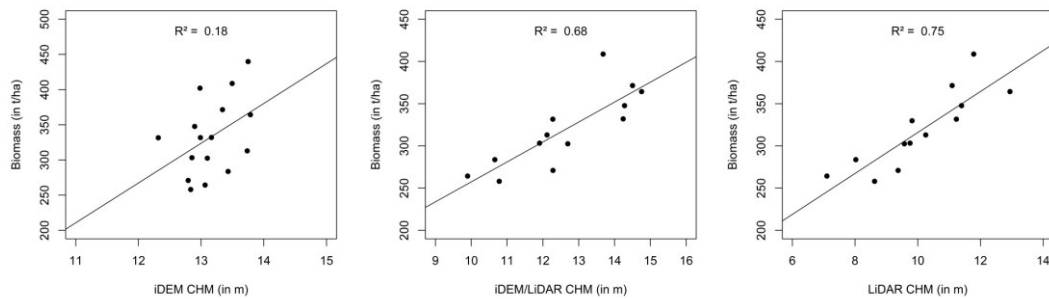
Fig. 6.7: Regression of canopy height models versus aboveground biomass

Despite the low coefficient of determination for the CHM$_{iDEM}$, the 10-fold-crossvalidation resulted in a moderate average RMSE of 54.1 t/ha representing 16.3 % of the mean biomass. As expected due to the substantial higher R^2 the other CHMs resulted in substantially lower average RMSEs of 24.5 t/a (7.5 %; CHM$_{iDEM/LiDAR}$) and 21.3 t/ha (6.5 %, CHM$_{LiDAR}$), respectively. The uniform CHM$_{iDEM}$ resulted in weak biomass differences along the transect, whereas the CHM$_{iDEM/LiDAR}$ and CHM$_{LiDAR}$ biomass estimation clearly indicated high biomass in the west close to the river and lower biomass in the east and at the top of the peat dome (Fig. 6.8). However, the range of all biomass estimation was quite similar in forested areas with about 200 t/ha and 500 t/ha.
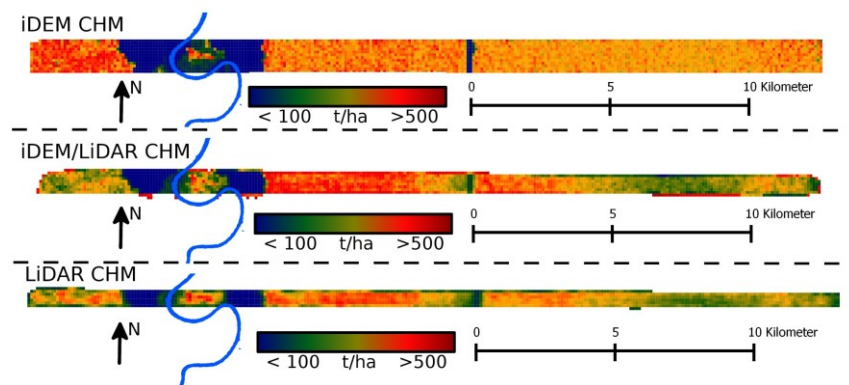
Fig. 6.8: Comparison of aboveground biomass estimation from CHM$_{iDEM}$, CHM$_{iDEM/LiDAR}$ & CHM$_{LiDAR}$

6.6 Discussion

6.6.1 Height accuracy and implications for canopy height models

The results indicated a high accuracy for the iDEM DSM for surfaces without forest cover, which is expected to further improve with the availability of WorldDEM™. Thus the iDEM DSM already fulfilled the height accuracy specified for the WorldDEM™ product (Airbus Defence and Space 2014). However, the surface height variability in areas with vegetation cover of the iDEM DSM was small compared to LiDAR DSM. These differences have multiple reasons. Firstly, the acquisition geometry of an InSAR and LiDAR system is different. The iDEM was acquired with a space borne SAR interferometer, which acquired the data in sidelooking geometry. This results in a lower probability to detect the ground or smaller trees in openings of the forest canopy compared to a nadir looking system like LiDAR. Secondly, the resolution of both systems is different. LiDAR acquired the data with one meter resolution. The iDEM was derived from TanDEM-X StripMap data with a resolution of about 3 m and was posted to 12 m (Wessel et al. 2013). Thirdly, short wavelength of X-band interacts mainly with constituents of the upper canopy resulting in a low penetration depth (Solberg et al. 2010, Dobson et al. 1995). In addition, the measured surface height, often called InSAR height, is a combination of the height and density of the forest in X-band (Treuhaft & Siqueira 2004, Askne et al. 2013). Differences in signal sampling resolution and averaging for noise reduction in combination with side-looking geometry and low penetration depth explain the lower amplitude and variation of the iDEM compared to LiDAR. In contrast, LiDAR acquired the data with a high resolution of about 0.5 m mainly in nadir from a helicopter resulting in a higher probability to detect the height of smaller trees and even openings in the forest canopy. This could explain the small overestimation of iDEM compared to LiDAR despite the penetration depth of X-band InSAR.

Wallington et al. (2004) found low accuracies for DTM generated from X-band InSAR interpolation, resulting in low accuracies in the canopy height model (RMSE = 23.5 m). In contrast, the iDEM DTM achieved high accuracies with and without vegetation cover fulfilling the WorldDEM™ specifications. This suggests that the iDEM DTM can be used for canopy height model calculation. Nevertheless, the reconstruction and quality of the terrain model largely depends on ground visibility and complexity of the terrain. Generally, the actual terrain height values are lowest where the highest vegetation existed, whereas highest terrain values are present where the lowest vegetation occurred. The iDEM DTM did not represent the shape of the terrain in areas where bare earth within the forest was not visible. Therefore,

the DTM follows the canopy surface thus resulting in an almost constant canopy height model. The inaccuracies of iDEM DSM and iDEM DTM propagated into the canopy height estimation. The CHM_{iDEM} resulted in a uniform forest canopy, whereas the LiDAR showed trends of higher vegetation in the west and lower vegetation on top of the peat dome and in the east of the top. Therefore, the canopy surface is uniform, but not the terrain underneath. Nevertheless, the RMSE of the CHM_{iDEM} is low and similar to other canopy height model estimations with InSAR (Neeff et al. 2005, Balzter et al. 2007, Rombach & Moreira 2003, Hyde et al. 2006). As expected, canopy height models with combining InSAR surface height and LiDAR terrain height achieved higher accuracies (Sexton et al. 2009). Nevertheless, the CHM_{iDEM} based on a single data source achieved comparable accuracies in dense tropical forest. However, the derivation of the WorldDEM DTM still is a limitation, which can potentially result in inaccuracies especially in difficult terrain and closed forests.

6.6.2 Biomass estimation with canopy height models

The biomass estimations resulted in relative RMSE of 16 % for TanDEM-X based CHM_{iDEM} compared to 6.5 % for LiDAR based CHM_{LiDAR} and 7.5 % for the combination of both sources ($CHM_{iDEM/LiDAR}$). Since the CHM_{LiDAR} and $CHM_{iDEM/LiDAR}$ resulted in a similar RMSE, it could be argued that the iDEM DSM is suitable to estimate aboveground biomass with high accuracy in cases where an accurate terrain model exists. However, a highly accurate DTM is often not available on larger scales. In this case, the iDEM DTM is a useful option to produce a CHM and estimate the aboveground biomass. This has impact on the accuracy, but could be still sufficient for biomass estimations (RMSE=16 %) as indicated by this study.

It was previously found that LiDAR compared to InSAR resulted in significantly lower RMSE in biomass estimations in boreal forests or temperate forests (Rahlf et al. 2014, Naesset et al. 2011, Hyde et al. 2006). This was not confirmed by this study in tropical forests showing similar strength of correlation to biomass for $CHM_{iDEM/LiDAR}$ and CHM_{LiDAR}. The height and density of the forest influence the resulting surface height of X-band InSAR estimate, whereas both parameters explain the biomass variation to a large extent (Askne et al. 2013, Treuhaft & Siqueira 2004, Solberg et al. 2010). Therefore, it could be argued that the InSAR surface height estimation can achieve comparable accuracies to LiDAR. The iDEM as precursor for WorldDEM™ performed similar to previously investigated biomass estimations in tropical forests based on airborne InSAR canopy height models (Neeff et al. 2005, Gama et al. 2010, Treuhaft et al. 2009). For instance, Treuhaft et al. (2009) estimated the aboveground biomass of tropical forests in Costa Rica resulting in an accuracy of 30 %, whereas 14 - 19 % were attributed to InSAR errors. Neeff et al. (2005)

reported a cross-validated RMSE of 46.1 t/ha on basis of an InSAR CHM and P-band backscatter, whereas Gama et al. 2010 reported a RMSE of 16 t/ha (20 % of mean biomass).

> Biomass estimations in tropical peat swamp forest were mainly based on combination of field measurements and LiDAR data (Boehm et al. 2013, Kronseder et al. 2012, Englhart et al. 2013, Ballhorn et al. 2011). Kronseder et al. (2012) estimated the biomass via LiDAR with a RMSE of 95 t/ha (41 %) in the tropical peat swamp forest of the Sebangau Catchment. Boehm et al. (2013) and Englhart et al. (2013) achieved accuracies in their biomass estimation of 20 % and 50 t/ha with LiDAR in peat swamp forests. SAR data was also frequently used to estimate biomass of tropical peat swamp forests (Englhart et al. 2011, Morel et al. 2011, Schlund et al. 2015). However, SAR backscatter based methods suffer mostly from saturation effects. Morel et al. (2011) suggested a saturation at 88 t/ha for L-band from ALOS PALSAR, whereas Englhart et al. (2011) reported a saturation of 80 t/ha for X-band. The biomass of the investigated area is largely exceeding this saturation limit for most of the forest area. Exploiting the phase of the SAR signal using the coherence increased the saturation level and accuracy (Schlund et al. 2015). The measurement of the canopy height for estimating biomass could overcome the current saturation limitations for short wavelength SAR systems.

6.6.3 Up-scaling of biomass measurements to LiDAR dataset

Only a few field measurements are necessary to transform LiDAR metrics to biomass (Asner et al. 2009b). A prerequisite of this assumption is the distribution of the field measurements over the entire range of biomass. The biomass of the used field plots ranged from 250 t/ha to 440 t/ha. The field measurements were sampled systematically on a transect over the peat dome. Therefore, it could be assumed that the whole range of biomass was covered despite the difficult terrain accessibility. Nevertheless, more ground reference could potentially improve the estimation of biomass and its uncertainties using an explicit validation data set. In general, studies in tropical peat swamp forests need more field measured data to increase confidentiality. However, as explained before this is hardly achievable due to their remoteness and frequently high water tables (Lawson et al. 2014, Phillips 1998).

> Additional errors may result from different acquisition dates of field measurements and remote sensing data (i.e. the LiDAR dataset 2007 vs. 2014). However, the study area is part of a conservation area where the forests are relatively undisturbed since the abandonment of the Mega Rice Project in 1999 (Aldhous 2004). Moreover, investigations showed that the biomass increases only marginally in undisturbed peat swamp forests of Central Kalimantan as well as in the study area (Boehm et al. 2012, Englhart et al. 2013, Sweda et al. 2012).

Therefore, it can be concluded that inconsistencies between the different acquisition dates are minimal and may not affect the results substantially.

GPS localization is also an error source to be considered. However, assuming no drastic change of the forest structure within the field plots and sampling the biomass to 0.1 ha or coarser minimizes the error of GPS localization inaccuracies.

Another source of error to be considered is the transformation of field measurements to biomass with allometric equations. Lawson et al. (2014) suggested pan-tropical equations could not be suitable to apply on tropical peat land. This should be tested, but it could be argued that the advantage of using a local model with low number of samples will not compensate the potential bias compared to pan-tropical equations with large number of samples (Chave et al. 2005, Manuri et al. 2014, Lawson et al. 2014). Therefore, several pan-tropical allometric equations were tested in order to select the most appropriate for biomass estimation in the peat swamp forest investigated. The results of the allometric equations differed significantly (see Section 6.4.2) and thus the choice was guided by the goal to attain similar values as other studies conducted in peat swamp forests. In addition, statistical values of the field measurements were compared to other studies in order to achieve comparable results. The statistical distributions of dbh and tree height measured in peat swamp forests were similar to other studies (Page et al. 1999, Nishimua et al. 2007, Boehm et al. 2013).

The field measurements resulted in an average biomass of 330 t/ha, whereas the range was 250 t/ha to 450 t/ha. The derived biomass is in the order of other studies in peat swamp forests of south-east Asia (Table 6.4). Therefore, it can be concluded that the biomass values used in this study are representative and can be used for the purpose of this study. The differences in those estimates could of course be related to the different geographical locations and the associated conditions as well as different allometric equations used for biomass calculation.

Tab. 6.4: Comparison of aboveground biomass values from different studies in southeast Asia

Aboveground biomass (in t/ha)	Area	Source
0-370	Sebangau national park (Central Kalimantan)	Boehm et al. (2013), Englhart et al. (2011), Kronseder et al. (2012)
228	Sebangau national park (Central Kalimantan)	Kronseder et al. (2012)
248-311	Sebangau national park	Waldes & Page (2002)

	(Central Kalimantan)	
264-397	South-east Asia	Verwer & Meer (2010)
287-491	Thailand	Kaneko (1992)
359.6±76.4	Java, Borneo and Peninsular Malaysia	Koh et al. (2011), Koh et al. (2012), Murdiyarso et al. (2010)

6.7 Conclusions

Although based on iDEM precursor data, the results of this study show that WorldDEM™ has high potential for estimation of canopy height models and aboveground biomass of tropical forests. Due to the global consistency of WorldDEM™ and its expected high accuracy, the investigations have shown that up-scaling from field samples to a canopy height model can achieve reliable accuracies for aboveground biomass estimations in tropical forest. WorldDEM™ is especially appropriate in remote tropical areas where other means would be either too expensive or even not possible.

The iDEM (especially in combination with an accurate DTM) resulted in a canopy height model, showing high correlation with biomass (R^2 = 0.68). However, an accurate DTM is not always available. The iDEM or WorldDEM™ can be used for reconstructing a terrain model, which achieving a high accuracy in relatively flat terrain. The combination of iDEM DSM and iDEM DTM resulted in a reliable estimation of a canopy height model, with a RMSE of 5 m compared to LiDAR reference. This resulted in a moderate cross-validated RMSE for aboveground biomass of 54 t/ha (16 %), which is comparable to other studies in tropical peat swamp forests based on InSAR or LiDAR biomass estimation. Therefore, it could be argued that this solution can be used where no accurate DTM is available resulting in lower but still reliable accuracy. The WorldDEM™ will be globally available resulting in potential cost-efficient and consistent estimations on a large up to worldwide scale compared to LiDAR.

Acknowledgments

References

Airbus Defence and Space (2014). *WorldDEM.Technical Product Specification*. 1.0, Airbus Defence and Space: Geo-Intelligence Program Line.

Aldhous, P. (2004). Borneo is burning. *Nature*, 432, 144–146.

Askne, J., Santoro, M., Smith, G. & Fransson, J. (2003). Multitemporal repeat-pass SAR interferometry of boreal forests. *IEEE Transactions on Geoscience and Remote Sensing* (7), 41, 1540–1550.

Askne, J. I., Fransson, J. E., Santoro, M., Soja, M. J. & Ulander, L. M. (2013). Model-Based Biomass Estimation of a Hemi-Boreal Forest from Multitemporal TanDEM-X Acquisitions. *Remote Sensing* (11), 5, 5574–5597.

Asner, G. P., Flint Hughes, R., Varga, T. A., Knapp, D. E. & Kennedy-Bowdoin, T. (2009b). Environmental and Biotic Controls over Aboveground Biomass Throughout a Tropical Rain Forest. *Ecosystems* (2), 12, 261–278.

Ballhorn, U., Jubanski, J. & Siegert, F. (2011). ICESat/GLAS Data as a Measurement Tool for Peatland Topography and Peat Swamp Forest Biomass in Kalimantan, Indonesia. *Remote Sensing* (9), 3, 1957–1982.

Balzter, H. (2001). Forest mapping and monitoring with interferometric synthetic aperture radar (InSAR). *Progress in Physical Geography* (2), 25, 159–177.

Balzter, H., Rowland, C. & Saich, P. (2007). Forest canopy height and carbon estimation at Monks Wood National Nature Reserve, UK, using dual-wavelength SAR interferometry. *Remote Sensing of Environment* (3), 108, 224–239.

Boehm, H. D. V., Liesenberg, V. & Limin, S. H. (2013). Multi-Temporal Airborne LiDAR-Survey and Field Measurements of Tropical Peat Swamp Forest to Monitor Changes. *IEEE Journal of Selected Topics in Applied Earth Observations and Remote Sensing* (3), 6, 1525–1530.

Boehm, H. D., Liesenberg, V., Sweda, T., Tsuzuki, H. & Limin, S. (2012). Multitemporal airborne LiDAR-surveys in 2007 and 2011 over tropical peat swamp forest environments in Central Kalimantan, Indonesia. In: *Proceedings of the 14th international peat congress, Stockholm, Sweden, 3-8 June 2012.*

Breiman, L., Friedman, J., Stone, C. J. & Olshen, R. A. (1984). *Classification and regression trees*. CRC press: Wadsworth.

Breiman, L. (1996). Stacked Regressions. *Machine Learning* (1), 24, 49–64.

Breiman, L. & Spector, P. (1992). Submodel Selection and Evaluation in Regression. The X-Random Case. *International Statistical Review* (3), 60, 291–319.

Brown, S., Gillespie, A. J. R. & Lugo, A. E. (1989). Biomass estimation methods for tropical forests with applications to forest inventory data. *Forest Science*, 35, 881–902.

Brown, S. & Iverson, L. R. (1992). Biomass estimates for tropical forests. *World Resources Review*, 4, 366–384.

Brown, S. & Lugo, A. E. (1992). Aboveground biomass estimates for tropical moist forests of the Brazilian Amazon. *Interciencia*, 17, 8–18.

Castro, K. L., Sanchez-Azofeifa, G. A. & Rivard, B. (2003). Monitoring secondary tropical forests using space-borne data: Implications for Central America. *International Journal of Remote Sensing* (9), 24, 1853–1894.

Chave, J., Rejou-Mechain, M., Burquez, A., Chidumayo, E., Colgan, M. S., Delitti, W. B., Duque, A., Eid, T., Fearnside, P. M., Goodman, R. C., Henry, M., Martinez-Yrizar, A., Mugasha, W. A., Muller-Landau, H. C., Mencuccini, M., Nelson, B. W., Ngomanda, A., Nogueira, E. M., Ortiz-Malavassi, E., Pelissier, R., Ploton, P., Ryan, C. M., Saldarriaga, J. G. & Vieilledent, G. (2014). Improved allometric models to estimate the aboveground biomass of tropical trees. *Global Change Biology* (10), 20, 3177–3190.

Chave, J., Andalo, C., Brown, S., Cairns, M., Chambers, J., Eamus, D, Folster, H, Fromard, F., Higuchi, N., Kira, T (2005). Tree allometry and improved estimation of carbon stocks and balance in tropical forests. *Oecologia* (1), 145, 87– 99.

Dandois, J. P. & Ellis, E. C. (2013). High spatial resolution three-dimensional mapping of vegetation spectral dynamics using computer vision. *Remote Sensing of Environment*, 136, 259–276.

Dobson, M., Ulaby, F., Pierce, L., Sharik, T., Bergen, K., Kellndorfer, J., Kendra, J., Li, E., Lin, Y., Nashashibi, A., Sarabandi, K. & Siqueira, P. (1995). Estimation of forest biophysical characteristics in Northern Michigan with SIR-C/X-SAR. *IEEE Transactions on Geoscience and Remote Sensing* (4), 33, 877–895.

Drake, J. B., Dubayah, R. O., Clark, D. B., Knox, R. G., Blair, J. B., Hofton, M. A., Chazdon, R. L., Weishampel, J. F. & Prince, S. (2002). Estimation of tropical forest structural characteristics using large-footprint lidar. *Remote Sensing of Environment*, 79, 305–319.

Englhart, S., Keuck, V. & Siegert, F. (2011). Aboveground biomass retrieval in tropical forests - The potential of combined X- and L-band SAR data use. *Remote Sensing of Environment*, 115, 1260–1271.

Englhart, S., Jubanski, J. & Siegert, F. (2013). Quantifying Dynamics in Tropical Peat Swamp Forest Biomass with Multi-Temporal LiDAR Datasets. *Remote Sensing* (5), 5, 2368–2388.

Eriksson, L., Santoro, M., Wiesmann, A. & Schmullius, C. (2003). Multitemporal JERS repeat-pass coherence for growing-stock volume estimation of Siberian forest. *IEEE Transactions on Geoscience and Remote Sensing* (7), 41, 1561– 1570.

Fransson, J. E. S., Smith, G., Askne, J. & Olsson, H. (2001). Stem volume estimation in boreal forests using ERS-1/2 coherence and SPOT XS optical data. *International Journal of Remote Sensing* (14), 22, 2777–2791.

Gama, F. F., Dos Santos, J. R. & Mura, J. C. (2010). Eucalyptus Biomass and Volume Estimation Using Interferometric and Polarimetric SAR Data. *Remote Sensing* (4), 2, 939–956.

Gibbs, H. K., Brown, S., Niles, J. O. & Foley, J. A. (2007). Monitoring and estimating tropical forest carbon stocks: making REDD a reality. *Environmental Research Letters*, 2, 1–13.

Hajnsek, I. & Hoekman, D. H. (2005). *Final Report, INDREX II - Indonesian Radar Experiment Campaign over Tropical Forest in L- and P-band, Version 1, 14 June 2006, ESA Contract RFQ/3-11077/04/NL/CB, Report ESA*. DLR and Wageningen University: Wageningen.

Hooijer, A., Page, S., Canadell, J. G., Silvius, M., Kwadijk, J., Wosten, H. & Jauhiainen, J. (2010). Current and future CO2 emissions from drained peatlands southeast Asia.. *Biogeosciences* (5), 7, 1505–1514.

Hyde, P., Dubayah, R., Walker, W., Blair, J. B., Hofton, M. & Hunsaker, C. (2006). Mapping forest structure for wildlife habitat analysis using multi-sensor (LiDAR, SAR/InSAR, ETM+, Quickbird) synergy. *Remote Sensing of Environment* (12), 102, 63–73.

Jauhiainen, J., Takahashi, H., Heikkinen, J. E. P., Martikainen, P. J. & Vasander, H. (2005). Carbon fluxes from a tropical peat swamp forest floor. *Global Change Biology* (10), 11, 1788–1797.

Kaneko, N. (1992). Comparison of forest structure of tropical peat swamp forests in Southern Thailand and Malaysia. In: Kyuma, K., Vijarnsorn, P. & Zakaria, A. (Eds.): *Coastal lowland ecosystems in Southern Thailand and Malaysia*: Kyoto.

Kasischke, E. S., Melack, J. M. & Dobson, M. C. (1997). The use of imaging radars for ecological applications: A review. *Remote Sensing of Environment* (2), 59, 141–156.

Kellndorfer, J., Walker, W., Pierce, L., Dobson, C., Fites, J. A., Hunsaker, C., Vona, J. & Clutter, M. (2004). Vegetation height estimation from Shuttle Radar Topography Mission and National Elevation Datasets. *Remote Sensing of Environment* (3), 93, 339–358.

Koch, B. (2010). Status and future of laser scanning, synthetic aperture radar and hyperspectral remote sensing data for forest biomass assessment. *ISPRS Journal of Photogrammetry and Remote Sensing*, 65, 581–590.

Koch, B., Heyder, U. & Weinacker, H. (2006). Detection of individual tree crowns in airborne Lidar data. *Photogrammetric Engineering & Remote Sensing* (72), 4, 357–363.

Koehl, M., Lister, A., Scott, C., Baldauf, T. & Plugge, D. (2011). Implications of sampling design and sample size for national carbon accounting systems. *Carbon Balance and Management* (1), 6, 1–20.

Koh, L., Miettinen, J., Liew, S. & Ghazoula, J. (2011). Remotely sensed evidence of tropical peatland conversion to oil palm. *Proceedings of the National Academy of Science of the United States of America (PNAS)* (12), 108, 5127–5132.

Koh, L., Gibbs, H., Potapov, P. & Hansen, M. (2012). REDDcalculator.com: A webbased decision-support tool for implementing Indonesia's forest moratorium. *Methods in Ecology and Evolution*, 3, 310–316.

Kohavi, R. (1995). A study of cross-validation and bootstrap for accuracy estimation and model selection. In: *International Joint Conference on Artificial Intelligence (IJCAI)*,1137–1145.

Krieger, G., Moreira, A., Fiedler, H., Hajnsek, I., Werner, M., Younis, M. & Zink, M. (2007). TanDEM-X: A Satellite Formation for High-Resolution SAR Interferometry. *IEEE Transactions on Geoscience and Remote Sensing* (11), 45, 3317– 3341.

Kronseder, K., Ballhorn, U., Boehm, V. & Siegert, F. (2012). Above ground biomass estimation across forest types at different degradation levels in Central Kalimantan using LiDAR data. *International Journal of Applied Earth Observation and Geoinformation* (0), 18, 37–48.

Lawson, I., Kelly, T., Aplin, P., Boom, A., Dargie, G., Draper, F., Hassan, P., Hoyos-Santillan, J., Kaduk, J., Large, D., Murphy, W., Page, S., Roucoux, K., Sjogersten, S., Tansey, K., Waldram, M., Wedeux, B. & Wheeler, J. (2014). Improving estimates of tropical peatland area, carbon storage, and greenhouse gas fluxes. *Wetlands Ecology and Management* (6), 22, 1–20.

Le Toan, T., Beaudoin, A., Riom, J. & Guyon, D. (1992). Relating forest biomass to SAR data. *IEEE Transactions on Geoscience and Remote Sensing* (2), 30, 403–411.

Lefsky, M. A., Harding, D. J., Keller, M., Cohen, W. B., Carabajal, C. C., Del Bom Espirito-Santo, F., Hunter, M. O. & Oliveira, R. de (2005). Estimates of forest canopy height and aboveground biomass using ICESat. *Geophysical Research Letters* (22), 32, 1–4.

Liesenberg, V., Boehm, H. D., Joosten, H. & Limin, S. (2013). Spatial and temporal variation of above ground biomass in tropical dome-shaped peatlands measured by airborne LiDAR. *Proceedings of international symposium on wild fire and carbon management in peat-forest in Indonesia*, 1, 99–117.

Luckman, A., Baker, J. & Wegmueller, U. (2000). Repeat-Pass Interferometric Coherence Measurements of Disturbed Tropical Forest from JERS and ERS Satellites. *Remote Sensing of Environment* (3), 73, 350–360.

Luckman, A., Baker, J., Honzak, M. & Lucas, R. (1998). Tropical Forest Biomass Density Estimation Using JERS-1 SAR: Seasonal Variation, Confidence Limits, and Application to Image Mosaics. *Remote Sensing of Environment* (2), 63, 126–139.

Manuri, S., Brack, C., Nugroho, N. P., Hergoualch, K., Novita, N., Dotzauer, H., Verchot, L., Putra, C. A. S. & Widyasari, E. (2014). Tree biomass equations for tropical peat swamp forest ecosystems in Indonesia. *Forest Ecology and Management*, 334, 241–253.

Martin, A. R. & Thomas, S. C. (2011). A Reassessment of Carbon Content in Tropical Trees. *PLoS ONE* (8), 6, 1–9.

Mitchard, E., Saatchi, S., Lewis, S., Feldpausch, T., Woodhouse, I., Sonke, B., Rowland, C. & Meir, P. (2011). Measuring biomass changes due to woody encroachment and deforestation/degradation in a forest-savanna boundary region of central Africa using multi-temporal L-band radar backscatter. *Remote Sensing of Environment* (11), 115, 2861–2873.

Molinaro, A. M., Simon, R. & Pfeiffer, R. M. (2005). Prediction error estimation: a comparison of resampling methods. *Bioinformatics* (15), 21, 3301–3307.

Morel, A. C., Saatchi, S. S., Malhi, Y., Berry, N. J., Banin, L., Burslem, D., Nilus, R. & Ong, R. C. (2011). Estimating aboveground biomass in forest and oil palm plantation in Sabah, Malaysian Borneo using ALOS PALSAR data. *Forest Ecology and Management* (9), 262, 1786 –1798.

Murdiyarso, D., Hergoualc'h, K. & Verchot, L. (2010). Opportunities for reducing greenhouse gas emissions in tropical peatlands. *Proceedings of the National Academy of Science of the United States of America (PNAS)* (46), 107, 19655–19660.

Naesset, E., Gobakken, T., Solberg, S., Gregoire, T. G., Nelson, R., Stahl, G. & Weydahl, D. (2011). Model-assisted regional forest biomass estimation using LiDAR and InSAR as auxiliary data: A case study from a boreal forest area.
Remote Sensing of Environment (12), 115, 3599–3614.

Neeff, T., Dutra, L. V., Santos, J. R. dos, Freitas, C. d. C. & Araujo, L. S. (2005). Tropical Forest Measurement by Interferometric Height Modeling and P-Band Radar Backscatter. *Forest Science* (6), 51, 585–594.

Nishimua, T. B., Suzuki, E., Kohyama, T. & Tsuyuzaki, S. (2007). Mortality and Growth of Trees in Peat-swamp and Heath Forests in Central Kalimantan After Severe Drought. *Vegetatio* (2), 188, 165–177.

Olander, L. P., Gibbs, H. K., Steininger, M., Swenson, J. J. & Murray, B. C. (2008). Reference scenarios for deforestation and forest degradation in support of REDD: a review of data and methods. *Environmental Research Letters*, 3, 1–11.

Page, S. E., Rieley, J. O. & Banks, C. J. (2011). Global and regional importance of the tropical peatland carbon pool. *Global Change Biology* (2), 17, 798–818.

Page, S. E., Rieley, J. O., Shotyk, O. W. & Weiss, D. (1999). Interdependence of peat and vegetation in a tropical peat swamp forest. *Philosphoical Transaction of the Royal Society*, 354, 1885–1897.

Page, S. E., Siegert, F., Rieley, J. O., Boehm, H.-D. V., Jaya, A. & Limin, S. (2002). The amount of carbon released from peat and forest fires in Indonesia during 1997. *Nature* (6911), 420, 61–65.

Phillips, V. D. (1998). Peatswamp ecology and sustainable development in Borneo. *Biodiversity & Conservation* (5), 7, 651–671.

Pitz, W. & Miller, D. (2010). The TerraSAR-X Satellite. *IEEE Transactions on Geoscience and Remote Sensing* (2), 48, 615 –622.

Rahlf, J., Breidenbach, J., Solberg, S., Naesset, E. & Astrup, R. (2014). Comparison of four types of 3D data for timber volume estimation. *Remote Sensing of Environment*, 155, 325–333.

Rahman, M. M., Csaplovics, E. & Koch, B. (2008). Satellite estimation of forest carbon using regression models. *International Journal of Remote Sensing* (23), 29, 6917–6936.

Reyes, G., Brown, S., Chapman, J. & Lugo, A. E. (1992). *Wood densities of tropical tree species*. USDA Forest Service: New Orleans.

Rombach, M. & Moreira, J. (2003). Description and applications of the multipolarized dual band OrbiSAR-1 InSAR sensor. In: *Proceedings of the International Radar Conference 2003*,245–250.

Saatchi, S. S., Soares, J. V. & Alves, D. S. (1997). Mapping deforestation and land use in amazon rainforest by using SIR-C imagery. *Remote Sensing of Environment* (2), 59, 191 –202.

Santoro, M., Askne, J., Smith, G. & Fransson, J. E. (2002). Stem volume retrieval in boreal forests from ERS-1/2 interferometry. *Remote Sensing of Environment* (1), 81, 19 –35.

Santoro, M., Shvidenko, A., McCallum, I., Askne, J. & Schmullius, C. (2007). Properties of ERS-1/2 coherence in the Siberian boreal forest and implications for stem volume retrieval. *Remote Sensing of Environment* (2), 106, 154 –172.

Schlerf, M., Atzberger, C. & Hill, J. (2005). Remote sensing of forest biophysical variables using HyMap imaging spectrometer data. *Remote Sensing of Environment* (2), 95, 177–194.

Schlund, M., Poncet, F. von, Kuntz, S., Schmullius, C. & Hoekman, D. H. (2015). TanDEM-X data for aboveground biomass retrieval in a tropical peat swamp forest. *Remote Sensing of Environment*, 158, 255–266.

Seber, G. A. F. & Lee, A. J. (2003). *Linear regression analysis*. Wiley & Sons: New Jersey.

Sexton, J., Bax, T., Siqueira, P., Swenson, J. & Hensley, S. (2009). A comparison of lidar, radar, and field measurements of canopy height in pine and hardwood forests of southeastern North America. *Forest Ecology and Management* (3), 257, 1136–1147.

Solberg, S., Weydahl, D. & Astrup, R. (2015). Temporal Stability of X-Band Single-Pass InSAR Heights in a Spruce Forest: Effects of Acquisition Properties and Season. *IEEE Transactions on Geoscience and Remote Sensing* (3), 53, 1607–1614.

Solberg, S., Astrup, R., Gobakken, T., Naesset, E. & Weydahl, D. J. (2010). Estimating spruce and pine biomass with interferometric X-band SAR. *Remote Sensing of Environment* (10), 114, 2353 –2360.

Solberg, S., Astrup, R., Breidenbach, J., Nilsen, B. & Weydahl, D. (2013). Monitoring spruce volume and biomass with InSAR data from TanDEM-X. *Remote Sensing of Environment*, 139, 60–67.

Sorensen, K. W. (1993). Indonesian peat swamp forests and their role as a carbon sink. *Chemosphere* (6), 27, 1065 –1082.

St-Onge, B., Hu, Y. & Vega, C. (2008). Mapping the height and aboveground biomass of a mixed forest using lidar and stereo Ikonos images. *International Journal of Remote Sensing* (5), 29, 1277–1294.

Sweda, T., Tsuzuki, H., Maeda, Y., Boehm, V. & Limin, S. (2012). Above- and belowground carbon budget of degraded tropical peatland revealed by multitemporal airborne laser altimetry. In: *Proceedings of the 14th international peat congress, Stockholm, Sweden, 3-8 June 2012*.

Treuhaft, R. N., Chapman, B. D., Santos, J. R. dos, Goncalves, F. G., Dutra, L. V., Graca, P. M. L. A. & Drake, J. B. (2009). Vegetation profiles in tropical forests from multibaseline interferometric synthetic aperture radar, field, and lidar measurements. *Journal of Geophysical Research: Atmospheres* (23), 114, 1–16.

Treuhaft, R. N. & Siqueira, P. R. (2004). The calculated performance of forest structure and biomass estimates from interferometric radar. *Waves in Random Media* (2), 14, 345–358.

Verwer, C. & Meer, P. van der (2010). *Carbon pools in tropical peat forests - Towards a reference value for forest biomass carbon in relatively undisturbed peat swamp forests in Southeast Asia*. Wageningen University and Research Center (Alterrareport 2108): Wageningen.

Wagner, W., Luckman, A., Vietmeier, J., Tansey, K., Balzter, H., Schmullius, C., Davidson, M., Gaveau, D., Gluck, M., Le Toan, T. (2003). Large-scale mapping of

boreal forest in SIBERIA using ERS tandem coherence and JERS backscatter data. *Remote Sensing of Environment* (2), 85, 125–144.

Waldes, N. J. L. & Page, S. E. (2002). Forest structure and tree diversity of a peat swamp forest in Central Kalimantan, Indonesia. In: *Proceedings of International Symposium on Tropical Peatlands, Jakarta (Indonesia), 22-08-2002-23-08-2002, BPPT*.

Wallington, E., Izzawati & Woodhouse, I. (2004). Forest height estimation from Xband SAR. In: *IEEE International Geoscience and Remote Sensing Symposium (IGARSS) 2004*,2393–2396.

Werf, G. R. van der, Morton, D. C., DeFries, R. S., Olivier, J. G. J., Kasibhatla, P. S., Jackson, R. B., Collatz, G. J. & Randerson, J. T. (2009). CO2 emissions from forest loss. *Nature Geoscience*, 2, 737–738.

Wessel, B., Fritz, T., Busche, T., Braeutigam, B., Krieger, G. & Zink, M. (2013). *TanDEM-X. Ground Segment. DEM Products Specification Document. Issue: 3.0*. Deutsches Zentrum fuer Luft- und Raumfahrt (DLR): Oberpfaffenhofen.

6 WorldDEM^{TM} data for canopy height and aboveground biomass retrieval in a
  127
tropical peat swamp forest

Weydahl, D. J., Sagstuen, J., Dick, O. B. & Ronning, H. (2007). SRTM DEM accuracy assessment over vegetated areas in Norway. *International Journal of Remote Sensing* (16), 28, 3513–3527.

7 Discussion & outlook

After Lawson et al. (2014) active remote sensing systems could be potentially successfully used in tropical peat swamp forests, but also in tropical forests in general (e.g. Englhart et al. 2011, Le Toan et al. 2011, Treuhaft et al. 2015, De Grandi et al. 2015). This was proved in the study on hand with TanDEM-X. It could be shown that active bistatic radar remote sensing can support improved mapping of tropical peat swamp forest compared to monostatic systems (75 % vs. 85 %). TanDEMX achieved comparable or even better results than other classifications in tropical (peat swamp) forests. Especially the classification of different forest classes and small scale objects were improved compared to other classifications of peat swamp forests in Southeast Asia (Wijedasa et al. 2012, Miettinen et al. 2008, Miettinen et al. 2012). The high accuracy and detection of small scale objects due to the high resolution can be beneficial e.g. in a forest fragmentation analysis, being of high importance in assessing ecosystem services and the biodiversity of forests (Dong et al. 2014, Wijedasa et al. 2012).

The classification approach tested on TanDEM-X can generally be transferred to tropical forests, whereas also comparable or improved results were achieved in this study with TanDEM-X in forest classification and degraded forest mapping (Schlund et al. 2014a, Schlund et al. 2014b, Santos et al. 2010, Morel et al. 2011, Longepe et al. 2011). The potential to differentiate different forest classes and the high resolution are the most significant advantages of TanDEM-X. The relationship of interferometric coherence and biophysical parameters supports classifications with a higher level of detail and accuracy compared to classifications without interferometric coherence. Therefore, TanDEM-X has a high potential to be utilized in the context of forest mapping and forest degradation monitoring. Another advantage is the global availability for the years 2010-2014 (Krieger et al. 2007), which could establish a baseline for LULUCF (Land Use, Land-Use Change and Forestry) suggested from the IPCC (2003) and in REDD+ MRV concepts. For instance, TanDEM-X classifications can be considered as benchmark mapping and represent the status quo of land cover. TanDEM-X amplitude and future SAR data could then be used in automated change detection algorithms, whereas changes within forest land are considered as forest disturbance or deforestation (Poncet et al. 2014).

De Grandi et al. (2015) showed the potential of spatial wavelet analysis with Cband data for the differentiation of intact and degraded forest. The necessity to use high frequency radar like C- and X-band was stressed in order to use data interacting with upper canopy constituents (De Grandi et al. 2015). High resolution such as in TanDEM-X could be used also in this analysis and would potentially improve the

differentiation of intact and degraded forest in addition to the inteferometric coherence (Schlund et al. 2014a, De Grandi et al. 2015). Such a spatial wavelet analysis would increase the usage of amplitude data in classification schemes (De Grandi et al. 2015).

First tests of transferability to other test areas achieved similar promising results (e.g. Poncet et al. 2014, Schlund et al. 2014b). Nevertheless, it is worth noting that the Mawas study area has a homogenous landscape and does not contain any agroforestry plantations. Heterogeneous landscapes and tree plantations resulted in confusions and degraded the classification accuracy (Poncet et al. 2014, Schlund et al. 2014b). Hierarchical classification and/or synergetic approaches with optical data could improve classification results, which is especially the case in heterogeneous landscapes (Schlund et al. 2014b). Hame et al. (2013a) suggested a multi-stage approach using optical and radar data as well. The analysis was examined applying a supervised classification demanding user interaction. But the exploration and implementation of automatic or semi-automatic classifications should be investigated in the future, as first trials with unsupervised techniques achieved promising results.

The second major part of the study investigated aboveground biomass estimation with TanDEM-X. The potential of TanDEM-X was also shown here, whereas again the interferometric capabilities of TanDEM-X were most important. Both described approaches after Koch (2010) were applied. First, the aboveground biomass was directly correlated with backscatter and interferometric coherence. As expected, the backscatter correlation was weak ($R^2 = 0.3$, Schlund et al. 2015, Englhart et al. 2011, Castro et al. 2003, Gama et al. 2010). This is mainly based on high biomass values in this tropical peat swamp forest and low penetration depth of X-band resulting in low saturation values (Schlund et al. 2015, Englhart et al. 2011, Gama et al. 2010). In contrast, the interferometric coherence achieved higher accuracies in biomass estimation ($R^2 = 0.5$ & RMSE=53 t/ha [14 %]) showing similar results to other studies using interferometric coherence of C-band in boreal forests (Schlund et al. 2015, Cartus et al. 2011, Santoro et al. 2002, Santoro et al. 2007). This proofs the relationship of volume decorrelation with forest structure and tree height (Schlund et al. 2015, Schlund et al. 2013, Kugler et al. 2014) being correlated to the biomass (Schlund et al. 2015). The volume decorrelation increases with increasing biomass resulting in lower coherence (Schlund et al. 2015, Treuhaft et al. 2015).

This correlation was investigated with an empirical model and similar relationships were observed in other study areas. Treuhaft et al. (2015) estimated biomass also with a linear function from TanDEM-X coherence and phase with an accuracy of 52 to 62 t/ha (29 % - 35 %) in tropical forests of Brazil. However,

empirical models are dependent on training data from field measurements or other data sources. Fur-

thermore, the exact correlation and resulting model is also dependent on additional parameters like baseline, incidence angle, etc. This can limit the transferability of the models depending on individual training data. These limitations can be resolved partially by using semi-empirical models. However, most semi-empirical models also need training data (Askne et al. 2013, Askne & Santoro 2014). For instance, the interferometric water-cloud model can be used. However, this model achieved comparable or less accuracies compared to the empirical model used (Schlund et al. 2015, Cartus et al. 2011, Santoro et al. 2002, Santoro et al. 2007, Askne et al. 2013, Askne & Santoro 2014).

Another approach to assess biomass is to estimate other biophysical parameters, like tree height or density, and correlate these results with the aboveground biomass (Koch 2010). InSAR heights of TanDEM-X were used to estimate vegetation height and were correlated with biomass (Schlund et al. without year). The InSAR height of a X-band system is assumed to represent a digital surface model on top of vegetation. The subtraction of a digital terrain model would result in a canopy height model. However, the existence of a DTM is a limiting factor in this approach. Different scenarios were analyzed in order to overcome this limitation. As expected the derivation of a canopy height model with LiDAR achieved best results, while a terrain model out of the TanDEM-X surface model achieved moderate results only (Schlund et al. without year). Nevertheless, this dataset is globally available due to the TanDEM-X mission objective. This is not the case for LiDAR at present. The correlation with the biomass was moderate to high (Schlund et al. without year). It is worth noting that error propagation needs to be taken into account. The estimation of canopy height may result in errors, which propagates in the biomass correlation. The biomass correlation contains errors as well.

Therefore, the extraction of a DTM could be improved in order to generate more accurate height estimations. Alternatively, other data sources like LiDAR or long wavelength SAR should be considered (Balzter et al. 2007, Solberg et al. 2010, Weydahl et al. 2007, Neeff et al. 2005, Rombach & Moreira 2003). The vegetation height is also assessable via semi-empirical models, like the Random Volume over Ground (RVoG) model (Kugler et al. 2014, Askne et al. 2013, Askne & Santoro 2014). However, certain limitations exist when using TanDEM-X in this model. The RVoG was developed for long-wavelength SAR (like L- or P-band) and quadpolarizations (Cloude & Papathanassiou 1998, Papathanassiou & Cloude 2001, Hajnsek et al. 2009, Neumann et al. 2010). Therefore, simplifications have to be applied for TanDEM-X. The necessary ground phase is extractable from LiDAR, which results in accurate height estimations (Kugler et al. 2014). However, a LiDAR dataset is again necessary for this approach in order to achieve accurate results especially in tropical

forests (Kugler et al. 2014). Furthermore, error propagation in biomass estimation exists also in this method, since first the vegetation height is assessed, which is then correlated with the biomass (Askne et al. 2013). Such error propagation should be investigated in further studies, especially in the tropics.

In general, different error sources exist in the biomass estimation with remote sensing. The reference measurement needs high location accuracy and must fit the remote sensing data in their location and timing. Furthermore, the aboveground biomass is mostly estimated via allometric equations. Different equations exist, which contains errors and may not fit heterogeneous tropical forest and tropical peat swamp forest in particular (Lawson et al. 2014). Biomass estimations of other studies in tropical peat swamp forests were compared in order to assess the biomass estimations (Schlund et al. 2015, Boehm et al. 2013, Englhart et al. 2011, Kronseder et al. 2012, Koh et al. 2011, Koh et al. 2012, Murdiyarso et al. 2010). The values of aboveground biomass in this study are in the range of other studies and thus were considered as representative for such an analysis.

In contrast to backscatter of TanDEM-X, the phase information of TanDEMX provides biomass estimation via interferometric coherence and interferometric height. This suggests that the phase information of X-band is more sensitive and correlated to forest structure (e.g. aboveground biomass) compared to the backscatter. The interferometric coherence and height can be combined. For instance, Treuhaft et al. (2015) combined phase height with coherence from TanDEM-X in order to estimate biomass in Tapajos National Forest, Brazil. The combination of both estimations can potentially improve the biomass assessment substantially. Similar findings were observed when combining biomass estimation with intensity and forest height estimation with polarimetric SAR interfometry of P-band data (Le Toan et al. 2011, Dubois-Fernandez et al. 2012). Le Toan et al. (2011) emphasized the complementarity of both measurements compensating the drawbacks of the other.

In addition, TanDEM-X biomass estimation via coherence and/or height can be used synergetically with other sensors and wavelengths. The combination of short and long wavelength backscatter did not substantially improve results (Naidoo et al. 2015, Luckman et al. 2000). But it can be expected that the combination of short wavelength interferometric and long wavelength backscatter information improves biomass estimations substantially. It is expected that the combination of optical data and TanDEM-X would not potentially improve biomass estimation since optical data is generally low correlated with biomass (Koch 2010). For instance, Hame et al. (2013b) did not observe improvements of biomass estimation by combining optical data with ALOS PALSAR.

8 Conclusions

The results show that TanDEM-X has a high potential as a highly valuable data source for forestry applications. Therefore, TanDEM-X could be recommended for REDD+ MRV systems. This is especially relevant in tropical countries where frequent cloud cover hinders the application of optical data resulting in spatially or timely inconsistent coverages and analysis.

TanDEM-X analysis is globally and consistently applicable. The bistatic properties of TanDEM-X mission show the most significant advantages. Interferometric coherence was the most significant of all tested features in land cover classifications. The classification results improved by 10 % with coherence, whereas the differentiation of different forest classes as well as forest/non-forest benefited from the coherence. The amplitudes and especially bistatic amplitude and ratio of monostatic and bistatic amplitude resulted in lower significance for classifications. Therefore, the incidence angle difference of monostatic and bistatic sensor is not large enough to measure different backscatter properties with the amplitude and did not result in higher information content.

The interferometric coherence exhibits information about forest structure due to the volume decorrelation. This is beneficial for classification purposes. In addition, the correlation of coherence with aboveground biomass was analyzed. A LiDAR dataset was used in order to up-scale the field estimated biomass and thus increased the number of observations substantially. The coherence correlated in that study with the aboveground forest biomass due to volume decorrelation ($R^2 = 0.5$). The volume decorrelation increased with the biomass and thus the coherence decreased. The amplitude resulted in lower correlations and accuracies ($R^2 = 0.3$). This was expected due to the short wavelength and subsequently low saturation value. In contrast, the phase information seemed more sensitive to biomass and thus the interferometric coherence achieved more accurate and less noisy results with more spatial detail for land cover classifications and biomass estimations compared to amplitude data. This is of high importance in forest applications as well as REDD+ MRV and is also beneficial for forest degradation monitoring.

The interferometric height, represented as iDEM, achieved an even higher correlation with the aboveground biomass ($R^2 = 0.68$) compared to coherence. The combination with an accurate digital terrain model resulted in high accuracies of biomass estimation (RMSE=24 t/ha [7.5 %]). However, a digital terrain model is not globally, consistently available. But a digital terrain model can be extracted

from TanDEM-X height models directly (in this case iDEM) as well. This did not represent the actual terrain height perfectly and resulted, in this study, in homogenous canopy heights. This propagated to a biomass estimation with overestimation in actual lower biomass and underestimation in actual higher biomass areas. Nevertheless, the cross-validated RMSE using this terrain model for biomass estimations was moderate with 54 t/ha (16 %). This dataset can be applied globally in a consistent way in contrast to LiDAR datasets.

These results indicate that TanDEM-X is a valuable and consistent data source for mapping and monitoring applications in tropical forests and beyond. Especially the interferometric information in form of coherence and height are promising. The interferometric coherence can be used for accurate land cover mapping and estimation of aboveground biomass. The interferometric height is valuable for biomass estimations as well. TanDEM-X data can thus be used as a starting point to deliver spatial distribution of biomass e.g. for stratification purposes. In the context of REDD+, this information supports measurement, verification, reporting (MRV) and forest degradation monitoring systems.

References

Airbus Defence and Space (2014). *WorldDEM.Technical Product Specification*. 1.0, Airbus Defence and Space: Geo-Intelligence Program Line.

Aldhous, P. (2004). Borneo is burning. *Nature*, 432, 144–146.

Almeida-Filho, R., Rosenqvist, A., Shimabukuro, Y. E. & Silva-Gomez, R. (2007). Detecting Deforestation with multitemporal L-band SAR imagery: a case study in western Brazilian Amazonia. *International Journal of Remote Sensing* (6), 28, 1383–1390.

Askne, J., Santoro, M., Smith, G. & Fransson, J. (2003). Multitemporal repeat-pass SAR interferometry of boreal forests. *IEEE Transactions on Geoscience and Remote Sensing* (7), 41, 1540–1550.

Askne, J. I., Fransson, J. E., Santoro, M., Soja, M. J. & Ulander, L. M. (2013). Model-Based Biomass Estimation of a Hemi-Boreal Forest from Multitemporal TanDEM-X Acquisitions. *Remote Sensing* (11), 5, 5574–5597.

Askne, J. & Santoro, M. (2014). On the Estimation of Boreal Forest Biomass From TanDEM-X Data Without Training Samples. *IEEE Geoscience and Remote Sensing Letters* (4), 12, 771–775.

Askne, J., Dammert, P., Ulander, L. & Smith, G. (1997). C-band repeat-pass interferometric SAR observations of the forest. *IEEE Transactions on Geoscience and Remote Sensing* (1), 35, 25–35.

Asner, G. P., Knapp, D. E., Balaji, A. & Paez-Acosta, G. (2009a). Automated mapping of tropical deforestation and forest degradation: CLASlite. *Journal of Applied Remote Sensing* (4), 3, 1–11.

Asner, G. P. (2009). Tropical forest carbon assessment: integrating satellite and airborne mapping approaches. *Environmental Research Letters*, 4, 1–11.

Asner, G. P., Flint Hughes, R., Varga, T. A., Knapp, D. E. & Kennedy-Bowdoin, T. (2009b). Environmental and Biotic Controls over Aboveground Biomass Throughout a Tropical Rain Forest. *Ecosystems* (2), 12, 261–278.

Asner, G. P., Powell, G. V. N., Mascaro, J., Knapp, D. E., Clark, J. K., Jacobson, J., Kennedy-Bowdoin, T., Balaji, A., Paez-Acosta, G., Victoria, E., Secada, L., Valqui, M. & Hughes, R. F. (2010). High-resolution forest carbon stocks and emissions in the Amazon. *Proceedings of the National Academy of Sciences* (38), 107, 16738–16742.

Baccini, A., Laporte, N., Goetz, S. J., Sun, M. & Dong, H. (2008). A first map of tropical Africa's above-ground biomass derived from satellite imagery. *Environmental Research Letters* (4), 3, 1–9.

Balzter, H. (2001). Forest mapping and monitoring with interferometric synthetic aperture radar (InSAR). *Progress in Physical Geography* (2), 25, 159–177.

Balzter, H., Rowland, C. & Saich, P. (2007). Forest canopy height and carbon estimation at Monks Wood National Nature Reserve, UK, using dual-wavelength SAR interferometry. *Remote Sensing of Environment* (3), 108, 224–239.

Bamler, R. & Hartl, P. (1998). Synthetic aperture radar interferometry. *Inverse Problems* (4), 14, R1–R54.

Beer, C., Lucht, W., Schmullius, C. & Shvidenko, A. (2006). Small net carbon dioxide uptake by Russian forests during 1981-1999. *Geophysical Research Letters* (15), 33, 1–4.

Boehm, H. D. V., Liesenberg, V. & Limin, S. H. (2013). Multi-Temporal Airborne LiDAR-Survey and Field Measurements of Tropical Peat Swamp Forest to Monitor Changes. *IEEE Journal of Selected Topics in Applied Earth Observations and Remote Sensing* (3), 6, 1525–1530.

Boehm, H.-D. & Siegert, F. (2001). Ecological impact of the onemillion hectare rice project in Central Kalimantan, Indonesia, using remote sensing and GIS. Land use change and (Il)-legal logging in Central Kalimantan, Indonesia. In: *22nd Asian Conference on Remote Sensing, 5-9 November 2001*.

Breidenbach, J., Ortiz, S. M. & Reich, M. (2010). Forest monitoring with TerraSARX: first results. *European Journal of Forest Research*, 129, 813–823.

Bruzzone, L., Marconcini, M., Wegmuller, U. & Wiesmann, A. (2004). An advanced system for the automatic classification of multitemporal SAR images. *IEEE Transactions on Geoscience and Remote Sensing* (6), 42, 1321–1334.

Cabral, A. I. R., Vasconcelos, M. J., Oom, D. & Sardinha, R. (2010). Spatial dynamics and quantification of deforestation in the central-plateau woodlands of Angola. *Applied Geography*, 31, 1185–1193.

Caicoya, A. T., Kugler, F., Hajnsek, I. & Papathanassiou, K. (2012). Boreal forest biomass classification with TanDEM-X. In: *IEEE International Geoscience and Remote Sensing Symposium (IGARSS), 2012*, 3439–3442.

Carreiras, J., Pereira, J., Campagnolo, M. & Shimabukuro, Y. (2006). Assessing the extent of agriculture/pasture and secondary succession forest in the Brazilian Legal Amazon using SPOT VEGETATION data. *Remote Sensing of Environment*, 101, 283–298.

Cartus, O., Santoro, M., Schmullius, C. & Li, Z. (2011). Large area forest stem volume mapping in the boreal zone using synergy of ERS-1/2 tandem coherence and MODIS vegetation continuous fields. *Remote Sensing of Environment* (3), 115, 931–943.

Castro, K. L., Sanchez-Azofeifa, G. A. & Rivard, B. (2003). Monitoring secondary tropical forests using space-borne data: Implications for Central America. *International Journal of Remote Sensing* (9), 24, 1853–1894.

Chitroub, S., Houacine, A. & Sansal, B. (2002). Statistical characterisation and modelling of SAR images. *Signal Processing* (1), 82, 69–92.

Cloude, S. (2009). *Polarisation: Applications in Remote Sensing*. Oxford University Press: Oxford.

Cloude, S. & Papathanassiou, K. (1998). Polarimetric SAR interferometry. *IEEE Transactions on Geoscience and Remote Sensing* (5), 36, 1551–1565.

Cutrona, L. (1990). Synthetic Aperture Radar. In: Skolnik, M. (Eds.): *Radar Handbook*. 2nd ed. McGraw-Hill: New York, 21.1 –21.23.

Dandois, J. P. & Ellis, E. C. (2013). High spatial resolution three-dimensional mapping of vegetation spectral dynamics using computer vision. *Remote Sensing of Environment*, 136, 259–276.

De Fries, R, Achard, F., Brown, S., Herold, M., Murdiyarso, D., Schlamadinger, B. & Souza Jr., C. de (2007). Earth observations for estimating greenhouse gas emissions from deforestation in developing countries. *Environmental Science & Policy*, 10, 385–394.

De Grandi, E. C., Mitchard, E., Woodhouse, I. H. & De Grandi, G. D. (2015). Spatial Wavelet Statistics of SAR Backscatter for Characterizing Degraded Forest: A Case Study From Cameroon. *IEEE Journal of Selected Topics in Applied Earth Observations and Remote Sensing*, 99, 1–13.

De Sy, V., Herold, M., Achard, F., Asner, G. P., Held, A., Kellndorfer, J. & Verbesselt, J. (2012). Synergies of multiple remote sensing data sources for REDD+ monitoring. *Current Opinion in Environmental Sustainability* (6), 4, 696–706.

Del Frate, F., Pacifici, F. & Solimini, D. (2008). Monitoring Urban Land Cover in Rome, Italy, and Its Changes by Single-Polarization Multitemporal SAR Images. *IEEE Journal of Selected Topics in Applied Earth Observations and Remote Sensing* (2), 1, 87–97.

Dobson, M., Ulaby, F., Pierce, L., Sharik, T., Bergen, K., Kellndorfer, J., Kendra, J., Li, E., Lin, Y., Nashashibi, A., Sarabandi, K. & Siqueira, P. (1995). Estimation of forest biophysical characteristics in Northern Michigan with SIR-C/X-SAR. *IEEE Transactions on Geoscience and Remote Sensing* (4), 33, 877–895.

Dong, J., Xiao, X., Sheldon, S., Biradar, C., Zhang, G., Dinh Duong, N., Hazarika, M., Wikantika, K., Takeuhci, W. & Moore III, B. (2014). A 50-m Forest Cover Map in Southeast Asia from ALOS/PALSAR and Its Application on Forest Fragmentation Assessment. *PLoS ONE* (1), 9, 1–12.

Drake, J. B., Dubayah, R. O., Clark, D. B., Knox, R. G., Blair, J. B., Hofton, M. A., Chazdon, R. L., Weishampel, J. F. & Prince, S. (2002). Estimation of tropical forest structural characteristics using large-footprint lidar. *Remote Sensing of Environment*, 79, 305–319.

Dubois-Fernandez, P., Cantalloube, H., Vaizan, B., Krieger, G., Horn, R., Wendler, M. & Giroux, V. (2006). ONERA-DLR bistatic SAR campaign: planning, data acquistiton, and first analysis of bistatic scattering behaviour of natural and urban targets. *IEE Proceedings - Radar, Sonar and Navigation* (3), 153, 214– 223.

Dubois-Fernandez, P., Toan, T. L., Daniel, S., Oriot, H., Chave, J., Blanc, L., Villard, L., Davidson, M. & Petit, M. (2012). The TropiSAR Airborne Campaign in French Guiana: Objectives, Description, and Observed Temporal Behavior of the Backscatter Signal. *IEEE Transactions on Geoscience and Remote Sensing* (8), 50, 3228–3241.

Durand, J., Gimonet, B. & Perbos, J. (1987). Speckle in SAR Images: An Evaluation of Filtering Techniques. *Advanced Space Research* (11), 7, 301–304.

Engdahl, M. & Hyyppa, J. (2003). Land-cover classification using multitemporal ERS-1/2 InSAR data. *IEEE Transactions on Geoscience and Remote Sensing* (7), 41, 1620–1628.

Englhart, S., Keuck, V. & Siegert, F. (2011). Aboveground biomass retrieval in tropical forests - The potential of combined X- and L-band SAR data use. *Remote Sensing of Environment*, 115, 1260–1271.

Englhart, S., Jubanski, J. & Siegert, F. (2013). Quantifying Dynamics in Tropical Peat Swamp Forest Biomass with Multi-Temporal LiDAR Datasets. *Remote Sensing* (5), 5, 2368–2388.

Franke, J., Navratil, P., Keuck, V., Peterson, K. & Siegert, F. (2012). Monitoring Fire and Selective Logging Activities in Tropical Peat Swamp Forests. *IEEE Journal of Selected Topics in Applied Earth Observations and Remote Sensing* (6), 5, 1811– 1820.

Fritz, T. (2012). *TanDEM-X. Ground Segment. TanDEM-X Experimental Product Description. Issue: 1.2*. Deutsches Zentrum fuer Luft- und Raumfahrt (DLR): Oberpfaffenhofen.

Fritz, T. & Eineder, M. (2013). *TerraSAR-X Ground Segment. Basic Product Specification Document. Issue: 1.9*. Deutsches Zentrum fuer Luft- und Raumfahrt (DLR): Oberpfaffenhofen.

Gama, F. F., Dos Santos, J. R. & Mura, J. C. (2010). Eucalyptus Biomass and Volume Estimation Using Interferometric and Polarimetric SAR Data. *Remote Sensing* (4), 2, 939–956.

Germer, J. & Sauerborn, J. (2008). Estimation of the impact of oil palm plantation establishment on greenhouse gas balance. *Environment, Development and Sustainability* (6), 10, 697–716.

Gibbs, H. K., Brown, S., Niles, J. O. & Foley, J. A. (2007). Monitoring and estimating tropical forest carbon stocks: making REDD a reality. *Environmental Research Letters*, 2, 1–13.

GOFC-GOLD (2012). *A sourcebook of methods and procedures for monitoring and reporting an-thropogenic greenhouse gas emissions and removals associated with deforestation, gains and losses of carbon stocks in forests remaining forests, and forestation. GOFC-GOLD Report version COP18-1*. Wageningen University: Wageningen.

Gonzalez, P., Asner, G. P., Battles, J. J., Lefsky, M. A., Waring, K. M. & Palace, M. (2010). Forest carbon densities and uncertainties from Lidar, QuickBird, and field measurements in California. *Remote Sensing of Environment* (7), 114, 1561–1575.

Gupta, K. & Gupta, R. (2007). Despeckle and geographical feature extraction in SAR images by wavelet transform. *ISPRS Journal of Photogrammetry & Remote Sensing* (6), 62, 473–484.

Hajnsek, I., Kugler, F., Lee, S.-K. & Papathanassiou, K. (2009). Tropical-ForestParameter Estimation by Means of Pol-InSAR: The INDREX-II Campaign. *IEEE Transactions on Geoscience and Remote Sensing* (2), 47, 481–493.

Hame, T., Kilpi, J., Ahola, H., Rauste, Y., Antropov, O., Rautiainen, M., Sirro, L. & Bounpone, S. (2013a). Improved Mapping of Tropical Forests With Optical and SAR Imagery, Part I: Forest Cover and Accuracy Assessment Using MultiResolution Data. *IEEE Journal of Selected Topics in Applied Earth Observations and Remote Sensing* (1), 6, 74–91.

Hame, T., Rauste, Y., Antropov, O., Ahola, H. & Kilpi, J. (2013b). Improved Mapping of Tropical Forests With Optical and SAR Imagery, Part II: Above Ground Biomass Estimation. *IEEE Journal of Selected Topics in Applied Earth Observations and Remote Sensing* (1), 6, 92–101.

Hansen, M. C., Potapov, P. V., Moore, R., Hancher, M., Turubanova, S. A., Tyukavina, A., Thau, D., Stehman, S. V., Goetz, S. J., Loveland, T. R., Kommareddy, A., Egorov, A., Chini, L., Justice, C. O. & Townshend, J. R. G. (2013). HighResolution Global Maps of 21st-Century Forest Cover Change. *Science* (6160), 342, 850–853.

Hansen, M., Shimabukuro, Y., Potapov, P. & Pittman, K. (2008). Comparing annual MODIS and PRODES forest cover change data for advancing monitoring of Brazilian forest cover. *Remote Sensing of Environment*, 112, 3784–3793.

Hanssen, R. (2001). *Radar interferometry: data interpretation and error analysis.*

Kluwer Academic: Dordrecht.

Henderson, F. & Lewis, A. (1998). Introduction. In: Henderson, F. & Lewis, A. (Eds.): *Principles & Applications of Imaging Radar.* 3rd ed. John Wiley & Sons: New York, 1–8.

Hoekman, D., Vissers, M. A. M. & Wielaard, N. (2010). PALSAR Wide-Area Mapping of Borneo: Methodology and Map Validation. *IEEE Journal of Selected Topics in Applied Earth Observations and Remote Sensing* (4), 3, 605–617.

Hooijer, A., Page, S., Canadell, J. G., Silvius, M., Kwadijk, J., Wosten, H. & Jauhiainen, J. (2010). Current and future CO2 emissions from drained peatlands southeast Asia.. *Biogeosciences* (5), 7, 1505–1514.

Huang, S. & Liu, D. (2007). Some uncertain factor analysis and improvement in spaceborne synthetic aperture radar imaging. *Signal Processing* (12), 87, 3202–2317.

IPCC (2003). *Good Practice Guidance for Land Use, Land-Use Change and Forestry*. IGES: Kanagawa.

Kell, R. (1965). On the derivation of bistatic RCS from monostatic measurements. *Proceedings of the IEEE* (8), 53, 983–988.

Kellndorfer, J., Walker, W., Pierce, L., Dobson, C., Fites, J. A., Hunsaker, C., Vona, J. & Clutter, M. (2004). Vegetation height estimation from Shuttle Radar Topography Mission and National Elevation Datasets. *Remote Sensing of Environment* (3), 93, 339–358.

Klausing, H. & Holpp, W. (2000). *Radar mit realer und synthetischer Apertur: Konzeption und Realisierung*. Oldenbourg: Mu¨nchen.

Knott, E. (1990). Radar Cross Section. In: Skolnik, M. (Eds.): *Radar Handbook*. 2nd ed. McGraw-Hill: New York, 11.1 –11.52.

Koch, B. (2010). Status and future of laser scanning, synthetic aperture radar and hyperspectral remote sensing data for forest biomass assessment. *ISPRS Journal of Photogrammetry and Remote Sensing*, 65, 581–590.

Koehl, M., Lister, A., Scott, C., Baldauf, T. & Plugge, D. (2011). Implications of sampling design and sample size for national carbon accounting systems. *Carbon Balance and Management* (1), 6, 1–20.

Koh, L., Miettinen, J., Liew, S. & Ghazoula, J. (2011). Remotely sensed evidence of tropical peatland conversion to oil palm. *Proceedings of the National Academy of Science of the United States of America (PNAS)* (12), 108, 5127–5132.

Koh, L., Gibbs, H., Potapov, P. & Hansen, M. (2012). REDDcalculator.com: A webbased decision-support tool for implementing Indonesia's forest moratorium. *Methods in Ecology and Evolution*, 3, 310–316.

Krieger, G. & Moreira, A. (2006). Spaceborne bi- and multistatic SAR: potential and challenges. *IEEE Proceedings - Radar, Sonar and Navigation* (3), 153, 184– 198.

Krieger, G., Moreira, A., Fiedler, H., Hajnsek, I., Werner, M., Younis, M. & Zink, M. (2007). TanDEM-X: A Satellite Formation for High-Resolution SAR Interferometry. *IEEE Transactions on Geoscience and Remote Sensing* (11), 45, 3317– 3341.

Krieger, G., Hajnsek, I., Papathanassiou, K., Younis, M. & Moreira, A. (2010). Interferometric Synthetic Aperture Radar (SAR) Missions Employing Formation Flying. *Proceedings of the IEEE* (5), 98, 816–843.

Kronseder, K., Ballhorn, U., Boehm, V. & Siegert, F. (2012). Above ground biomass estimation across forest types at different degradation levels in Central Kalimantan using LiDAR data. *International Journal of Applied Earth Observation and Geoinformation* (0), 18, 37–48.

Kugler, F., Schulze, D., Hajnsek, I., Pretzsch, H. & Papathanassiou, K. (2014). TanDEM-X Pol-InSAR Performance for Forest Height Estimation. *IEEE Transactions on Geoscience and Remote Sensing* (10), 52, 6404–6422.

Kuntz, S. (2010). Potential of spaceborne SAR for monitoring the tropical environments. *Tropical Ecology*, 51, 3–10.

Lawson, I., Kelly, T., Aplin, P., Boom, A., Dargie, G., Draper, F., Hassan, P., Hoyos-Santillan, J., Kaduk, J., Large, D., Murphy, W., Page, S., Roucoux, K., Sjogersten, S., Tansey, K., Waldram, M., Wedeux, B. & Wheeler, J. (2014). Improving estimates of tropical peatland area, carbon storage, and greenhouse gas fluxes. *Wetlands Ecology and Management* (6), 22, 1–20.

Le Toan, T., Beaudoin, A., Riom, J. & Guyon, D. (1992). Relating forest biomass to SAR data. *IEEE Transactions on Geoscience and Remote Sensing* (2), 30, 403–411.

Le Toan, T., Quegan, S., Davidson, M., Balzter, H., Paillou, P., Papathanassiou, K., Plummer, S., Rocca, F., Saatchi, S., Shugart, H. & Ulander, L. (2011). The BIOMASS mission: Mapping global forest biomass to better understand the terrestrial carbon cycle. *Remote Sensing of Environment* (11), 115, 2850–2860.

Leckie, D. (1998). Forestry Applications using imaging radar. In: Henderson, F. & Lewis, A. (Eds.): *Principles & Applications of Imaging Radar*. 3rd ed. John Wiley & Sons: New York, 435–510.

Lefsky, M. A., Harding, D. J., Keller, M., Cohen, W. B., Carabajal, C. C., Del Bom Espirito-Santo, F., Hunter, M. O. & Oliveira, R. de (2005). Estimates of forest canopy height and aboveground biomass using ICESat. *Geophysical Research Letters* (22), 32, 1–4.

Lewis, A. & Henderson, F. (1998). Radar Fundamentals: The Geoscience Perspective. In: Henderson, F. & Lewis, A. (Eds.): *Principles & Applications of Imaging Radar*. 3rd ed. John Wiley & Sons: New York, 132–183.

Lillesand, T., Kiefer, R. & Chipman, J. (2008). *Remote sensing and image interpretation*. 6th ed., John Wiley & Sons: Hoboken.

Longepe, N., Rakwatin, P., Isoguchi, O., Shimada, M., Uryu, Y. & Yulianto, K. (2011). Assessment of ALOS PALSAR 50 m Orthorectified FBD Data for Regional Land Cover Classification by Support Vector Machines. *IEEE Transactions on Geoscience and Remote Sensing* (6), 49, 2135–2150.

Lu, D. (2006). The potential and challenge of remote sensing-based biomass estimation. *International Journal of Remote Sensing* (7), 27, 1297–1328.

Lucas, R., Held, A., Phinn, S. & Saatchi, S. (2004). Tropical forests. In: Ustin, S. (Eds.): *Remote Sensing for natural ressource management and environmental monitoring*. 3rd ed. John Wiley & Sons: 239–316.

Luckman, A., Baker, J. & Wegmueller, U. (2000). Repeat-Pass Interferometric Coherence Measurements of Disturbed Tropical Forest from JERS and ERS Satellites. *Remote Sensing of Environment* (3), 73, 350–360.

Madsen, S. & Zebker, H. (1998). Imaging Radar Interferometry. In: Henderson, F. & Lewis, A. (Eds.): *Principles and applications of imaging radar*. Wiley & Sons: New York, 359 –380.

Madsen, S., Zebker, H. & Martin, J. (1993). Topographic mapping using radar interferometry: processing techniques. *IEEE Transactions on Geoscience and Remote Sensing* (1), 31, 246 –256.

Martin, A. R. & Thomas, S. C. (2011). A Reassessment of Carbon Content in Tropical Trees. *PLoS ONE* (8), 6, 1–9.

Massonnet, D. & Souyris, J. (2008). *Imaging with synthetic aperture radar*. EPFL Press: Lausanne.

Miettinen, J., Wong, C. M. & Liew, S. C. (2008). New 500A m spatial resolution landˆ cover map of the western insular Southeast Asia region. *International Journal of Remote Sensing* (20), 29, 6075–6081.

Miettinen, J., Shi, C., Tan, W. J. & Liew, S. C. (2012). 2010 land cover map of insular Southeast Asia in 250-m spatial resolution. *Remote Sensing Letters* (1), 3, 11–20.

Mitchard, E. T., Saatchi, S. S., Baccini, A., Asner, G. P., Goetz, S. J., Harris, N. L. & Brown, S. (2013). Uncertainty in the spatial distribution of tropical forest biomass: a comparison of pan-tropical maps. *Carbon Balance and Management* (10), 8, 1–13.

Mitchard, E., Saatchi, S., Lewis, S., Feldpausch, T., Woodhouse, I., Sonke, B., Rowland, C. & Meir, P. (2011). Measuring biomass changes due to woody encroachment and deforestation/degradation in a forest-savanna boundary region of central Africa using multi-temporal L-band radar backscatter. *Remote Sensing of Environment* (11), 115, 2861–2873.

Morel, A. C., Saatchi, S. S., Malhi, Y., Berry, N. J., Banin, L., Burslem, D., Nilus, R. & Ong, R. C. (2011). Estimating aboveground biomass in forest and oil palm plantation in Sabah, Malaysian Borneo using ALOS PALSAR data. *Forest Ecology and Management* (9), 262, 1786 –1798.

Muhamad, N. Z. & Rieley, J. O. (2002). Management of tropical peatlands in Indonesia: Mega reclamation project in Central Kalimantan. In: Rieley, J. O., Page, S. E. & Setiadi, B. (Eds.): *Proceedings of the International Symposium on Tropical Peatland* . BPPT and Indonesian Peat association: Jakarta, 155–162.

Murdiyarso, D., Hergoualc'h, K. & Verchot, L. (2010). Opportunities for reducing greenhouse gas emissions in tropical peatlands. *Proceedings of the National Academy of Science of the United States of America (PNAS)* (46), 107, 19655–19660.

Myneni, R. B., Dong, J., Tucker, C. J., Kaufmann, R. K., Kauppi, P. E., Liski, J., Zhou, L., Alexeyev, V. & Hughes, M. K. (2001). A large carbon sink in the woody biomass of Northern forests. *Proceedings of the National Academy of Sciences* (26), 98, 14784–14789.

Naidoo, L., Mathieu, R., Main, R., Kleynhans, W., Wessels, K., Asner, G. & Leblon, B. (2015). Savannah woody structure modelling and mapping using multi-frequency (X-, C- and L-band) Synthetic Aperture Radar data. *ISPRS Journal of Photogrammetry & Remote Sensing*, 105, 234–250.

Neeff, T., Dutra, L. V., Santos, J. R. dos, Freitas, C. d. C. & Araujo, L. S. (2005). Tropical Forest Measurement by Interferometric Height Modeling and P-Band Radar Backscatter. *Forest Science* (6), 51, 585–594.

Neumann, M., Ferro-Famil, L. & Reigber, A. (2010). Estimation of Forest Structure, Ground, and Canopy Layer Characteristics From Multibaseline Polarimetric Interferometric SAR Data. *IEEE Transactions on Geoscience and Remote Sensing* (3), 48, 1086 –1104.

Nezry, E., Mougin, E., Lopes, A. & Gastellu-Etchegorry, J. (1993). Tropical vegetation mapping with combined visible and SAR spareborne data. *International Journal of Remote Sensing*, 14, 2165–2184.

Olander, L. P., Gibbs, H. K., Steininger, M., Swenson, J. J. & Murray, B. C. (2008). Reference scenarios for deforestation and forest degradation in support of REDD: a review of data and methods. *Environmental Research Letters*, 3, 1–11.

Otukei, J. R., Blaschke, T., Collins, M. & Maghsoudi, Y. (2011). Analysis of ALOS PALSAR and TerraSAR-X data for protected area mapping: A case of the Bwindi Impenetrable National Park-Uganda. In: *IEEE International Geoscience and Remote Sensing Symposium (IGARSS), 2011*,348–351.

Page, S. E., Rieley, J. O. & Banks, C. J. (2011). Global and regional importance of the tropical peatland carbon pool. *Global Change Biology* (2), 17, 798–818.

Page, S. E., Rieley, J. O., Shotyk, O. W. & Weiss, D. (1999). Interdependence of peat and vegetation in a tropical peat swamp forest. *Philosphoical Transaction of the Royal Society*, 354, 1885–1897.

Page, S. E., Siegert, F., Rieley, J. O., Boehm, H.-D. V., Jaya, A. & Limin, S. (2002). The amount of carbon released from peat and forest fires in Indonesia during 1997. *Nature* (6911), 420, 61–65.

Papathanassiou, K. & Cloude, S. (2001). Single-baseline polarimetric SAR interferometry. *IEEE Transactions on Geoscience and Remote Sensing* (11), 39, 2352– 2363.

Phillips, V. D. (1998). Peatswamp ecology and sustainable development in Borneo. *Biodiversity & Conservation* (5), 7, 651–671.

Pitz, W. & Miller, D. (2010). The TerraSAR-X Satellite. *IEEE Transactions on Geoscience and Remote Sensing* (2), 48, 615 –622.

Poncet, F. v., Schlund, M. & Kuntz, S. (2014). Synergy of TanDEM-X bistatic data and TerraSAR-X to map the state and evolution of forest degradation. In: *ForestSAT2014*.

Potapov, P. V., Turubanova, S. A., Hansen, M. C., Adusei, B., Broich, M., Altstatt, A., Mane, L. & Justice, C. O. (2012). Quantifying forest cover loss in Democratic Republic of the Congo, 2000-2010, with Landsat ETM data. *Remote Sensing of Environment*, 122, 106–116.

Rahman, M. M., Csaplovics, E. & Koch, B. (2008). Satellite estimation of forest carbon using regression models. *International Journal of Remote Sensing* (23), 29, 6917– 6936.

Raney, R. (1998). Radar Fundamentals: Technical Perspective. In: Henderson, F. & Lewis, A. (Eds.): *Principles & Applications of Imaging Radar*. 3rd ed. John Wiley & Sons: New York, 9–131.

Reiche, J., Souzax, C., Hoekman, D., Verbesselt, J., Persaud, H. & Herold, M. (2013). Feature Level Fusion of Multi-Temporal ALOS PALSAR and Landsat Data for

Mapping and Monitoring of Tropical Deforestation and Forest Degradation. *IEEE Journal of Selected Topics in Applied Earth Observations and Remote Sensing* (5), 6, 2159–2173.

Reiche, J., Verbesselt, J., Hoekman, D. & Herold, M. (2015). Fusing Landsat and SAR time series to detect deforestation in the tropics. *Remote Sensing of Environment*, 156, 276–293.

Richards, J. (2009). *Remote Sensing with Imaging Radar*. Springer: Berlin.

Rombach, M. & Moreira, J. (2003). Description and applications of the multipolarized dual band OrbiSAR-1 InSAR sensor. In: *Proceedings of the International Radar Conference 2003*, 245–250.

Rosen, P., Hensley, S., Joughin, I., Li, F., Madsen, S., Rodriguez, E. & Goldstein, R. (2000). Synthetic aperture radar interferometry. *Proceedings of the IEEE* (3), 88, 333 –382.

Rosenqvist, A., Milne, A., Lucas, R., Imhoff, M. & Dobson, C. (2003). A review of remote sensing technology in support of the Kyoto Protocol. *Environmental Science & Policy*, 6, 441–455.

Saatchi, S. S., Houghton, R. A., Dos Santos Alvala, R. C., Soares, J. V. & Yu, Y. (2007). Distribution of aboveground live biomass in the Amazon basin. *Global Change Biology* (4), 13, 816–837.

Saatchi, S. S., Soares, J. V. & Alves, D. S. (1997). Mapping deforestation and land use in amazon rainforest by using SIR-C imagery. *Remote Sensing of Environment* (2), 59, 191 –202.

Saatchi, S., Marlier, M., Chazdon, R. L., Clark, D. B. & Russell, A. E. (2011b). Impact of spatial variability of tropical forest structure on radar estimation of aboveground biomass. *Remote Sensing of Environment* (11), 115, 2836–2849.

Saatchi, S. S., Harris, N. L., Brown, S., Lefsky, M., Mitchard, E. T. A., Salas, W., Zutta, B. R., Buermann, W., Lewis, S. L., Hagen, S., Petrova, S., White, L., Silman, M. & Morel, A. (2011a). Benchmark map of forest carbon stocks in tropical regions across three continents. *Proceedings of the National Academy of Science of the United States of America (PNAS)* (24), 108, 9899–9904.

Sanden, J. J. van der & Hoekman, D. H. (1999). Potential of Airborne Radar To Support the Assessment of Land Cover in a Tropical Rain Forest Environment. *Remote Sensing of Environment*, 68, 26 –40.

Santoro, M., Askne, J., Smith, G. & Fransson, J. E. (2002). Stem volume retrieval in boreal forests from ERS-1/2 interferometry. *Remote Sensing of Environment* (1), 81, 19 –35.

Santoro, M., Shvidenko, A., McCallum, I., Askne, J. & Schmullius, C. (2007). Properties of ERS-1/2 coherence in the Siberian boreal forest and implications for stem volume retrieval. *Remote Sensing of Environment* (2), 106, 154 –172.

Santos, J. R., Mura, J. C., Kux, H. J. H., Garcia, C. E., Kuntz, S., Brown, I. F. & Pantoja, N. V. (2010). Classification of TerraSAR-X imagery for the characterization of Amazon tropical forests. In: *30th EARSeL Symposium: Remote Sensing for Science, Education and Culture*,vol. 31, 329–334.

Schlerf, M., Atzberger, C. & Hill, J. (2005). Remote sensing of forest biophysical variables using HyMap imaging spectrometer data. *Remote Sensing of Environment* (2), 95, 177–194.

Schlund, M., Poncet, F. v., Kuntz, S. & Hoekman, D. H. (2013). Relationship of canopy cover with TanDEM-X features in a tropical peat swamp forest. In: Jekel, T., Car, A., Strobl, J. & Griesebner, G. (Eds.): *GI Forum 2013. Creating the GISociety* . VDE: Offenbach, 109–113.

Schlund, M., Poncet, F. v., Kuntz, S., Boehm, H. D.-V., Hoekman, D. & Schmullius, C. (without year). WorldDEM data for canopy height and aboveground biomass retrieval in a tropical peat swamp forest. *submitted*, NA, NA.

Schlund, M., Herrera Cruz, V. & Poncet, F. v. (2014b). Synergetic use of TanDEMX and RapidEye to support object based Land Use/Land cover Mapping. *South Eastern European Journal of Earth Observation and Geomatics* (2), 3, 595–600.

Schlund, M., Poncet, F. von, Hoekman, D. H., Kuntz, S. & Schmullius, C. (2014a). Importance of bistatic SAR features from TanDEM-X for forest mapping and monitoring. *Remote Sensing of Environment*, 151, 16–26.

Schlund, M., Poncet, F. von, Kuntz, S., Schmullius, C. & Hoekman, D. H. (2015). TanDEM-X data for aboveground biomass retrieval in a tropical peat swamp forest. *Remote Sensing of Environment*, 158, 255–266.

Sexton, J., Bax, T., Siqueira, P., Swenson, J. & Hensley, S. (2009). A comparison of lidar, radar, and field measurements of canopy height in pine and hardwood forests of southeastern North America. *Forest Ecology and Management* (3), 257, 1136–1147.

Sgrenzaroli, M., Baraldi, A., De Grandi, G., Eva, H. & Achard, F. (2004). A novel approach to the classification of regional-scale Radar mosaics for tropical vegetation mapping. *IEEE Transactions on Geoscience and Remote Sensing* (11), 42, 2654–2669.

Shimabukuro, Y. E., Batista, G. T., Mello, E. M. K., Moreira, J. C. & Duarte,

V. (1998). Using shade fraction image segmentation to evaluate deforestation in Landsat Thematic Mapper images of the Amazon Region. *International Journal of Remote Sensing* (3), 19, 535–541.

Simard, M., Saatchi, S. & De Grandi, G. (2000). The use of decision tree and multiscale texture for classification of JERS-1 SAR data over tropical forest. *IEEE Transactions on Geoscience and Remote Sensing* (5), 38, 2310–2321.

Simard, M., Grandi, G. D., Saatchi, S. & Mayaux, P. (2002). Mapping tropical coastal vegetation using JERS-1 and ERS-1 radar data with a decision tree classifier. *International Journal of Remote Sensing* (7), 23, 1461–1474.

Simard, M., Pinto, N., Fisher, J. B. & Baccini, A. (2011). Mapping forest canopy height globally with spaceborne lidar. *Journal of Geophysical Research*, 116, 1– 12.

Skolnik, M. (1990). An introduction to radar. In: Skolnik, M. (Eds.): *Radar Handbook*. 2nd ed. McGraw-Hill: 1.1 –11.21.

Soja, M., Persson, H. & Ulander, L. (2015). Estimation of Forest Biomass From Two-Level Model Inversion of Single-Pass InSAR Data. *IEEE Transactions on Geoscience and Remote Sensing* (9), 53, 5083–5099.

Solberg, S., Astrup, R., Gobakken, T., Naesset, E. & Weydahl, D. J. (2010). Estimating spruce and pine biomass with interferometric X-band SAR. *Remote Sensing of Environment* (10), 114, 2353 –2360.

Solberg, S., Astrup, R., Breidenbach, J., Nilsen, B. & Weydahl, D. (2013). Monitoring spruce volume and biomass with InSAR data from TanDEM-X. *Remote Sensing of Environment*, 139, 60–67.

Sorensen, K. W. (1993). Indonesian peat swamp forests and their role as a carbon sink. *Chemosphere* (6), 27, 1065 –1082.

Souza, C., Roberts, D. & Cochrane, M. (2005). Combining spectral and spatial information to map canopy damage from selective logging and forest fires. *Remote Sensing of Environment*, 98, 329–343.

St-Onge, B., Hu, Y. & Vega, C. (2008). Mapping the height and aboveground biomass of a mixed forest using lidar and stereo Ikonos images. *International Journal of Remote Sensing* (5), 29, 1277–1294.

Strozzi, T., Dammert, P., Wegmuller, U., Martinez, J.-M., Askne, J., Beaudoin, A. & Hallikainen, N. (2000). Landuse mapping with ERS SAR interferometry. *IEEE Transactions on Geoscience and Remote Sensing* (2), 38, 766 –775.

Thenkabail, P. S., Enclona, E. A., Ashton, M. S., Legg, C. & Dieu, M. J. D. (2004). Hyperion, IKONOS, ALI, and ETM+ sensors in the study of African rainforests. *Remote Sensing of Environment*, 90, 23–43.

Treuhaft, R., Goncalves, F., Santos, J. dos, Keller, M., Palace, M., Madsen, S., Sullivan, F. & Graca, P. (2015). Tropical-Forest Biomass Estimation at X-Band From the Spaceborne TanDEM-X Interferometer. *IEEE Geoscience and Remote Sensing Letters* (2), 12, 239–243.

Ulaby, F. & Dobson, D. (1989). *Handbook of radar scattering statistics for terrain*. Artech House: Norwood.

Ulaby, F., Moore, R. & Fung, A. (1981). *Microwave Remote Sensing: Microwave remote sensing fundamentals and radiometry*. Artech House: Norwood.

Ulaby, F., Moore, R. & Fung, A. (1982). *Microwave Remote Sensing: Radar remote sensing and surface scattering and emission theory*. Artech House: Norwood.

Ullmann, T., Lumsdon, P., Poncet, F. v., Esch, T., Lang, O., Tinz, M., Kuntz, S. & Dech, S. (2012). Application of quadpolarimetric TerraSAR-X data for landcover characterization in tropical regions - A case study in South Kalimantan, Indonesia. In: *IEEE International Geoscience and Remote Sensing Symposium (IGARSS), 2012*, 5133–5136.

Villard, L. & Borderies, P. (2015). On the use of virtual ground scatterers to localize double and triple bounce scattering mechanisms for bistatic SAR. *Journal of Electromagnetic Waves and Applications* (5), 29, 626–635.

Walker, W., Stickler, C., Kellndorfer, J., Kirsch, K. & Nepstad, D. (2010). LargeArea Classification and Mapping of Forest and Land Cover in the Brazilian Amazon: A Comparative Analysis of ALOS/PALSAR and Landsat Data Sources. *IEEE Journal of Selected Topics in Applied Earth Observations and Remote Sensing* (4), 3, 594–604.

Walterscheid, I., Brenner, A. & Ender, J. (2004). Results on bistatic synthetic aperture radar. *Electronics Letters* (19), 40, 1224–1225.

Walterscheid, I., Ender, J., Brenner, A. & Loffeld, O. (2006). Bistatic SAR Processing and Experiments. *IEEE Transactions on Geoscience and Remote Sensing* (10), 44, 2710 –2717.

Wegmuller, U. & Werner, C. (1995). SAR interferometric signatures of forest. *IEEE Transactions on Geoscience and Remote Sensing* (5), 33, 1153 –1161.

Werf, G. R. van der, Morton, D. C., DeFries, R. S., Olivier, J. G. J., Kasibhatla, P. S., Jackson, R. B., Collatz, G. J. & Randerson, J. T. (2009). CO2 emissions from forest loss. *Nature Geoscience*, 2, 737–738.

Werninghaus, R. & Buckreuss, S. (2010). The TerraSAR-X Mission and System Design. *IEEE Transactions on Geoscience and Remote Sensing* (2), 48, 606 –614.

Weydahl, D. J., Sagstuen, J., Dick, O. B. & Ronning, H. (2007). SRTM DEM accuracy assessment over vegetated areas in Norway. *International Journal of Remote Sensing* (16), 28, 3513–3527.

Wich, S. A., Meijaard, E., Marshall, A. J., Husson, S., Ancrenaz, M., Lacy, R. C., Schaik, C. P. van, Sugardjito, J., Simorangkir, T., Traylor-Holzer, K., Doughty, M., Supriatna, J., Dennis, R., Gumal, M., Knott, C. D. & Singleton, I. (2008). Distribution and conservation status of the orang-utan (Pongo spp.) on Borneo and Sumatra: how many remain?. *Oryx*, 42, 329–339.

Wijedasa, L. S., Sloan, S., Michelakis, D. G. & Clements, G. R. (2012). Overcoming Limitations with Landsat Imagery for Mapping of Peat Swamp Forests in Sundaland. *Remote Sensing* (9), 4, 2595–2618.

Willis, N. (1990). Bistatic Radar. In: Skolnik, M. (Eds.): *Radar Handbook*. 2nd ed. McGraw-Hill: New York, 25.1 –25.35.

Willis, N. (1991). *Bistatic Radar*. SciTech Publishing: Raleigh.

Woesten, J. H. M., Clymans, E., Page, S. E., Rieley, J. O. & Limin, S. H. (2008). Peat-water interrelationships in a tropical peatland ecosystem in Southeast Asia. *Catena* (2), 73, 212–224.

Zhou, X., Chang, N.-B. & Li, S. (2009). Applications of SAR Interferometry in Earth and Environmental Science Research. *Sensors* (3), 9, 1876–1912.

Erklärung zu Eigenanteilen an Publikationen & Zweitpublikationsrechten bei einer kumulativen Dissertation

Hiermit bestätige ich, Michael Schlund, dass für den Artikel *"Importance of bistatic SAR features from TanDEM-X for forest mapping and monitoring"* erschienen in *Remote Sensing of Environment* die Zweitpublikationsrechte im Rahmen der kumulativen Dissertation *"Utilization of bistatic TanDEM-X data to derive land cover information"* vorliegen. Lizenzvereinbarung zwischen Michael Schlund und Elsevier, bereitgestellt von *Copyright Clearance Center (CCC)*, wurde geschlossen am 21.06.2015.

Schlund, M., F. von Poncet, S. Kuntz, D.H. Hoekman & C. Schmullius (2014). Importance of bistatic SAR features from TanDEM-X for forest mapping and monitoring. *Remote Sensing of Environment* 151, 16-26.

	M.Schlund	F.vonPoncet	S.Kuntz	D.H.Hoekman	C.Schmullius
Konzeption des Forschungsansatzes	x	x	x		x
Planung der Untersuchungen	x	x			
Datenerhebung	x			x	
Datenanalyse und -interpretation	x				
Schreiben des Manuskripts	x	x	x	x	x
Vorschlag Anrechnung Publikationsäquivalente	1				

Hiermit bestätige ich, Michael Schlund, dass für den Artikel *"TanDEM-X data for aboveground biomass retrieval in a tropical peat swamp forest"* erschienen in *Remote Sensing of Environment* die Zweitpublikationsrechte im Rahmen der kumulativen Dissertation *"Utilization of bistatic TanDEM-X data to derive land cover information"* vorliegen. Lizenzvereinbarung zwischen Michael Schlund und Elsevier,

Schlund, M., F. von Poncet, S. Kuntz, C. Schmullius & D.H. Hoekman (2015). TanDEM-X data for aboveground biomass retrieval in a tropical peat swamp forest. *Remote Sensing of Environment* 158, 255-266.

| | M.Schlund | S.Kuntz | | | |
| | F.von Poncet | C.Schmullius | D.H.Hoekman | | |

	M.Schlund	F.von Poncet	S.Kuntz	C.Schmullius	D.H.Hoekman
Konzeption des Forschungsansatzes	x	x	x	x	
Planung der Untersuchungen	x				
Datenerhebung	x				x
Datenanalyse und -interpretation	x	x			
Schreiben des Manuskripts	x	x	x	x	x
Vorschlag Anrechnung Publikationsäquivalente	1				

Original Research Paper

Dear Mr. Michael Schlund,

Your submission entitled "WorldDEM data for canopy height and aboveground biomass retrieval in a tropical peat swamp forest" has been received by ISPRS Journal of Photogrammetry and Remote Sensing.

Thank you for submitting your work to this journal.

Kind regards,

Elsevier Editorial System

ISPRS Journal of Photogrammetry and Remote Sensing

Schlund, M., F. von Poncet, S. Kuntz, H.D.-V. Boehm, D.H. Hoekman & C. Schmullius (2015). WorldDEM™ data for canopy height and aboveground biomass retrieval in a tropical peat swamp forest. *ISPRS Journal of Photogrammetry & Remote Sensing*. (Status: submitted)

M.Schlund   F.vonPoncet   U.Ballhorn   N.Boehm   J.C.Schmullius   S.Kuntz

	M.Schlund	F.vonPoncet	U.Ballhorn	N.Boehm	J.C.Schmullius	S.Kuntz
Konzeption des Forschungsansatzes	x	x	x			x
Planung der Untersuchungen	x	x				
Datenerhebung	x			x	x	
Datenanalyse und -interpretation	x		x			
Schreiben des Manuskripts	x	x	x	x	x	x
Vorschlag Anrechnung Publikationsäquivalente	1					

Für alle in dieser kumulativen Dissertation verwendeten Manuskripte liegen die notwendigen Genehmigungen der Verlage ("Reprint permissions") für die Zweitpublikation vor.

Die Ko-Autoren der in dieser kumulativen Dissertation verwendeten Manuskripte sind sowohl über die Nutzung, als auch über die oben angegebenen Eigenanteile informiert und stimmen dem zu.

Michael Schlund, Ort, Datum

Ich bin mit der Abfassung der Dissertation als publikationsbasiert, d.h. kumulativ, einverstanden und bestätige die vorstehenden Angaben. Eine entsprechend begründete Befürwortung mit Angabe des wissenschaftlichen Anteils des Doktoranden/der Doktorandin an den verwendeten Publikationen werde ich parallel an den Rat der Fakultät der Chemisch-Geowissenschaftlichen Fakultät richten.

Prof. Dr. C. Schmullius, Ort, Datum

Curriculum Vitae

Personal details

Name	Michael Schlund
Address	Alpenblick 22
	88718 Daisendorf - Germany
Mobile	+49 176 21136811
Date of birth	June 24, 1985
Place of birth	Sonneberg - Germany
Nationality	German

Academic education

09-2012   GIONET summer school at the University of Leicester
                 "Remote sensing of land cover and forest in GMES"

Since 02-2011 Friedrich-Schiller-University Jena *PhD
                 student*

2008 - 2011   Friedrich-Schiller-University Jena
                 Master of Science Geoinformatics (Grade: 1.4)

2005 - 2008   Friedrich-Schiller-University Jena
                 Bachelor of Science Geography (Grade: 2.3)

1996 - 2004   Heinrich-Heine grammar school in Sonneberg

1992 - 1996   Primary school Wolkenrasen in Sonneberg

Relevant work experience

08-2014 - 09-   Field measurements & training given for aboveground tree
2014   biomass estimations in Mawas, Kalimantan, Indonesia

05-2013 - 07- Field measurements & training given for aboveground tree 2013 biomass estimations in Mawas, Kalimantan, Indonesia

08-2012 Training classes given at CERSGIS (Centre for Remote Sensing & GIS), University of Ghana, Accra, Ghana

03-2010 - 08- Internship at Infoterra GmbH
2010

07-2009 - 12- Scientific assistant at Department of earth observation at 2009 Friedrich-Schiller-University Jena

09-2007 - 02- Scientific assistant at Department of Geoinformatics, Geohydrol2009 ogy and Modelling at Friedrich-Schiller-University Jena

04-2009 Assistant at General Assembly of European Geoscience Union

04-2008 - 05- Internship at Department of economic geography at Friedrich2008 Schiller-University Jena

04-2007 Assistant at General Assembly of European Geoscience Union

IT skills

- Advanced skills in remote sensing software packages like ERDAS Imagine, PCI Geomatica, ENVI & eCognition

- Advanced skills in radar remote sensing software packages like PolSARpro, SARscape & Gamma

- Advanced skills in programming language R

- Advanced skills in GIS like ArcGIS & ArcView
- Basic skills in programming language IDL, Matlab and bash scripting

- Basic skills in typesetting software TeX

- Experienced user of all office applications, E-Mail & internet

Languages

- German: fluent

- English: fluent

- Spanish: basic knowledge

Hobbies

- Football, cycling, reading, traveling

Selbstständigkeitserklärung

Ich erkläre, dass mir die geltende Promotionsordnung der Fakultät bekannt ist; dass ich die Dissertation selbst angefertigt, keine Textabschnitte eines Dritten oder eigener Prüfungsarbeiten ohne Kennzeichnung übernommen und alle von mir benutzten Hilfsmittel, persönlichen Mitteilungen und Quellen in meiner Arbeit angegeben habe; das mich folgende Personen bei der Auswahl und Auswertung des Materials sowie bei der Herstellung des Manuskripts unterstützt haben:

- Ko-Autoren der Veröffentlichungen

- Henrike Manthey

- Constanze Graesche

dass die Hilfe eines Promotionsberaters nicht in Anspruch genommen wurde und dass Dritte weder unmittelbar noch mittelbar geldwerte Leistungen von mir für Arbeiten erhalten haben, die im Zusammenhang mit dem Inhalt der vorgelegten Dissertation stehen; dass ich die Dissertation noch nicht als Prüfungsarbeit für eine staatliche oder andere wissenschaftliche Prüfung eingereicht habe;
dass ich nicht die gleiche, eine in wesentlichen Teilen ähnliche oder eine andere Abhandlung bei einer anderen Hochschule als Dissertation eingereicht habe.

Daisendorf, den 10.09.2015   Michael Schlund